12-1-2020

Antibody profiling of patients with prostate cancer reveals differences in antibody signatures among disease stages

Hemanth K Potluri

Tun Lee Ng

Michael A Newton

Jin Zhang

Christopher A Maher

See next page for additional authors

Authors

Hemanth K Potluri, Tun Lee Ng, Michael A Newton, Jin Zhang, Christopher A Maher, Peter S Nelson, and Douglas G McNeel

Antibody profiling of patients with prostate cancer reveals differences in antibody signatures among disease stages

Hemanth K Potluri,[1] Tun Lee Ng,[2] Michael A Newton,[2] Jin Zhang,[3] Christopher A Maher,[3] Peter S Nelson,[4] Douglas G McNeel [ORCID] [1]

[1]Medicine, University of Wisconsin-Madison, Madison, Wisconsin, USA
[2]Biostatistics and Medical Informatics, University of Wisconsin-Madison, Madison, Wisconsin, USA
[3]Medicine, Washington University in Saint Louis, Saint Louis, Missouri, USA
[4]Human Biology Division, Fred Hutchinson Cancer Research Center, Seattle, Washington, USA

Correspondence to
Dr Douglas G McNeel;
dm3@medicine.wisc.edu

ABSTRACT

Background Previous studies of prostate cancer autoantibodies have largely focused on diagnostic applications. So far, there have been no reports attempting to more comprehensively profile the landscape of prostate cancer-associated antibodies. Specifically, it is unknown whether the quantity of antibodies or the types of proteins recognized change with disease progression.

Methods A peptide microarray spanning the amino acid sequences of the gene products of 1611 prostate cancer-associated genes was synthesized. Serum samples from healthy male volunteers (n=15) and patients with prostate cancer (n=85) were used to probe the array. These samples included patients with various clinical stages of disease: newly diagnosed localized prostate cancer (n=15), castration-sensitive non-metastatic prostate cancer (nmCSPC, n=40), castration-resistant non-metastatic prostate cancer (n=15) and castration-resistant metastatic disease (n=15). The patients with nmCSPC received treatment with either standard androgen deprivation therapy (ADT) or an antitumor DNA vaccine encoding prostatic acid phosphatase. Serial sera samples from these individuals were also used to probe the array, to secondarily determine whether this approach could be used to detect treatment-related changes.

Results We demonstrated that this peptide array yielded highly reproducible measurements of serum IgG levels. We found that the overall number of antibody responses did not increase with disease burden. However, the composition of recognized proteins shifted with clinical stage of disease. Our analysis revealed that the largest difference was between patients with castration-sensitive and castration-resistant disease. Patients with castration-resistant disease recognized more proteins associated with nucleic acid binding and gene regulation compared with men in other groups. Our longitudinal data showed that treatments can elicit antibodies detectable by this array, and notably vaccine-treated patients developed increased responses to more proteins over the course of treatment than did ADT-treated patients.

Conclusions This study represents the largest survey of prostate cancer-associated antibodies to date. We have been able to characterize the classes of proteins recognized by patients and determine how they change with disease burden. Our findings further demonstrate the potential of this platform for measuring antigen spread and studying responses to immunomodulatory therapies.

BACKGROUND

It has been previously reported that patients with cancer develop antibodies to autologous proteins.[1 2] This phenomenon has been described across a wide variety of cancer types, including colon, melanoma, bladder, lung and prostate.[3–7] These antibodies may arise due to overexpression of self-antigens, inflammation or tumor cell lysis.[8] Studies of serum antibodies may be particularly attractive for a variety of diagnostic applications because serum samples are relatively easy to obtain, antibodies can be present at early stages of disease and antibodies can be present at high levels even when their target antigen is expressed at low levels. In contrast, monitoring serum proteins in patients with cancer has been more challenging because they are often much less abundant and have more variable expression over time.[9 10] Antibody presence can also provide information about the relative immunogenicity of a given antigen. Many groups have used naturally existing antibody responses in patients with cancer to identify targets for antibody therapies or vaccination strategies.[11–13] Similarly, profiling antibody responses has been used to detect antigen spread following immunotherapy.[14] Thus, further study of these antibodies may have important implications for cancer diagnostics, biomarkers of response to therapy and in guiding the design and targets of future therapies.

In the case of prostate cancer, several groups have developed methods to evaluate serum antibodies.[7 15 16] Chinnaiyan *et al* used phage display to screen patient serum for responses against many candidate prostate cancer-associated peptides. They identified

22 proteins against which antibody responses could distinguish patients with prostate cancer and healthy individuals more reliably than detection of serum prostate-specific antigen (PSA) protein. Taylor *et al* and Ummanni *et al* took similar approaches, probing prostate tumor lysates with patient serum and then performing mass spectrometry to identify the proteins that reacted more with serum of cancer patient than control serum. Our group has also interrogated patient serum samples to discover prostate tumor-associated antibodies using ELISA for known prostate cancer tumor antigens and the serological identification of antigens by recombinant expression (SEREX) methodology to identify antibody targets from tissue expression libraries.[17–19] These previous studies of antibodies in patients with prostate cancer focused primarily on diagnostic applications or on changes in antibody responses. This approach has resulted in the discovery of small panels of shared antigens that may be useful for monitoring development of disease or response to treatment. However, to date, no studies have performed a more complete profile of the repertoires of prostate cancer-associated antibodies in individuals. In addition, data on whether the quantity or composition of antibody responses differ between patients with different disease severity are lacking.

Early studies were able to characterize antibodies against small numbers of antigens, but advancements such as phage display and now microarray-based platforms have made it possible to develop more thorough profiles of antibodies in patients with cancer. We sought to develop a microarray capable of detecting serum IgG responses against peptides using gene products from genes highly expressed in prostate cancer and predicted products of open reading frames (ORFs) from prostate cancer-associated long non-coding RNAs (lncRNAs). Our goal was to evaluate the number and character of proteins recognized by individuals with different clinical stages of disease, and secondarily whether a peptide microarray could be used to detect changes in antibody profiles following cancer treatment.

Here, we describe the use of the largest reported prostate cancer-specific peptide microarray. We demonstrate that the composition of antibodies does change with stage, with the largest differences evident between patients with castration-resistant disease and castration-sensitive disease, but the overall number of proteins recognized by these antibodies does not change with stage. We provide a detailed examination of the types of proteins that are recognized in patients with different clinical stages of prostate cancer and that have received treatment. We detect many more proteins with increased antibody recognition following vaccination than following androgen deprivation therapy (ADT), suggesting that the microarray platform could be used to measure prostate cancer-associated antigen spread as a future direction.

METHODS

Patient populations

Sera were previously collected from male volunteer blood donors without cancer (n=15, controls), or patients with prostate cancer (n=85). Sera from patients were grouped according to stage of disease: newly diagnosed localized prostate cancer (new Dx, n=15), castration-sensitive non-metastatic prostate cancer (nmCSPC, n=40), castration-resistant non-metastatic prostate cancer (nmCRPC, n=15) and castration-resistant metastatic disease (mCRPC, n=15). Sera were also collected serially from the individuals with nmCSPC, who were enrolled on clinical trials in which 20 patients were treated with standard ADT (gonadotropin-releasing hormone analog given every 3 months)[20] and the other 20 were treated with an investigational antitumor DNA vaccine encoding prostatic acid phosphatase (PAP; pTVG-HP, with granulocyte-macrophage colony-stimulating factor co-delivered as a vaccine adjuvant, given every 14 days for 6 administrations).[21] Sera were collected at baseline, and at 3 months and 6 months following initiation of treatment for these patients. All samples were stored between −20°C and −80°C until use for analysis.

Antigen selection

Gene products from 1463 of the most highly expressed transcripts in prostate cancer[22 23] and 148 predicted ORFs in prostate cancer were selected for inclusion on the array (online supplemental table 1). Gene products included 125 antigens previously identified as recognized by IgG from patients with prostate cancer.[24] The potential ORFs were selected from a list by Iyer *et al* of long RNAs with in silico evidence of coding potential.[25] There were 74 transcripts designated as having a 'Cancer Association', 'prostate' tissue association and category of 'tucp' (transcript of unknown coding potential).[26] ORFs were then predicted using EMBOSS: getorf, with the top two longest ORFs for each long RNA included on the microarray.

Peptide array synthesis and antibody screening

Peptide synthesis was performed as previously described, using a light-directed array synthesis in a Roche Nimblegen (Madison, Wisconsin, USA) maskless array synthesizer.[27] Cycles of amino acid coupling were repeated until 16-mer peptides were synthesized on arrays containing 12 replicates of 177,604 peptides per subarray. Sera were diluted 1:100 with binding buffer (0.1 M Tris, 1% alkali-soluble casein, 0.05% Tween-20), incubated overnight at 4°C and washed. IgG was detected using an Alexa Fluor 647-labeled antihuman IgG secondary antibody (Jackson ImmunoResearch Labs, West Grove, Pennsylvania, USA). After final washing, arrays were dried and read using a Roche MS 200 microarray scanner, and signals were extracted using Roche internally developed software. Fluorescent signals were converted into arbitrary units (AU) with intensity plots ranging from 0 to 65 000 AU. Spatial correction, background correction and quantile normalization were performed on raw array signal intensities by Roche as

previously described.[28] All samples were evaluated in triplicate on separate arrays. Samples were considered positive for an antibody response at a given probe if the signal crossed 2^{12} fluorescence units, with a sliding scale p value <0.05 in at least two of three technical replicates.[28] A binding buffer only control was also run to confirm the absence of signal above the 2^{12} threshold.

Data analysis

Data analyses were performed in R V.3.6.2[29] and RStudio[30] using many available extension packages and visualization tools as well as custom scripts. To support reproducibility, workflow details are supplied in an R markdown document and the rendered online supplemental statistical. These materials are also available at: https://github.com/wiscstatman/immunostat-prostate

Array reproducibility

Pearson's correlation coefficients were calculated for each pair of observations of fluorescence data, creating a 345×345 matrix. The Fisher transformation was then applied before averaging coefficients together to assess reproducibility of the array. In a complementary analysis (online supplemental statistical section 2.3), a peptide-specific linear mixed-effects model was fit to measure the relative size of technical variation to biological variation in this system. This used the R package lme4[31] on log-transformed fluorescence intensity levels to compute variance components while adjusting for possible fixed effects of disease stage.

Differences between clinical groups

Analysis of variance (ANOVA) with the Tukey's Honest Significant Differences post-test was used to compare the overall numbers of proteins and peptides recognized among patients with different clinical stages. Peptide-specific logistic regression testing for cancer-stage effects while controlling the false discovery rate (FDR) using the Benjamini-Hochberg (BH) method was also performed (online supplemental statistical section 2.4).

We reasoned that detectable antibody signatures between clinical groups may be present below the threshold of the stringent definition of a positive peptide. To test for such signals in the fluorescence intensity data, peptide-specific ANOVA according to the rank-based Kruskal-Wallis (KW) procedure was applied, followed by filtering peptides with significant clinical-group effects at 5% FDR by the BH method. Subject data were preprocessed to collapse triplicate profiles per person to a single, consensus profile per person by using median per peptide (online supplemental statistical section 2.5). The rank-based KW procedure is robust to distributional anomalies and is expected to provide a conservative assessment of antibody-profile differences between the clinical groups.[32] Peptides exhibiting sufficiently small BH-adjusted KW p value were examined for differences in various pairwise comparisons, which invoked both a median fold-change filter (at least twofold difference)

as well as a significance filter by two-sample Wilcoxon rank-sum p value, again with BH adjustment at 5% FDR (online supplemental statistical section 2.6).

Temporal changes

A linear mixed-effects model was fit to each peptide, separately for the groups of vaccinated patients and ADT-administered patients, to determine if there was an increase in signal over time, again using lme4; this allows a linear increase or decrease in mean log-transformed intensity over time per subject and per peptide. Patient-specific random effects allow for among subject variation in the temporal response, while a fixed time effect per peptide expresses the average response over subjects in that clinical group. Statistical significance was assessed using both the Kenward Roger and Satterthwaite approximate F tests[33] using the R package lmerTest[34] as well as BH for FDR control (online supplemental statistical section 3). Peptides with a coefficient of at least 0.3333 and a BH-adjusted p value <0.05 were considered to have increased antibody response over time.

Gene ontology analysis

Gene ontology (GO) analysis was performed using *allez*.[35] The set of all proteins on the microarray was used as the background list and the subset of proteins of interest was used as the target list, with a Bonferroni-corrected p value threshold of 0.05 in *allez*. The output was visualized using waterfall plots in *allez*. These reveal dominant functional categories enriched in the protein list while accounting for set redundancies.[36 37]

UniProt analysis

Proteins from the array were matched with UniProt IDs using UniGene IDs when available and protein names otherwise. Data were then retrieved from UniProt[38] on gene names, protein length and subcellular location. UniProt may designate a protein with multiple subcellular localizations, in which case all localizations were kept in the analysis. This sometimes leads to percentages that add up to over 100%.

RESULTS

A prostate cancer-specific peptide microarray was able to reproducibly measure antibody signatures from serum of healthy individuals and patients with prostate cancer

To characterize antibody responses to a wide variety of prostate cancer-associated proteins in patients with prostate cancer, we designed a peptide microarray able to be screened with patient sera. This array included peptides spanning the amino acid sequences of 1463 of the most abundantly expressed gene products in metastatic prostate cancer,[22 23] including 125 proteins identified in previous studies examining serum antibody responses in patients with prostate cancer.[24 39] We also included peptides spanning the predicted amino acid sequences of 148 potential open reading frames (ORFs) from
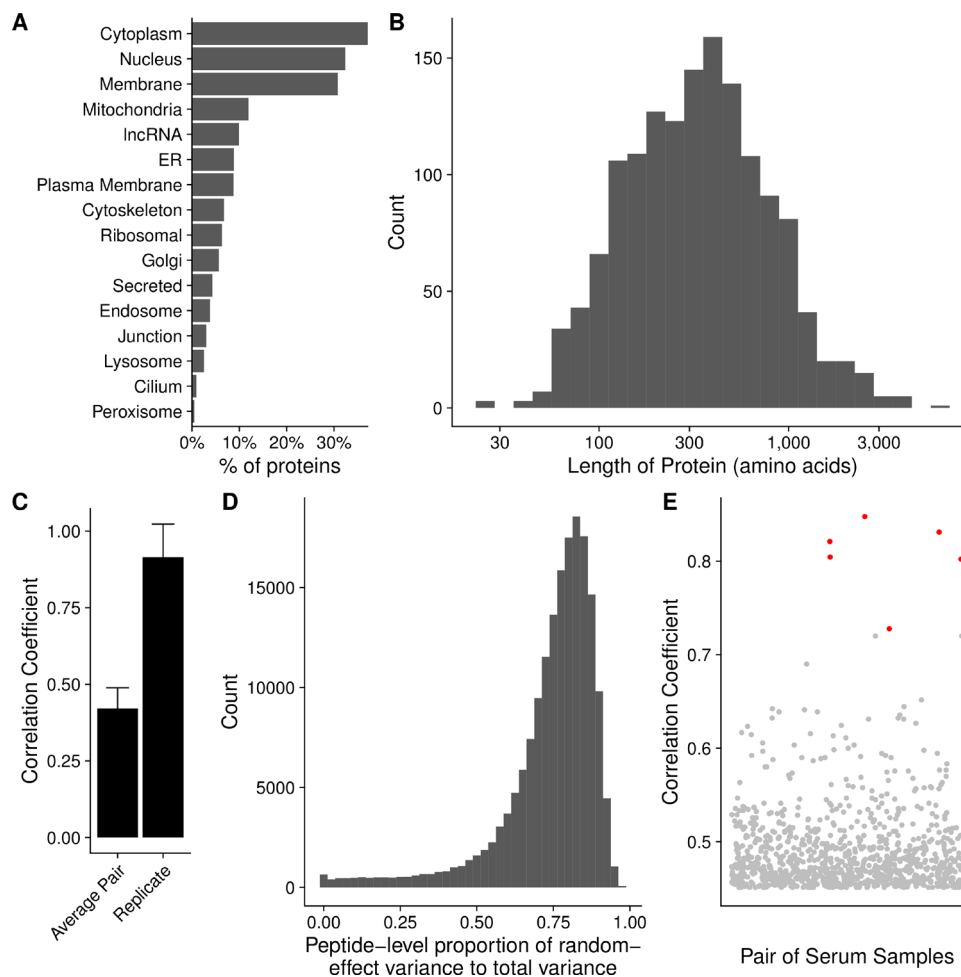
Figure 1 A prostate cancer-specific peptide microarray was able to reproducibly measure antibody signatures from serum of healthy individuals and patients with prostate cancer. Summary of the (A) subcellular localization and (B) length in amino acids of all 1611 unique proteins on the array according to UniProt. (C) The mean correlation coefficient among all pairs of different individuals (average pair) compared with the average correlation coefficient among all technical replicates (replicate). Error bars represent SD. (D) Histogram depicting the ratio of the biological variation to the total variation of the array data for each peptide as estimated by a linear mixed-effects model. (E) Each point represents the correlation coefficient between antibody responses in two different serum samples. Points marked in red are instances when the same individual had serum collected at two different time points with different stages of disease. ER, endoplasmic reticulum; lncRNA, long non-coding RNAs.

lncRNAs that have been shown to be highly expressed in prostate cancer. We included these given their strong association with prostate cancer. While most would likely serve as negative controls as they would not be expected to encode gene products, other groups have shown that some lncRNAs may be translated into unstable peptides or even functional proteins, especially with the dysregulation induced by cancer.[40–42] Hence, we reasoned that a few might serve as antibody targets in patients with prostate cancer.

The 16-mer peptides spanning the amino acid sequences of these 1611 gene products, and overlapping by 12 amino acids, were used to generate a microarray comprising 177 604 peptides. The complete list of probes and corresponding proteins is available in online supplemental table 1. The manufacture of the array and synthesis of peptides was performed as previously described.[43] The characteristics of the proteins included in the array are summarized in figure 1, using data retrieved from

UniProt.[38] Sixty-nine per cent of proteins included were those typically localized within the cytoplasm or nucleus, or that traffic between the two compartments (figure 1A). Approximately 6% of the proteins were localized to the ribosomes. The median protein length was 483 amino acids (figure 1B).

We next assayed serum samples collected from controls and patients with different stages of prostate cancer for peptide-specific IgG responses using the microarray. Examples of the primary data are shown in online supplemental figure 1A,B. To assess the reproducibility of the assay, we calculated Pearson's correlation coefficents between each pair of technical replicates and found high correlation on average among replicates (figure 1C). To determine the degree of variability among serum samples, we calculated the mean correlation coefficient across all pairs of distinct serum samples. We observed low correlation between the average pair of serum samples (figure 1C). In a complementary approach, we fit a linear
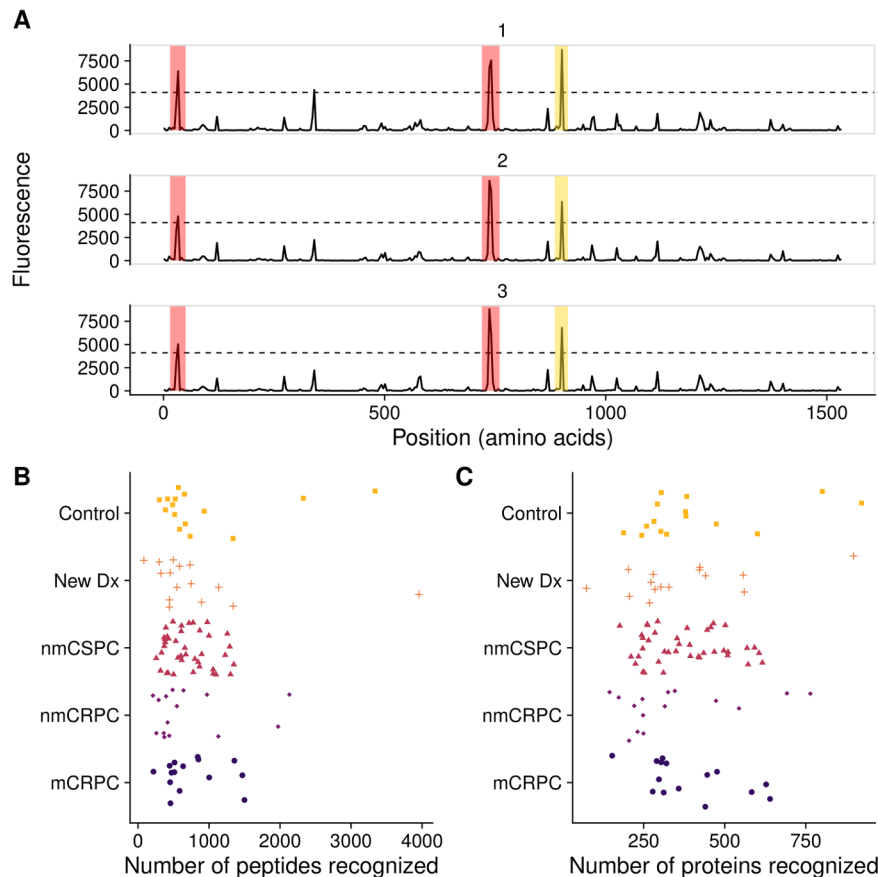
Figure 2 Frequency of protein recognition did not correlate with stage of disease. (A) Example microarray data for technical replicates of a single protein (ADT14) with the 2^{12} signal threshold indicated by the dashed line. Positive calls are marked in red. In yellow is a negative call that did not meet the sliding window criterion. The number of (B) peptides and (C) proteins recognized by each patient, categorized by clinical stage of disease. mCRPC, castration-resistant metastatic disease; nmCRPC, castration-resistant non-metastatic prostate cancer; nmCSPC, castration-sensitive non-metastatic prostate cancer.

mixed-effects model to estimate the amount of biological variation and technical variation across our triplicate data for each peptide. We found that the average ratio of biological variation to total variation was 0.74, indicating low technical variation (figure 1D).

Included in this study were six patients who had serum collected at two different time points, when they had an early stage of disease and again when they had a later stage of disease. Notably, these serum samples from the same patients had especially high correlation coefficients (figure 1E). This suggests that while there is high variation among individuals, each particular individual had smaller variation in his antibody repertoire over time. These six patients had their first serum collection removed from further analysis to prevent inflating their impact on our results.

Frequency of protein recognition did not correlate with stage of disease

To determine whether the array could detect IgG to common prostate antigens, we first defined a 'positive' antibody response to individual peptides using previously described criteria.[28] Using binding buffer as a negative control, no peptides met these criteria (not shown). Two examples of positive responses are shown in figure 2A.

We specifically evaluated responses to peptides derived from well-defined prostate target antigens PSA, PAP and the androgen receptor (AR). Overall, 7.1% of patients with prostate cancer (13.3% of patients with mCRPC) assayed on the array displayed antibody responses against peptides derived from PSA, while 6.7% of controls had PSA responses; 8.2% of patients with prostate cancer (13.3% of patients with mCRPC) and 0% of controls had responses to PAP. Finally, 5.9% of patients with prostate cancer (13.3% of patients with mCRPC) and 20.0% of controls recognized peptides derived from the ligand-binding domain of AR. Given the small sample sizes, none of the antibody responses to these proteins was significantly different in frequency in patients with cancer compared with controls.

We next tested the hypothesis that patients with higher disease burden would recognize more peptides, potentially due to increased presentation of cancer-associated proteins.[44] We found no correlation between stage of disease and the number of probes recognized at either the peptide level or the protein level. The median numbers of proteins recognized were 321 for controls, 303 for new Dx, 353 for nmCSPC, 249 for nmCRPC and 320 for mCRPC (figure 2B,C). The median numbers
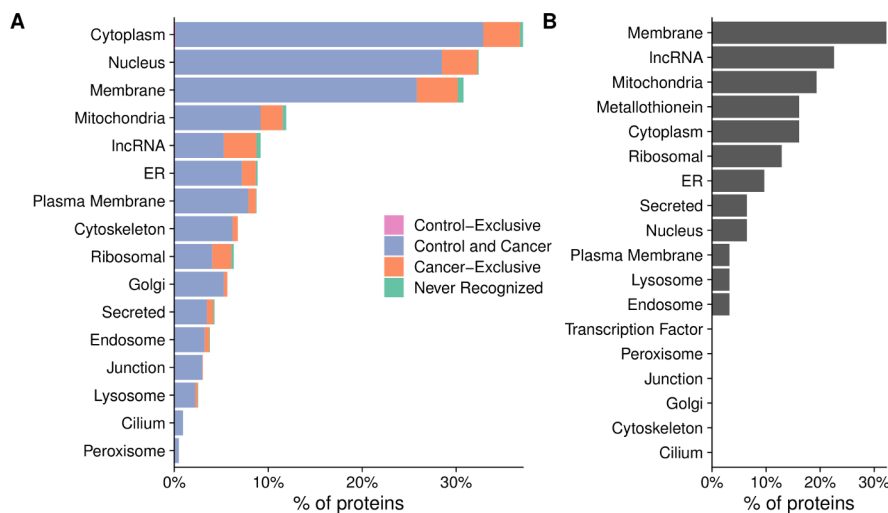
Figure 3 Nearly all proteins on the array were recognized by serum antibodies of patients with prostate cancer. Percentage of proteins that were recognized by only controls (*control-exclusive*), percentage of proteins recognized by at least one control and one cancer patient (*control and cancer*), percentage of proteins not recognized by any controls but recognized by at least one cancer patient (*cancer-exclusive*) and percentage not recognized at all (*never recognized*), categorized by subcellular localization. (B) Characteristics of the proteins that were not recognized by any controls or patients tested. The x-axis represents the percentage of the 41 proteins that were not recognized that fall into each category.

of peptides were 919 for controls, 832 for new Dx, 712 for nmCSPC, 708 for nmCRPC and 754 for mCRPC. We noted a substantial amount of heterogeneity in antibody responses among patients. For instance, the number of proteins recognized by controls ranged from 188 to 922. Similarly, we did not observe an association between subject age and number of proteins recognized (data not shown).

Nearly all proteins on the array were recognized by serum antibodies of patients with prostate cancer
Having established that there was a large diversity in antibody repertoires among patients, we next examined whether there were any broad trends in the types of proteins that were recognized. While only 0.4% of calls were positive overall, 20% of peptides were recognized by at least one subject. Nearly all proteins (1570 of 1611, 97%) had one or more peptides recognized by at least one subject. Conversely, there were no proteins that were recognized by all patients. Most proteins (1326 of 1611, 82%) were recognized by both controls and patients with cancer (figure 3A). As expected, one of the largest categories of proteins that were not recognized were ORFs from lncRNAs (figure 3B, online supplemental table 2); however, contrary to our expectations, the majority of lncRNAs (141 of 148, 95%) were recognized by at least one patient (figure 3A).

The composition of antibody targets changes with clinical stage of disease
We hypothesized that while the overall number of proteins recognized may not increase with burden of disease, the composition of proteins recognized may be different. We employed a KW test to identify peptides that had significantly different fluorescence intensities across clinical stages and controls. This test identified 13 279

significant peptides (online supplemental table 3). We used principal component analysis (PCA) to visualize the residual fluorescence levels after subtracting the grand mean fluorescence level for each peptide and observed that patients tended to group with other patients with the same clinical stage of disease (figure 4A). Patients with castration-resistant tumors, and mCRPC in particular, tended to cluster especially closely to one another. Notably, controls did not exhibit this clustering. We were particularly interested in the subset of peptides that had significantly different fluorescence signals in patients with cancer compared with controls. We identified these peptides by using a Wilcoxon rank-sum test and specifically focused on those that had differences in median fluorescence of at least twofold in patients with cancer compared with controls (figure 4B, left; online supplemental table 4). To discover which peptides were driving the especially strong clustering of patients with mCRPC, we repeated this procedure to find peptides with significantly different fluorescence in patients with mCRPC compared with all other patients (figure 5B, right; online supplemental table 5). Unexpectedly, we detected only 110 peptides associated with the cancer versus control comparison, but found 4246 peptides in the mCRPC versus all other comparisons.

We applied this same approach to identify the number of peptides that had significantly higher or lower signals in patients in one clinical stage of disease compared with patients in the previous clinical stage. The largest change in number of recognized peptides occurred between the castration-sensitive (nmCSPC) and castration-resistant (nmCRPC) populations (figure 4C; online supplemental tables 6–9). Examples of the fluorescence signals of peptides that are detected by this strategy are shown in figure 4D,E.
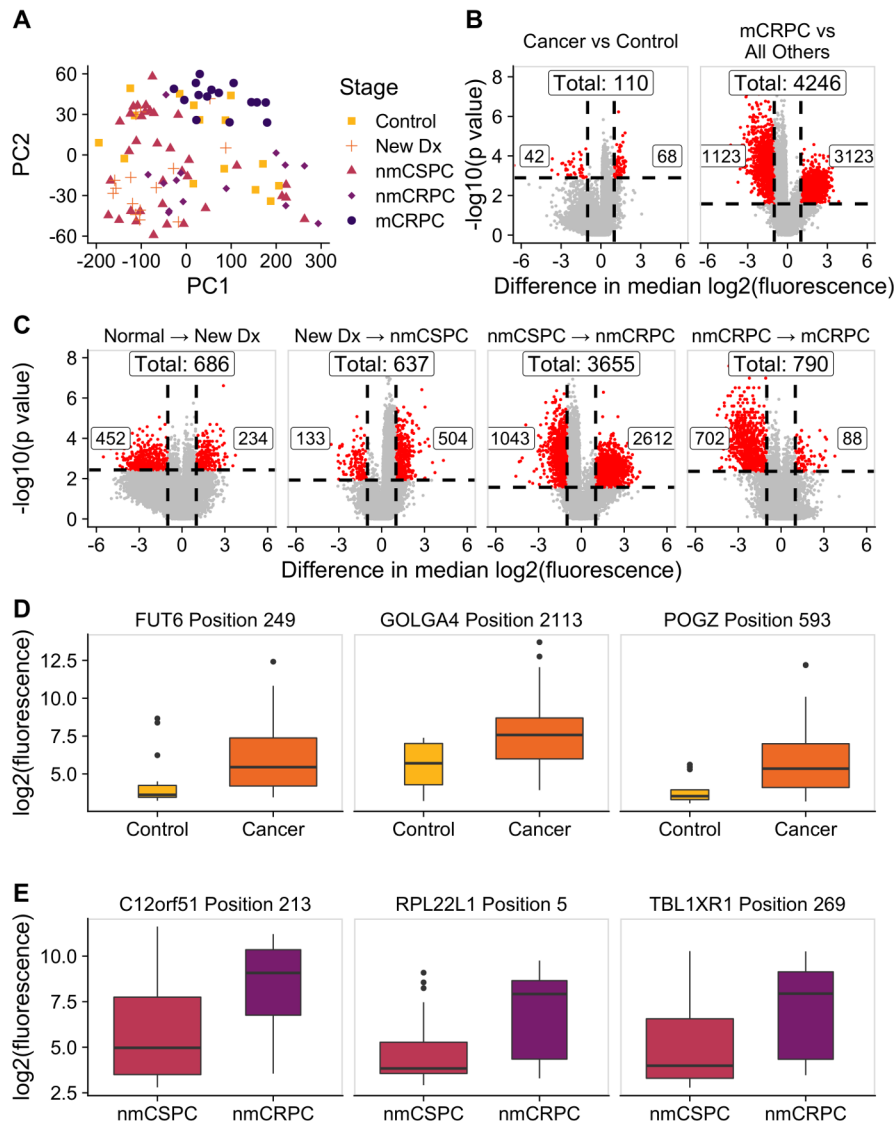
Figure 4 The composition of antibody targets changes with clinical stage of disease. (A) Principal component analysis plot obtained by using the set of 13 279 significantly changed peptides identified by the Kruskal-Wallis test then subtracting the grand mean of log2 fluorescence levels across patients for each peptide. Each point represents a patient, colored by clinical stage. (B) Volcano plots depicting peptides that met the 5% Benjamini-Hochberg (BH) false discovery rate (FDR) cut-off based on the Wilcoxon p values (horizontal lines) and had at least a twofold difference in median log2 fluorescence values between the stages being compared (vertical lines). The number of significantly increased peptides is shown on the right of each plot, the number of significantly decreased peptides is shown on the left, and the overall number of significantly changed peptides is shown at the top. Significant peptides are colored red. The left plot indicates peptides that had significantly different signals in patients with cancer compared with controls. The right plot indicates peptides that had significantly different signals in patients with mCRPC compared with all other groups. (C) Volcano plots indicating peptides that had significantly different signals between patients with consecutive clinical stages of disease. Box plots displaying fluorescence signals in (D) all patients with cancer compared with controls and (E) patients with nmCRPC compared with patients with nmCSPC in three example peptides that met both the twofold signal change and BH-adjusted p-value criteria. Box width is proportional to sample size. mCRPC, castration-resistant metastatic disease; nmCRPC, castration-resistant non-metastatic prostate cancer; nmCSPC, castration-sensitive non-metastatic prostate cancer.

Specific proteins were preferentially recognized in patients with cancer and patients with mCRPC

From our initial list of 13,279 peptides, we identified 6708 of these peptides that were significant in one of the six comparisons made in figure 4B,C. We visualized the residual fluorescence levels of these peptides after removing the grand mean for each peptide in figure 5A. As in figure 4A, we observed high similarity in antibody profiles between patients with the same stage of disease. We next more closely examined the sets of proteins we had identified earlier for common features and associations with cellular processes. GO analysis revealed that the genes corresponding to the 68 peptides that were recognized more robustly in patients with cancer compared with controls were associated with mRNA export from the nucleus and the cell-cell contact zone (figure 5B).
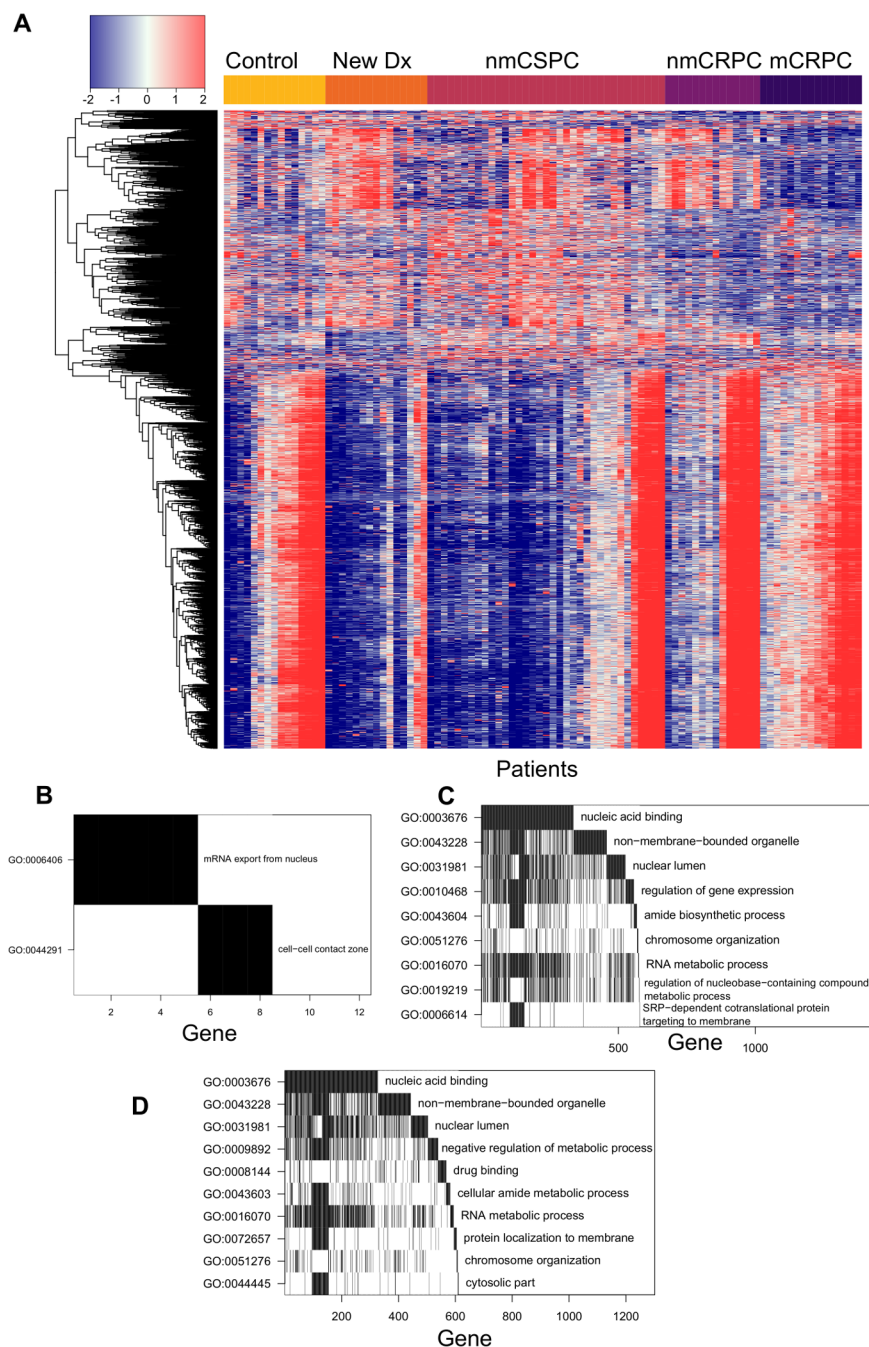
Figure 5 Specific proteins were preferentially recognized in patients with cancer and patients with mCRPC. (A) Heatmap depicting the difference in log2 fluorescence levels between each peptide in each patient and its grand mean across patients, displaying only the set of 6708 peptides that met the secondary selection criteria. Patients are grouped by stage across the x-axis, while peptides are clustered along the y-axis. (B) Waterfall plot depicting a gene ontology (GO) analysis of proteins that had significantly more antibody recognition in patients with cancer than controls. The top row indicates the GO term that encompasses the most genes corresponding to significant peptides. For the second row, these genes are then removed from the list and the GO term that encompasses the most genes in the remainder of the list is chosen. Genes identified by this process are counted along the x-axis to visualize overlapping GO terms. Waterfall plots depicting GO analysis of proteins that had significantly increased antibody responses in (C) patients with mCRPC compared with all other patients or (D) patients with nmCRPC compared with patients with nmCSPC. mCRPC, castration-resistant metastatic disease; nmCRPC, castration-resistant non-metastatic prostate cancer; nmCSPC, castration-sensitive non-metastatic prostate cancer.

GO analysis of the 3123 peptides that had particularly strong antibody responses in patients with mCRPC showed an enrichment for proteins associated with nucleic acid binding, RNA metabolism, gene regulation and downregulation of metabolism (figure 5C). One of the significant terms within the 'non-membrane-bounded organelle' term was the cytosolic large ribosomal subunit. To investigate the large difference in

Figure 6 Antitumor vaccination elicited increased antibody responses over time, unlike androgen deprivation therapy (ADT). (A) The mean correlation coefficient among all pairs of different individuals (*average pair*) compared with the average correlation coefficient among all technical replicates (*replicate*) and the average correlation among samples collected from the same patient at different time points (*same patient*). Error bars represent SD. (B) Volcano plots depicting peptides to which there was increased signal following treatment with ADT or vaccine by at least twofold every 3 months, corresponding to a coefficient of time fixed-effect of 0.3333 (vertical line), and met the 5% Benjamini-Hochberg (BH) false discovery rate (FDR) cut-off using both Kenward Roger (KR) and Satterthwaite F-tests. Significant peptides are colored red. (C) Example box plots displaying log2 fluorescence levels for three peptides at baseline, 3 months and 6 months, in patients treated with ADT or vaccine. PAP, prostatic acid phosphatase.

antibody repertoires between patients with nmCSPC and nmCRPC, we performed GO analysis on the 2612 peptides with significantly higher signal in nmCRPC than nmCSPC. We identified differences in recognition of proteins associated with nucleic acid binding, chromatin structure, amide metabolism and protein localization to the membrane (figure 5D).
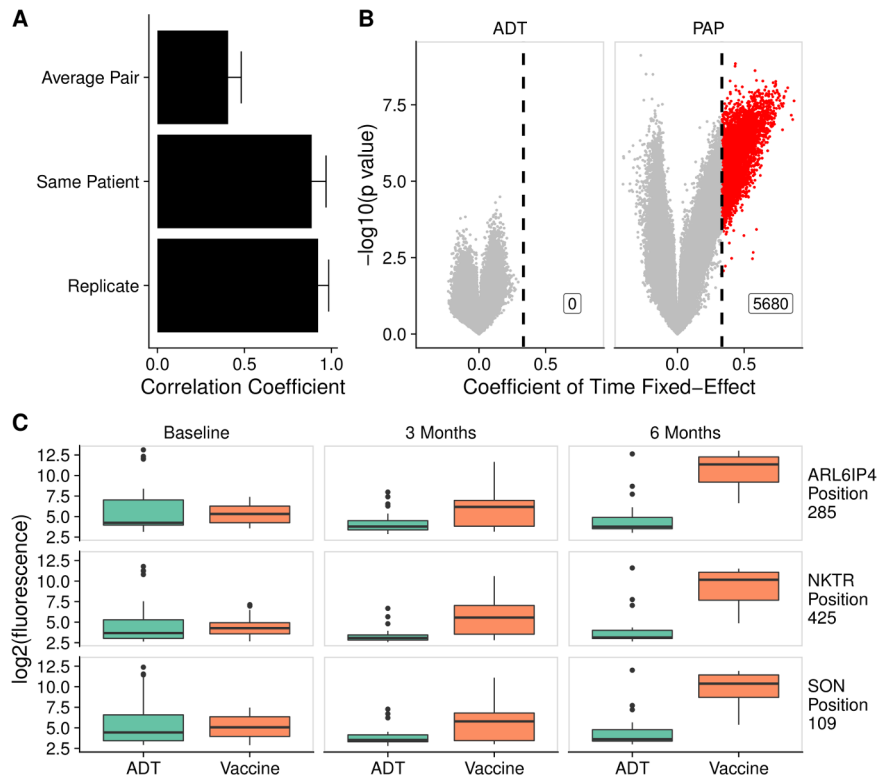
Antitumor vaccination elicited increased antibody responses over time, unlike androgen deprivation therapy

Based on our finding that individual patients tended to have relatively small variation in their antibody responses over time, we hypothesized that this could make the microarray particularly sensitive for detecting changes induced by treatment in a longitudinal analysis. To test the potential of this platform for studying treatment effects, we used the serial serum samples available from the 40 patients with nmCSPC who were treated with either ADT or an investigational DNA vaccine. Consistent with our observations in figure 1E, we found high correlation between samples from an individual patient over time (figure 6A).

We next fit a linear mixed-effects model to determine if there were any peptides against which there was increased signal over time. In the vaccine-treated patients, we found 5680 significant peptides that had a coefficient of time fixed-effect of at least 0.3333, indicating a twofold increase in signal every 3 months (online supplemental table 10). We were unable to detect any peptides against which ADT-treated patients developed increasing antibody signal over time using this procedure (figure 6B). Examples of the fluorescence levels of 3 peptides over time in ADT-treated and vaccine-treated patients are shown in figure 6C.

PAP-targeted DNA vaccination causes similar increases in antibodies against proteins associated with nucleic acid binding and gene regulation in multiple patients

We visualized the changes in peptide recognition over time in vaccine-treated patients by plotting the residuals of the null model in the heatmap in figure 7A. This further demonstrated that vaccine-treated patients had robust increases in antibody responses to these 5680 peptides. To characterize these peptides, we performed GO analysis. We found that a significantly enriched set of these antibodies were specific to nucleic acid binding proteins. There were also more antibodies against proteins associated with RNA metabolism, ion binding and ribosomal or
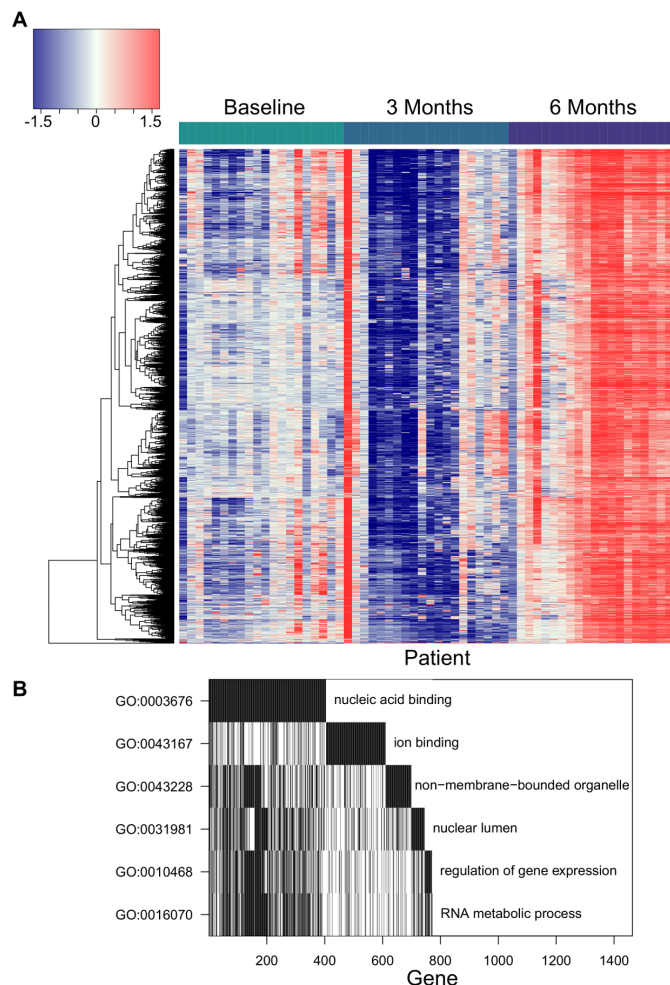
Figure 7 Prostatic acid phosphatase (PAP)-targeted DNA vaccination causes similar increases in antibodies against proteins associated with nucleic acid binding and gene regulation in multiple patients. (A) Heatmap of the fluorescence residuals from the null model for each of the 5680 peptides that were significantly increased in vaccine-treated patients. Samples from vaccine-treated patients at each collection time point (baseline, 3 months and 6 months) are grouped together along the x-axis, while peptides are clustered along the y-axis. The order of the columns (patients) is consistent across the three timepoints for ease of comparison. (B) Waterfall plot of gene ontology (GO) analysis of proteins recognized more following vaccine.

nucleolar cellular components than would be expected by chance (figure 7B).

DISCUSSION

The purpose of this study was to perform a comprehensive survey of tumor-associated serum antibody responses in patients with prostate cancer and to determine whether antibody profiles changed with disease progression. Previous examinations of serum antibodies in patients with prostate cancer focused mainly on diagnostic applications; thus, a more complete picture of patient antibody repertoires has been lacking. We addressed this by designing the largest reported prostate cancer-specific peptide microarray, capable of measuring IgG responses to over 177,000 peptides. Our major findings were (1) the microarray data were highly reproducible, (2) the overall number of peptides recognized was not greater in patients with more advanced disease, (3) the composition of patient antibody repertoires changed with later stages of disease, (4) most antibody signatures were largely stable within individuals over time and (5) this approach was able to track changes elicited by therapy in individuals.

Here, we have shown that this novel prostate cancer-specific peptide microarray yields highly reproducible measurements of serum IgG levels with high correlation of technical replicates and negligible background fluorescence signal. The microarray's measurements also exhibited generally strong concordance with existing literature on serum antibodies in patients with prostate cancer. A previous study using ELISA detected anti-PSA antibodies in 11% of patients with mCRPC.[44] Similarly, the microarray detected PSA responses in 13.3% of patients with mCRPC. Looking at PAP, ELISA detected antibody responses in 5.5% of patients, while the microarray detected antibody responses in 8.2% of patients with prostate cancer. On the other hand, ELISA detected antibodies specific for the AR ligand-binding domain in 17.1% of patients, whereas the microarray detected antibody responses in 5.9% of patients.[45]

Based on reports that individual proteins like PSA and PAP are more recognized in patients than controls, we hypothesized that patients with more advanced disease would have antibodies against more proteins. Previous studies have focused on the use of antibody profiling as a diagnostic tool to discover proteins that are recognized more in patients with prostate cancer than controls.[7 15 16] Because these studies focused only on antibodies that are enriched in patients with prostate cancer, they were unable to address this question of whether the overall number of antibody responses changes with clinical stage of disease. Our microarray approach also allowed us to examine the classes of proteins recognized by patients in each clinical stage.

Contrary to our expectations, we did not observe an increase in the number of peptides recognized with more advanced disease. While the overall number of antibody responses did not appear to increase, we found that the composition of proteins recognized changed. Interestingly, we discovered that the vast majority of predicted lncRNA ORF gene products were recognized by at least one subject, with a large proportion recognized exclusively in patients with cancer. This could be the result of unstable peptides being translated from lncRNAs at higher rates due to the dysregulation induced by prostate cancer. Alternatively, it is possible that some of these genes with predicted ORFs represented poorly annotated protein coding genes rather than true lncRNAs. We found significant changes in antibody responses against one of the lncRNAs, PCAT-14 (PRCAT104), in the transition to castration-resistant disease and non-metastatic to metastatic disease, but not in earlier stage

transitions. PCAT-14-specific antibodies also increased following vaccination. Interestingly, previous work has shown that PCAT-14 encodes a peptide and that loss of PCAT-14 is associated with metastatic progression and poor outcomes.[46–48] Further study of serum antibodies targeting this lncRNA is warranted.

We also found that the sets of proteins associated with patients with mCRPC and the transition from nmCSPC to nmCRPC were significantly enriched for ribosomal proteins and other non-membrane bound organelles. It is possible that the upregulation of the translational machinery required to support rapid cell division in cancer leads to a greater abundance in ribosomal proteins. This lends further credence to observations made by Wang *et al* that two of the five coding proteins they identified in their screen for prostate cancer-specific antibodies were ribosomal and the majority of the other proteins they identified came from untranslated regions.[7] In fact, we identified many of the same proteins when looking at mCRPC-associated proteins, such as BRD2, RPL13a, RPL22 and LAMR1. We also identified proteins detected by Taylor *et al*, and Ummanni *et al*, such as ACPP, VCP and PRDX6.[15 16] The increases in antibodies against proteins involved in gene regulation and RNA metabolism in patients with nmCRPC and mCRPC may be due to the large changes in transcription associated with the development of castration resistance.[49]

Despite the power of this approach, we were limited to observing antibody responses to 1611 proteins that are all highly expressed in prostate cancer and it is possible that there are humoral responses to other targets that may be expressed at lower levels that we did not capture. Our analysis was also limited by our relatively small sera sample size, with only 15 patients for most disease stages, including mCRPC. However, the fact that we were able to detect such large differences between disease stages with this sample size demonstrates the sensitivity of this approach. This sample size was sufficient to detect large changes in the antibody signatures in patients with castration-sensitive versus castration-resistant disease. These small sample sizes, however, limited any clinical interpretation or association of antibody signatures with long-term outcome, and these will be focuses of future study. We took a cross-sectional approach to identifying antibody profiles associated with each stage of disease rather than following individual patients across the lengthy natural history of prostate cancer, which also prevented us from observing changes in individual patients with different stages of disease. However, we were able to obtain longitudinal data from a subset of patients for a period of 6 months.

Our longitudinal analysis with sample collections at baseline, 3 months and 6 months revealed that it is possible to identify individual subjects at multiple time points based on their antibody signature. Others have demonstrated that healthy individuals have largely unchanged responses over time to a panel of self-antigens,[50 51] although we are, to our knowledge, the first to observe this phenomenon with an array of this size and the first to study it in the setting of prostate cancer. Despite this individual signature, we did observe common recognized proteins among patients with the same clinical stage of disease. Due to the lack of large random fluctuations in antibody responses over time, this platform appears particularly suited to identifying changes in individuals over time induced by disease or treatment. This demonstrates the potential value of this platform for future more extensive studies specifically evaluating antigen spread, to determine whether the development of antibody responses is associated with clinical outcome, and contrasting the effects of different immunotherapies on patient antibody repertoires.

Most strikingly, we have shown that treatments can modulate a patient's antibody repertoire, at least during a 6-month study period. We found that antigen-specific vaccination elicited greater increases in off-target antibody responses over time than did traditional targeted therapy, showing that this may be a method of quantifying antigen spread caused by treatment. Our data are consistent with previous findings examining antibody responses following treatment with Sipuleucel-T, but we were able to study a greater number of prostate cancer-associated peptides and compare the effects of immunotherapy with the effects of ADT.[14] These specific proteins to which patients receiving the PAP vaccine developed increasing responses may be useful as biomarkers of response to therapy. Interestingly, we did not identify any proteins to which patients receiving ADT developed increasing responses, in contrast to findings in our previous work.[18] It is possible that changes in antibody responses in ADT-treated patients were too low in magnitude to meet our selection criteria. These data suggest that ADT itself is not driving the majority of the dramatic differences in antibody profiles between patients with nmCSPC to nmCRPC. Rather, it may be a direct consequence of changes in the biology of the tumor and gene expression that occur during the development of castration resistance. Future studies will use this platform to identify antibody signature changes that are specific for various types of immunotherapies and quantifying the number and nature of antigens recognized following therapy. In particular, we are interested in studying in detail the associations between antibody responses and clinical outcomes, as we hypothesize that induction of antibodies to larger numbers of antigens, and potentially certain types of antigens, may lead to improved clinical outcomes such as prolonged progression-free survival and overall survival.

Disclaimer The content is solely the responsibility of the authors and does not necessarily represent the official views of the National Institutes of Health.

Competing interests DGM has ownership interest, has received research support and serves as consultant to Madison Vaccines, which has licensed intellectual property related to this content.

Patient consent for publication Not required.

Ethics approval Study protocols that permitted collection and use of human blood samples were reviewed and approved the University of Wisconsin Human Subjects' Review Board (IRB). All patients gave written informed consent for use of blood products for research.

Provenance and peer review Not commissioned; externally peer reviewed.

Data availability statement Data are available in a public, open access repository. Data are available on reasonable request. All data relevant to the study are included in the article or uploaded as supplementary information. Workflow details are supplied in an R markdown document and the rendered Statistical Supplement. These materials are also available at: https://github.com/wiscstatman/immunostat-prostate.

Supplemental material This content has been supplied by the author(s). It has not been vetted by BMJ Publishing Group Limited (BMJ) and may not have been peer-reviewed. Any opinions or recommendations discussed are solely those of the author(s) and are not endorsed by BMJ. BMJ disclaims all liability and responsibility arising from any reliance placed on the content. Where the content includes any translated material, BMJ does not warrant the accuracy and reliability of the translations (including but not limited to local regulations, clinical guidelines, terminology, drug names and drug dosages), and is not responsible for any error and/or omissions arising from translation and adaptation or otherwise.

ORCID iD
Douglas G McNeel http://orcid.org/0000-0003-1471-6723

REFERENCES

1 von Kleist S, Burtin P. On the specificity of autoantibodies present in colon cancer patients. *Immunology* 1966;10:507–15.
2 Gold JM, Freedman SO, Gold P. Human anti-CEA antibodies detected by radioimmunoelectrophoresis. *Nat New Biol* 1972;239:60–2.
3 Scanlan MJ, Chen YT, Williamson B, *et al*. Characterization of human colon cancer antigens recognized by autologous antibodies. *Int J Cancer* 1998;76:652–8.
4 Cai X, Garen A. Anti-Melanoma antibodies from melanoma patients immunized with genetically modified autologous tumor cells: selection of specific antibodies from single-chain Fv fusion phage libraries. *Proc Natl Acad Sci U S A* 1995;92:6537–41.
5 Grossman HB, Wedemeyer G, Stein J. Autologous antibodies to human bladder cancer. *Cancer Immunol Immunother* 1988;26:269-72.
6 Atakan S, Bayiz H, Sak S, *et al*. Autologous anti-SOX2 antibody responses reflect intensity but not frequency of antigen expression in small cell lung cancer. *BMC Clin Pathol* 2014;14:24.
7 Wang X, Yu J, Sreekumar A, *et al*. Autoantibody signatures in prostate cancer. *N Engl J Med* 2005;353:1224–35. doi:10.1056/NEJMoa051931
8 Zaenker P, Gray ES, Ziman MR. Autoantibody Production in Cancer--The Humoral Immune Response toward Autologous Antigens in Cancer Patients. *Autoimmun Rev* 2016;15:477–83.
9 Wandall HH, Blixt O, Tarp MA, *et al*. Cancer biomarkers defined by autoantibody signatures to aberrant O-glycopeptide epitopes. *Cancer Res* 2010;70:1306–13.
10 Wahrenbrock MG, Varki A. Multiple hepatic receptors cooperate to eliminate secretory mucins aberrantly entering the bloodstream:

11 are circulating cancer mucins the "tip of the iceberg"? *Cancer Res* 2006;66:2433–41.
11 Olson BM, McNeel DG, Antibody MDG. Antibody and T-cell responses specific for the androgen receptor in patients with prostate cancer. *Prostate* 2007;67:1729–39.
12 Silva WA, Gnjatic S, Ritter E, *et al*. Plac1, a trophoblast-specific cell surface protein, is expressed in a range of human tumors and elicits spontaneous antibody responses. *Cancer Immun* 2007;7:18.
13 Chen YT, Scanlan MJ, Sahin U, *et al*. A testicular antigen aberrantly expressed in human cancers detected by autologous antibody screening. *Proc Natl Acad Sci U S A* 1997;94:1914–8.
14 GuhaThakurta D, Sheikh NA, Fan L-Q, *et al*. Humoral immune response against nontargeted tumor antigens after treatment with Sipuleucel-T and its association with improved clinical outcome. *Clin Cancer Res* 2015;21:3619–30.
15 Taylor BS, Pal M, Yu J, *et al*. Humoral response profiling reveals pathways to prostate cancer progression. *Mol Cell Proteomics* 2008;7:600–11.
16 Ummanni R, Duscharla D, Barett C, *et al*. Prostate cancer-associated autoantibodies in serum against tumor-associated antigens as potential new biomarkers. *J Proteomics* 2015;119:218–29.
17 Smith HA, Maricque BB, Eberhardt J, *et al*. Igg responses to tissue-associated antigens as biomarkers of immunological treatment efficacy. *Journal of Biomedicine and Biotechnology* 2011;2011:1–10.
18 Morse MD, McNeel DG. Prostate cancer patients on androgen deprivation therapy develop persistent changes in adaptive immune responses. *Hum Immunol* 2010;71:496–504.
19 Dunphy EJ, Eickhoff JC, Muller CH, *et al*. Identification of antigen-specific IgG in sera from patients with chronic prostatitis. *J Clin Immunol* 2004;24:492–502.
20 Lang JM, Wallace M, Becker JT, *et al*. A randomized phase II trial evaluating different schedules of zoledronic acid on bone mineral density in patients with prostate cancer beginning androgen deprivation therapy. *Clin Genitourin Cancer* 2013;11:407–15.
21 McNeel DG, Dunphy EJ, Davies JG, *et al*. Safety and immunological efficacy of a DNA vaccine encoding prostatic acid phosphatase in patients with stage D0 prostate cancer. *J Clin Oncol* 2009;27:4047–54.
22 Robinson D, Van Allen EM, Wu Y-M, *et al*. Integrative clinical genomics of advanced prostate cancer. *Cell* 2015;162:454.
23 Kumar A, Coleman I, Morrissey C, *et al*. Substantial interindividual and limited intraindividual genomic diversity among tumors from men with metastatic prostate cancer. *Nat Med* 2016;22:369–78.
24 Maricque BB, Eickhoff JC, McNeel DG. Antibody responses to prostate-associated antigens in patients with prostatitis and prostate cancer. *Prostate* 2011;71:134–46.
25 Iyer MK, Niknafs YS, Malik R, *et al*. The landscape of long noncoding RNAs in the human transcriptome. *Nat Genet* 2015;47:199–208.
26 Cabili MN, Trapnell C, Goff L, *et al*. Integrative annotation of human large intergenic noncoding RNAs reveals global properties and specific subclasses. *Genes Dev* 2011;25:1915–27.
27 Mishra N, Caciula A, Price A, *et al*. Diagnosis of Zika virus infection by peptide array and enzyme-linked immunosorbent assay. *mBio* 2018;9. doi:10.1128/mBio.00095-18. [Epub ahead of print: 06 Mar 2018].
28 Lo KC, Sullivan E, Bannen RM, *et al*. Comprehensive profiling of the rheumatoid arthritis antibody repertoire. *Arthritis Rheumatol* 2020;72:242–50.
29 R Core Team. *R: a language and environment for statistical computing*. Vienna, Austria: R Foundation for Statistical Computing, 2019. https://www.R-project.org/
30 RStudio Team. *RStudio: integrated development environment for R*. Boston, MA: RStudio, Inc, 2019. http://www.rstudio.com/
31 Bates D, Mächler M, Bolker B, *et al*. Fitting Linear Mixed-Effects Models Using lme4. *J Stat Softw* 2015;67:1–48.
32 McDonald JH. *Handbook of biological statistics*. Baltimore, Maryland: Sparky House Publishing, 2014: 157–64.
33 Luke SG. Evaluating significance in linear mixed-effects models in R. *Behav Res Methods* 2017;49:1494–502.
34 Kuznetsova A, Brockhoff PB, Christensen RHB. lmerTest Package: Tests in Linear Mixed Effects Models. *J Stat Softw* 2017;82:1–26.
35 Newton MA, Quintana FA, den Boon JA, *et al*. Random-set methods identify distinct aspects of the enrichment signal in gene-set analysis. *Ann Appl Stat* 2007;1:85–106.
36 Hao L, He Q, Wang Z, *et al*. Limited agreement of independent RNAi screens for virus-required host genes owes more to false-negative than false-positive factors. *PLoS Comput Biol* 2013;9:e1003235.
37 Pleiman JK, Irving AA, Wang Z, *et al*. The conserved protective cyclic AMP-phosphodiesterase function PDE4B is expressed in the adenoma and adjacent normal colonic epithelium of mammals and silenced in colorectal cancer. *PLoS Genet* 2018;14:e1007611.

38 UniProt Consortium. UniProt: a worldwide hub of protein knowledge. *Nucleic Acids Res* 2019;47:D506–15.

39 Smith HA, Maricque BB, Eberhardt J, *et al*. Igg responses to tissue-associated antigens as biomarkers of immunological treatment efficacy. *J Biomed Biotechnol* 2011;2011:1–10.

40 Guo Z-W, Meng Y, Zhai X-M, *et al*. Translated long non-coding ribonucleic acid ZFAS1 promotes cancer cell migration by elevating reactive oxygen species production in hepatocellular carcinoma. *Front Genet* 2019;10:1111.

41 Ji Z, Song R, Regev A, *et al*. Many lncRNAs, 5'UTRs, and pseudogenes are translated and some are likely to express functional proteins. *eLife* 2015;4.

42 Ingolia NT, Lareau LF, Weissman JS. Ribosome profiling of mouse embryonic stem cells reveals the complexity and dynamics of mammalian proteomes. *Cell* 2011;147:789–802.

43 Yan Y, Sun N, Wang H, *et al*. Whole Genome-Derived Tiled peptide arrays detect prediagnostic autoantibody signatures in non-small-cell lung cancer. *Cancer Res* 2019;79:1549–57.

44 McNeel DG, Nguyen LD, Storer BE, *et al*. Antibody immunity to prostate cancer associated antigens can be detected in the serum of patients with prostate cancer. *J Urol* 2000;164:1825–9.

45 Olson BM, McNeel DG, Antibody MDG. Antibody and T-cell responses specific for the androgen receptor in patients with prostate cancer. *Prostate* 2007;67:1729–39.

46 White NM, Zhao SG, Zhang J, *et al*. Multi-Institutional analysis shows that low PCAT-14 expression associates with poor outcomes in prostate cancer. *Eur Urol* 2017;71:257–66.

47 Zhao SG, Chen WS, Li H, *et al*. The DNA methylation landscape of advanced prostate cancer. *Nat Genet* 2020;52:778–89.

48 Sayanjali. Genome-Wide transcriptome analysis of prostate cancer tissue identified overexpression of specific members of the human endogenous retrovirus-K family. Available: http://www.cancertm.com/article.asp?issn=2395-3977;year=2017;volume=3;issue=1;spage=1;epage=12;aulast=Sayanjali [Accessed 28 Jul 2020].

49 Toropainen S, Niskanen EA, Malinen M, *et al*. Global analysis of transcription in castration-resistant prostate cancer cells uncovers active enhancers and direct androgen receptor targets. *Sci Rep* 2016;6:33510.

50 Francoeur A-M. Antibody fingerprinting: a novel method for identifying individual people and animals. *Nat Biotechnol* 1988;6:822–5.

51 Neiman M, Hellström C, Just D, *et al*. Individual and stable autoantibody repertoires in healthy individuals. *Autoimmunity* 2019;52:1–11.

Vaccine-Increased

Seq ID	Unigene ID	Uniprot ID	Gene Names
1_HSPA1A_3303	Hs.274402	P0DMV8	HSPA1A HSP72 HSPA1 HSX70
100_AKAP17A_8227	Hs.522572	Q02040	AKAP17A CXYorf3 DXYS155E SFRS17A XE7
1000_H2AFY_9555	Hs.420272	O75367	H2AFY MACROH2A1
1001_ITPK1_3705	Hs.308122	Q13572	ITPK1
1002_PTPN11_5781	Hs.506852	Q06124	PTPN11 PTP2C SHPTP2
1003_EIF3J_8669	Hs.404056	O75822	EIF3J EIF3S1 PRO0391
1004_TRIP12_9320	Hs.591633	Q14669	TRIP12 KIAA0045 ULF
1006_YEATS2_55689	Hs.632575	Q9ULM3	YEATS2 KIAA1197
1007_SEL1L3_23231	Hs.479384	Q68CR1	SEL1L3 KIAA0746
1008_IDH1_3417	Hs.593422	O75874	IDH1 PICD
101_HSPH1_10808	Hs.36927	Q92598	HSPH1 HSP105 HSP110 KIAA0201
1010_LDLR_3949	Hs.213289	P01130	LDLR
1011_FAM129B_64855	Hs.522401	Q96TA1	NIBAN2 C9orf88 FAM129B
1012_MAP3K5_4217	Hs.186486	Q99683	MAP3K5 ASK1 MAPKKK5 MEKK5
1013_NEFH_4744	Hs.198760	P12036	NEFH KIAA0845 NFH
1014_RAP1B_5908	Hs.369920	P61224	RAP1B OK/SW-cl.11
1015_MCCC1_56922	Hs.47649	Q96RQ3	MCCC1 MCCA
1017_MT1E_4493	Hs.534330	P04732	MT1E
1022_TXNDC5_81567	Hs.150837	Q8NBS9	TXNDC5 TLP46 UNQ364/PRO700
1023_STRA13_201254	Hs.37616	O14503	BHLHE40 BHLHB2 DEC1 SHARP2 STRA13
1024_NPEPPS_9520	Hs.443837	P55786	NPEPPS PSA
1025_YIPF6_286451	Hs.82719	Q96EC8	YIPF6
1026_CLIP1_6249	Hs.524809	P30622	CLIP1 CYLN1 RSN
1027_SRSF7_6432	Hs.309090	Q16629	SRSF7 SFRS7
103_RPS25_6230	Hs.512676	P62851	RPS25
1031_SOCS7_30837	Hs.514132	O14512	SOCS7 NAP4 SOCS6
1032_C1orf9_51430	Hs.626306	Q9UBS9	SUCO C1orf9 CH1 OPT SLP1
1034_OCIAD2_132299	Hs.95835	Q56VL3	OCIAD2
1035_RAB35_11021	Hs.524788	Q15286	RAB35 RAB1C RAY
1036_WWC1_23286	Hs.484047	Q8IX03	WWC1 KIAA0869
1037_SUZ12_23512	Hs.730786	Q15022	SUZ12 CHET9 JJAZ1 KIAA0160
1038_ZNHIT1_10467	Hs.211079	O43257	ZNHIT1 CGBP1 ZNFN4A1
1039_ABAT_18	Hs.336768	P80404	ABAT GABAT
104_RPL23_9349	Hs.406300	P62829	RPL23
1040_DIAPH1_1729	Hs.529451	O60610	DIAPH1 DIAP1
1041_MLL_4297	Hs.258855	Q03164	KMT2A ALL1 CXXC7 HRX HTRX MLL MLL1 TRX1
1043_LEPROT_54741	Hs.23581	O15243	LEPROT LEPR OBR
1044_ZFP36L2_678	Hs.503093	P47974	ZFP36L2 BRF2 ERF2 RNF162C TIS11D
1045_STRBP_55342	Hs.694157	Q96SI9	STRBP SPNR
1046_SRRT_51593	Hs.111801	Q9BXP5	SRRT ARS2 ASR2
1048_TSPYL4_23270	Hs.284141	Q9UJ04	TSPYL4 KIAA0721
1049_ABLIM1_3983	Hs.438236	O14639	ABLIM1 ABLIM KIAA0059 LIMAB1
105_HIST2H2AA4_723790	Hs.731339	Q6FI13	HIST2H2AA3 H2AFO HIST2H2AA; HIST2H2AA4
1051_TRA2B_6434	Hs.533122	P62995	TRA2B SFRS10
1052_ARL6IP4_51329	Hs.103561	Q66PJ3	ARL6IP4
1055_KIAA0146_23514	Hs.381058	Q14159	SPIDR KIAA0146
1056_KIAA0355_9710	Hs.330073	O15063	KIAA0355
1057_SRRM1_10250	Hs.18192	Q8IYB3	SRRM1 SRM160

1058_SLC25A3_5250	Hs.144130	Q00325	SLC25A3 PHC OK/SW-cl.48
1059_NEMF_9147	Hs.655964	O60524	NEMF SDCCAG1
1060_CNP_1267	Hs.8752	P23582	NPPC CNP2
1062_BCLAF1_9774	Hs.486542	Q9NYF8	BCLAF1 BTF KIAA0164
1063_ITGAV_3685	Hs.436873	P06756	ITGAV MSK8 VNRA VTNR
1066_PDPK1_5170	Hs.459691	O15530	PDPK1 PDK1
1069_PTRH2_51651	Hs.12677	Q9Y3E5	PTRH2 BIT1 PTH2 CGI-147
107_RPS27_6232	Hs.546291	P42677	RPS27 MPS1
1070_MGST1_4257	Hs.389700	P10620	MGST1 GST12 MGST
1071_NRBP2_340371	Hs.521926	Q9NSY0	NRBP2 PP9320 TRG16
1073_GLTSCR1_29998	Hs.97244	Q9NZM4	BICRA GLTSCR1
1074_LTA4H_4048	Hs.524648	P09960	LTA4H LTA4
1075_WIPI2_26100	Hs.122363	Q9Y4P8	WIPI2 CGI-50
1076_TANC1_85461	Hs.61590	Q9C0D5	TANC1 KIAA1728
1077_NPM1_4869	Hs.557550	P06748	NPM1 NPM
1079_IST1_9798	Hs.46423	P53990	IST1 KIAA0174
1081_DDX3Y_8653	Hs.99120	O15523	DDX3Y DBY
1083_LAMC1_3915	Hs.609663	P11047	LAMC1 LAMB2
1084_RAB10_10890	Hs.467960	P61026	RAB10
1085_FAM117B_150864	Hs.471130	Q6P1L5	FAM117B ALS2CR13
1086_RBPJ_3516	Hs.479396	Q06330	RBPJ IGKJRB IGKJRB1 RBPJK RBPSUH
1088_PPIA_5478	Hs.356331	P62937	PPIA CYPA
1090_TSPYL5_85453	Hs.173094	Q86VY4	TSPYL5 KIAA1750
1091_RBBP6_5930		Q7Z6E9	RBBP6 P2PR PACT RBQ1 My038
1093_EIF1AX_1964	Hs.522590	P47813	EIF1AX EIF1A EIF4C
1094_IMPA1_3612	Hs.656694	P29218	IMPA1 IMPA
1096_ANKHD1_54882	Hs.594084	Q8IWZ3	ANKHD1 KIAA1085 MASK VBARP PP2500
1097_CCDC28A_25901	Hs.412019	Q8IWP9	CCDC28A C6orf80
1098_ARGLU1_55082	Hs.508644	Q9NWB6	ARGLU1
110_AMD1_262	Hs.159118	P17707	AMD1 AMD
1100_KIAA0494_9813	Hs.592859	O75071	EFCAB14 KIAA0494
1102_BRD1_23774	Hs.127950	O95696	BRD1 BRL BRPF2
1103_USO1_8615	Hs.292689	O60763	USO1 VDP
1104_CHMP3_51652	Hs.591582	Q9Y3E7	CHMP3 CGI149 NEDF VPS24 CGI-149
1105_SGK1_6446	Hs.510078	O00141	SGK1 SGK
1106_SLC22A23_63027	Hs.713588	A1A5C7	SLC22A23 C6orf85
1107_ACAT1_38	Hs.232375	P35610	SOAT1 ACACT ACACT1 ACAT ACAT1 SOAT STAT
1108_CUX1_1523	Hs.191482	P39880	CUX1 CUTL1
111_GDF15_9518	Hs.616962	Q99988	GDF15 MIC1 PDF PLAB PTGFB
1112_TGOLN2_10618	Hs.593382	O43493	TGOLN2 TGN46 TGN51
1113_PTPLB_201562	Hs.705480	Q6Y1H2	HACD2 PTPLB
1114_STAG3L1_54441	Hs.632310	P0CL83	STAG3L1
1115_ZNF350_59348	Hs.407694	Q9GZX5	ZNF350 ZBRK1
1116_CDKN1C_1028	Hs.106070	P49918	CDKN1C KIP2
112_RPL19_6143	Hs.381061	P84098	RPL19
1120_LAPTM4B_55353	Hs.492314	Q86VI4	LAPTM4B PSEC0001
1121_RPL22L1_200916	Hs.380933	Q6P5R6	RPL22L1
1122_NFIL3_4783	Hs.79334	Q16649	NFIL3 E4BP4 IL3BP1
1123_H2AFV_94239	Hs.488189	Q71UI9	H2AFV H2AV
1125_IGF2_3481	Hs.272259	P01344	IGF2 PP1446

1128_C5orf15_56951	Hs.730670	Q8NC54	KCT2 C5orf15 HTGN29
1129_EZH2_2146	Hs.444082	Q15910	EZH2 KMT6
113_LOC648771_648771			
1132_SH3RF1_57630	Hs.301804	Q7Z6J0	SH3RF1 KIAA1494 POSH POSH1 RNF142 SH3M
1133_SMARCA1_6594	Hs.152292	P28370	SMARCA1 SNF2L SNF2L1
1135_ARMC2_84071	Hs.645481	Q8NEN0	ARMC2
1137_KAT6A_7994	Hs.491577	Q92794	KAT6A MOZ MYST3 RUNXBP2 ZNF220
1138_SNRNP200_23020	Hs.246112	O75643	SNRNP200 ASCC3L1 HELIC2 KIAA0788
1139_NDUFA2_4695	Hs.534333	O43678	NDUFA2
114_SRRM2_23524	Hs.433343	Q9UQ35	SRRM2 KIAA0324 SRL300 SRM300 HSPC075
1141_EIF4A3_9775	Hs.389649	P38919	EIF4A3 DDX48 KIAA0111
1142_NOP56_10528	Hs.376064	O00567	NOP56 NOL5A
1143_PHF2_5253	Hs.211441	O75151	PHF2 CENP-35 KIAA0662
1145_PRR15L_79170	Hs.368260	Q9BU68	PRR15L ATAD4
1147_PPA1_5464	Hs.437403	Q15181	PPA1 IOPPP PP
1149_ARF3_377		P61204	ARF3
115_HMGN2_3151	Hs.181163	P05204	HMGN2 HMG17
1152_HIST1H4L_8368	Hs.533295	P62805	H4C1 H4/A H4FA HIST1H4A; H4C2 H4/I H4FI H
1154_CAMLG_819	Hs.529846	P49069	CAMLG CAML
1155_EIF5_1983	Hs.433702	P55010	EIF5
1156_PREPL_9581	Hs.727511	Q4J6C6	PREPL KIAA0436
1157_KRAS_3845	Hs.505033	P01116	KRAS KRAS2 RASK2
1158_SEMA4C_54910	Hs.516220	Q9C0C4	SEMA4C KIAA1739 SEMAI UNQ5855/PRO3448
1159_PIP4K2B_8396	Hs.730609	P78356	PIP4K2B PIP5K2B
116_TRIB1_10221	Hs.444947	Q96RU8	TRIB1 C8FW GIG2 TRB1
1160_CYFIP1_23191	Hs.26704	Q7L576	CYFIP1 KIAA0068
1161_LINC00116_205251	Hs.128499	Q8NCU8	MTLN LINC00116 NCRNA00116 SMIM37
1162_LIMS1_3987	Hs.597715	P48059	LIMS1 PINCH PINCH1
1163_CARS2_79587	Hs.508725	Q9HA77	CARS2 OK/SW-cl.10
1164_PTDSS1_9791	Hs.292579	P48651	PTDSS1 KIAA0024 PSSA
1167_BZW2_28969	Hs.487635	Q9Y6E2	BZW2 HSPC028 MSTP017
1168_MT1X_4501	Hs.374950	P80297	MT1X
1169_ILF2_3608	Hs.75117	Q12905	ILF2 NF45 PRO3063
117_DHX9_1660	Hs.191518	Q08211	DHX9 DDX9 LKP NDH2
1171_SF3B1_23451	Hs.632554	O75533	SF3B1 SAP155
1173_ATP1B1_481	Hs.291196	P05026	ATP1B1 ATP1B
1178_C12orf51_283450	Hs.530943	Q9Y4D8	HECTD4 C12orf51 KIAA0614
1179_CXXC5_51523	Hs.189119	Q7LFL8	CXXC5 HSPC195 TCCCIA00297
118_RPS7_6201	Hs.546287	P62081	RPS7
1180_ATP8B2_57198	Hs.435700	P98198	ATP8B2 ATPID KIAA1137
1182_PHF10_55274	Hs.435933	Q8WUB8	PHF10 BAF45A
1183_MDK_4192	Hs.82045	P21741	MDK MK1 NEGF2
1184_RIPK4_54101	Hs.517310	P57078	RIPK4 ANKRD3 DIK
1185_ST6GAL1_6480	Hs.207459	P15907	ST6GAL1 SIAT1
1186_WDR1_9948	Hs.128548	O75083	WDR1
1187_TDP2_51567	Hs.403010	O95551	TDP2 EAP2 TTRAP AD-022
1188_RIC8A_60626	Hs.592292	Q9NPQ8	RIC8A
1189_HDAC1_3065	Hs.26593	Q13547	HDAC1 RPD3L1
119_RPS10_6204	Hs.645317	P46783	RPS10
1190_HIST1H2AG_8969	Hs.51011	P0C0S8	H2AC11 H2AFP HIST1H2AG; H2AC13 H2AFC H

1191_JUND_3727		P17535	JUND
1192_CNKSR3_154043	Hs.16064	Q6P9H4	CNKSR3 MAGI1
1193_HIST1H2BH_8345	Hs.247815	Q93079	HIST1H2BH H2BFJ
1194_ANXA1_301	Hs.494173	P04083	ANXA1 ANX1 LPC1
1196_ZFP62_643836	Hs.509227	Q8NB50	ZFP62
1197_GNAQ_2776	Hs.269782	P50148	GNAQ GAQ
1199_PRKAR2A_5576	Hs.631923	P13861	PRKAR2A PKR2 PRKAR2
12_HSP90AA1_3320	Hs.525600	P07900	HSP90AA1 HSP90A HSPC1 HSPCA
120_NPIPL3_23117	Hs.632865	Q92617	NPIPB3 KIAA0220 NPIPL3
1200_C11orf96_387763	Hs.714890	Q7Z7L8	C11orf96 AG2
1201_UIMC1_51720	Hs.232721	Q96RL1	UIMC1 RAP80 RXRIP110
1202_CTNNA1_1495	Hs.445981	P35221	CTNNA1
1203_SRSF1_6426	Hs.68714	Q07955	SRSF1 ASF SF2 SF2P33 SFRS1 OK/SW-cl.3
1204_TAF15_8148	Hs.402752	Q16514	TAF12 TAF15 TAF2J TAFII20
1205_HIST1H2AH_85235	Hs.352225	Q96KK5	HIST1H2AH HIST1H2AI
1207_PAFAH1B1_5048	Hs.77318	P43034	PAFAH1B1 LIS1 MDCR MDS PAFAHA
1208_SCFD1_23256	Hs.369168	Q8WVM8	SCFD1 C14orf163 KIAA0917 STXBP1L2 FKSG23
1209_DDX1_1653	Hs.440599	Q92499	DDX1
121_OGT_8473	Hs.405410	O15294	OGT
1210_SYBU_55638	Hs.390738	Q9NX95	SYBU GOLSYN KIAA1472
1211_OCRL_4952	Hs.126357	Q01968	OCRL OCRL1
1212_PCF11_51585	Hs.128959	O94913	PCF11 KIAA0824
1215_ING5_84289	Hs.529172	Q8WYH8	ING5
1216_UBE2I_7329	Hs.302903	P63279	UBE2I UBC9 UBCE9
1218_CNOT2_4848	Hs.730666	Q9NZN8	CNOT2 CDC36 NOT2 HSPC131 MSTP046
1220_PKP3_11187	Hs.534395	Q9Y446	PKP3
1222_SMARCC2_6601	Hs.236030	Q8TAQ2	SMARCC2 BAF170
1223_EIF3M_10480	Hs.502244	Q7L2H7	EIF3M HFLB5 PCID1 GA17 PNAS-125
1224_RABGAP1_23637	Hs.271341	Q9Y3P9	RABGAP1 HSPC094
1225_RNF114_55905	Hs.144949	Q9Y508	RNF114 ZNF228 ZNF313
1226_PITPNA_5306	Hs.429819	Q00169	PITPNA PITPN
1227_HRASLS5_117245	Hs.410316	Q96KN8	PLAAT5 HRASLS5 HRLP5
123_NEDD4L_23327	Hs.185677	Q96PU5	NEDD4L KIAA0439 NEDL3
1230_MBOAT2_129642	Hs.467634	Q6ZWT7	MBOAT2 OACT2
1231_FAM49B_51571	Hs.126941	Q9NUQ9	FAM49B BM-009
1233_SUB1_10923	Hs.229641	P53999	SUB1 PC4 RPO2TC1
1234_MRPL33_9553	Hs.515879	O75394	MRPL33 C2orf1
1235_VAMP8_8673	Hs.714302	Q9BV40	VAMP8
1236_KLHDC10_23008	Hs.520710	Q6PID8	KLHDC10 KIAA0265
1238_IFITM1_8519	Hs.458414	P13164	IFITM1 CD225 IFI17
1240_NOP10_55505	Hs.14317	Q9NPE3	NOP10 NOLA3
1242_THOC2_57187	Hs.149991	Q8NI27	THOC2 CXorf3
1243_DUSP16_80824	Hs.536535	Q9BY84	DUSP16 KIAA1700 MKP7
1244_ETFB_2109	Hs.348531	P38117	ETFB FP585
1246_TAF1C_9013	Hs.153022	Q15572	TAF1C
1247_CRYL1_51084	Hs.370703	Q9Y2S2	CRYL1 CRY
1248_DHTKD1_55526	Hs.104980	Q96HY7	DHTKD1 KIAA1630
1249_ALDH1A3_220	Hs.459538	P47895	ALDH1A3 ALDH6
125_RPS27A_6233	Hs.546292	P62979	RPS27A UBA80 UBCEP1
1250_MRPS35_60488	Hs.311072	P82673	MRPS35 MRPS28 HDCMD11P MDS023 PSEC02

1251_SNX12_29934	Hs.260750	Q9UMY4	SNX12
1252_SMG1_23049	Hs.460179	Q96Q15	SMG1 ATX KIAA0421 LIP
1253_ANKRD11_29123	Hs.335003	Q6UB99	ANKRD11 ANCO1
1254_C19orf50_79036	Hs.369785	Q9BQD3	KXD1 C19orf50
1256_C19orf28_126321	Hs.656901	Q6NUT3	MFSD12 C19orf28
1257_PMVK_10654	Hs.30954	Q15126	PMVK PMKI
1258_SRSF10_10772	Hs.3530	O75494	SRSF10 FUSIP1 FUSIP2 SFRS13A TASR
1259_HPS4_89781	Hs.474436	Q9NQG7	HPS4 KIAA1667
126_ND4_4538	Hs.465808	P03905	MT-ND4 MTND4 NADH4 ND4
1260_C1orf63_57035	Hs.259412	Q9BUV0	RSRP1 C1orf63 HT033 NPD014
1261_PIGT_51604	Hs.437388	Q969N2	PIGT CGI-06 PSEC0163 UNQ716/PRO1379
1262_HSF1_3297	Hs.530227	Q00613	HSF1 HSTF1
1263_FBXO25_26260	Hs.438454	Q8TCJ0	FBXO25 FBX25
1264_CAST_831	Hs.436186	P20810	CAST
1267_PPAPDC1B_84513	Hs.567619	Q8NEB5	PLPP5 DPPL1 HTPAP PPAPDC1B
1268_XYLT2_64132	Hs.463416	Q9H1B5	XYLT2 XT2 UNQ3058/PRO9878
1270_EIF2AK1_27102	Hs.728827	Q9BQI3	EIF2AK1 HRI KIAA1369 PRO1362
1272_GTPBP4_23560	Hs.215766	Q9BZE4	GTPBP4 CRFG NOG1
1273_NFIA_4774	Hs.191911	Q12857	NFIA KIAA1439
1275_SNRPB2_6629	Hs.280378	P08579	SNRPB2
1277_FABP5_2171	Hs.408061	Q01469	FABP5
1279_MFN2_9927	Hs.376681	O95140	MFN2 CPRP1 KIAA0214
128_RPL35A_6165	Hs.529631	P18077	RPL35A GIG33
1280_FZD4_8322	Hs.591968	Q9ULV1	FZD4
1281_SNRPE_6635	Hs.334612	P62304	SNRPE
1282_RARS_5917	Hs.654907	P54136	RARS
1283_TCEAL3_85012	Hs.311776	Q969E4	TCEAL3 MSTP072
1284_MGP_4256	Hs.365706	P08493	MGP MGLAP GIG36
1285_MICAL2_9645	Hs.501928	O94851	MICAL2 KIAA0750 MICAL2PV1 MICAL2PV2
1286_BCL6_604	Hs.478588	P41182	BCL6 BCL5 LAZ3 ZBTB27 ZNF51
1287_MYO6_4646	Hs.149387	Q9UM54	MYO6 KIAA0389
1289_MSH6_2956	Hs.445052	P52701	MSH6 GTBP
1292_RAN_5901	Hs.194718	P62826	RAN ARA24 OK/SW-cl.81
1293_AMACR_23600	Hs.508343	Q9UHK6	AMACR
1294_CAPRIN1_4076	Hs.471818	Q14444	CAPRIN1 GPIAP1 GPIP137 M11S1 RNG105
1296_EXOC7_23265	Hs.514496	Q9UPT5	EXOC7 EXO70 KIAA1067
1297_NRD1_4898	Hs.584782	O43847	NRDC NRD1
1298_MYO19_80179	Hs.302051	Q96H55	MYO19 MYOHD1
1299_SYPL1_6856	Hs.80919	Q16563	SYPL1 SYPL
13_H3F3A_3020	Hs.533624	P84243	H3-3A H3.3A H3F3 H3F3A PP781; H3-3B H3.3B
1303_RUFY1_80230	Hs.306769	Q96T51	RUFY1 RABIP4 ZFYVE12
1305_PSMD1_5707	Hs.3887	Q99460	PSMD1
1306_SLC38A1_81539	Hs.533770	Q9H2H9	SLC38A1 ATA1 NAT2 SAT1 SNAT1
1307_TSG101_7251	Hs.523512	Q99816	TSG101
1309_RAB3IP_117177	Hs.258209	Q96QF0	RAB3IP RABIN8
131_POM121_9883	Hs.655217	Q96HA1	POM121 KIAA0618 NUP121 POM121A
1310_TADA3_10474	Hs.386390	O75528	TADA3 ADA3 TADA3L
1311_TBC1D14_57533	Hs.518611	Q9P2M4	TBC1D14 KIAA1322
1312_TAB2_23118	Hs.269775	Q9NYJ8	TAB2 KIAA0733 MAP3K7IP2
1314_RCN1_5954	Hs.97887	Q15293	RCN1 RCN

1316_DNAJB1_3337	Hs.515210	P25685	DNAJB1 DNAJ1 HDJ1 HSPF1
1317_MYC_4609	Hs.202453	P01106	MYC BHLHE39
1318_GANAB_23193	Hs.595071	Q14697	GANAB G2AN KIAA0088
1319_ARL6IP5_10550	Hs.730695	O75915	ARL6IP5 DERP11 JWA PRA2 PRAF3 HSPC127
132_RPL21_6144	Hs.381123	P46778	RPL21
1320_FARSB_10056	Hs.471452	Q9NSD9	FARSB FARSLB FRSB HSPC173
1321_MLLT4_4301	Hs.614974	P55196	AFDN AF6 MLLT4
1322_NIT2_56954	Hs.439152	Q9NQR4	NIT2 CUA002
1324_KIAA1430_57587	Hs.535734	Q9P2B7	CFAP97 KIAA1430
1325_KIAA1324_57535	Hs.708190	Q6UXG2	KIAA1324 EIG121 UNQ2426/PRO4985
1326_PPP1CC_5501	Hs.79081	P36873	PPP1CC
1327_SELENBP1_8991	Hs.632460	Q13228	SELENBP1 SBP
1328_MT1L_4500	Hs.647358	Q93083	MT1L
1330_PDIA4_9601	Hs.93659	P13667	PDIA4 ERP70 ERP72
1332_IP6K2_51447	Hs.595983	Q9UHH9	IP6K2 IHPK2 TCCCIA00113
1333_TMCO3_55002	Hs.317593	Q6UWJ1	TMCO3 C13orf11 UNQ2419/PRO4976
1334_HGSNAT_138050	Hs.600384	Q68CP4	HGSNAT TMEM76
1335_KTN1_3895	Hs.509414	Q86UP2	KTN1 CG1 KIAA0004
1337_SIDT2_51092	Hs.712144	Q8NBJ9	SIDT2 CGI-40 PSEC0072 UNQ685/PRO1325
1338_TOP1MT_116447	Hs.528574	Q969P6	TOP1MT
1339_RNASET2_8635	Hs.529989	O00584	RNASET2 RNASE6PL
134_CD99_4267	Hs.522805	P14209	CD99 MIC2 MIC2X MIC2Y
1343_DAAM1_23002	Hs.654934	Q9Y4D1	DAAM1 KIAA0666
1344_SEC31A_22872	Hs.370024	O94979	SEC31A KIAA0905 SEC31L1 HSPC275 HSPC334
1345_ENOSF1_55556	Hs.369762	Q7L5Y1	ENOSF1 RTS TYMSAS
1348_ARFIP1_27236	Hs.416089	P53367	ARFIP1
1349_NMT1_4836	Hs.532790	P30419	NMT1 NMT
1350_MDH1_4190	Hs.526521	P40925	MDH1 MDHA
1353_LAS1L_81887	Hs.522675	Q9Y4W2	LAS1L MSTP060
1354_SET_6418	Hs.436687	Q9NQR1	KMT5A PRSET7 SET07 SET8 SETD8
1355_SIVA1_10572	Hs.112058	O15304	SIVA1 SIVA
1356_MT1H_4496	Hs.438462	P80294	MT1H
1357_BZW1_9689	Hs.355983	Q7L1Q6	BZW1 BZAP45 KIAA0005
1358_TOM1L2_146691	Hs.462379	Q6ZVM7	TOM1L2
1359_SP3_6670	Hs.531587	Q02447	SP3
136_RPL17_6139	Hs.374588	P18621	RPL17
1360_DCAF13_25879	Hs.532265	Q9NV06	DCAF13 WDSOF1 HSPC064
1361_IARS_3376	Hs.445403	P41252	IARS
1362_ADD1_118	Hs.183706	P35611	ADD1 ADDA
1363_LEF1_51176	Hs.555947	Q9UJU2	LEF1
1367_KIF13B_23303	Hs.444767	Q9NQT8	KIF13B GAKIN KIAA0639
1368_VEZF1_7716	Hs.463569	Q14119	VEZF1 DB1 ZNF161
1369_JUNB_3726	Hs.25292	P17275	JUNB
137_RPL14_9045	Hs.730621	P50914	RPL14
1370_GOLPH3_64083	Hs.408909	Q9H4A6	GOLPH3 GPP34
1373_TPM3_7170	Hs.644306	P06753	TPM3
1374_PSMA6_5687	Hs.446260	P60900	PSMA6 PROS27
1375_ARID4B_51742	Hs.575782	Q4LE39	ARID4B BRCAA1 RBBP1L1 RBP1L1 SAP180
1376_MORF4L2_9643	Hs.326387	Q15014	MORF4L2 KIAA0026 MRGX
1377_TRIM2_23321	Hs.435711	Q9C040	TRIM2 KIAA0517 RNF86

1378_CHD7_55636	Hs.20395	Q9P2D1	CHD7 KIAA1416
1379_KPNA4_3840	Hs.730660	O00629	KPNA4 QIP1
138_RPL37_6167	Hs.80545	P61927	RPL37
1380_PSMD3_5709	Hs.12970	O43242	PSMD3
1382_PGC_5225	Hs.1867	Q86YN6	PPARGC1B PERC PGC1 PGC1B PPARGC1
1383_SYNCRIP_10492	Hs.571177	O60506	SYNCRIP HNRPQ NSAP1
1385_ITGB1_3688	Hs.643813	P05556	ITGB1 FNRB MDF2 MSK12
1386_RALGAPA2_57186	Hs.472285	Q2PPJ7	RALGAPA2 C20orf74 KIAA1272
1387_RPA1_6117	Hs.461925	P27694	RPA1 REPA1 RPA70
139_BBS5_129880	Hs.233398	Q8N3I7	BBS5
1390_BEX2_84707	Hs.398989	Q9BXY8	BEX2
1391_PDIA5_10954	Hs.477352	Q14554	PDIA5 PDIR
1392_C20orf108_116151	Hs.143736	Q96KR6	FAM210B C20orf108 PSEC0265
1393_PSMB7_5695	Hs.213470	Q99436	PSMB7 Z
1394_PCGF3_10336	Hs.144309	Q3KNV8	PCGF3 RNF3 RNF3A
1395_CCT6A_908	Hs.82916	P40227	CCT6A CCT6 CCTZ
1396_HIST2H2AB_317772	Hs.664173	Q8IUE6	HIST2H2AB
1397_SAR1B_51128	Hs.432984	Q9Y6B6	SAR1B SARA2 SARB
1398_BANP_54971	Hs.461705	Q8N9N5	BANP BEND1 SMAR1
14_UBOX5_22888	Hs.654646	O94941	UBOX5 KIAA0860 RNF37 UBCE7IP5 UIP5
1400_FOXJ3_22887	Hs.26023	Q9UPW0	FOXJ3 KIAA1041
1402_A2M_2	Hs.212838	P01023	A2M CPAMD5 FWP007
1403_HGS_9146	Hs.730823	O14964	HGS HRS
1404_DPYSL3_1809	Hs.519659	Q14195	DPYSL3 CRMP4 DRP3 ULIP ULIP1
1405_ATXN2_6311	Hs.460499	Q99700	ATXN2 ATX2 SCA2 TNRC13
1407_FXR1_8087	Hs.478407	P51114	FXR1
1408_ESRP2_80004	Hs.592053	Q9H6T0	ESRP2 RBM35B PP7059
1409_MAP2K3_5606	Hs.514012	P46734	MAP2K3 MEK3 MKK3 PRKMK3 SKK2
141_CAMKK2_10645	Hs.297343	Q96RR4	CAMKK2 CAMKKB KIAA0787
1411_MAFG_4097	Hs.252229	O15525	MAFG
1417_XRN1_54464	Hs.435103	Q8IZH2	XRN1 SEP1
1418_YBX1_4904	Hs.473583	P67809	YBX1 NSEP1 YB1
1419_TBL1XR1_79718	Hs.715026	Q9BZK7	TBL1XR1 IRA1 TBLR1
142_RPL13_6137	Hs.410817	P26373	RPL13 BBC1 OK/SW-cl.46
1420_TCF3_6929	Hs.371282	P15923	TCF3 BHLHB21 E2A ITF1
1421_DUSP12_11266	Hs.416216	Q9UNI6	DUSP12
1423_CHCHD7_79145	Hs.436913	Q9BUK0	CHCHD7
1424_ITPRIPL2_162073	Hs.530899	Q3MIP1	ITPRIPL2
1425_SSRP1_6749	Hs.523680	Q08945	SSRP1 FACT80
1426_FAM164A_51101	Hs.271876	Q96GY0	ZC2HC1A C8orf70 FAM164A CGI-62
1427_PFKM_5213	Hs.75160	P08237	PFKM PFKX
1428_MRPS14_63931	Hs.654858	O60783	MRPS14
1429_FRMD8_83786	Hs.578433	Q9BZ67	FRMD8 FKSG44
143_STX16_8675	Hs.307913	O14662	STX16
1430_DLD_1738	Hs.131711	P09622	DLD GCSL LAD PHE3
1431_ZNF462_58499	Hs.370379	Q96JM2	ZNF462 KIAA1803
1433_SASH1_23328	Hs.193133	O94885	SASH1 KIAA0790 PEPE1
1434_PKN2_5586	Hs.440833	Q16513	PKN2 PRK2 PRKCL2
145_IGFBP7_3490	Hs.479808	Q16270	IGFBP7 MAC25 PSF
146_SMPD4_55627	Hs.516450	Q9NXE4	SMPD4 KIAA1418 SKNY

Supplemental material

BMJ Publishing Group Limited (BMJ) disclaims all liability and responsibility arising from any reliance placed on this supplemental material which has been supplied by the author(s)

J Immunother Cancer

147_RPL36_25873	Hs.432485	Q9Y3U8	RPL36
149_RPS11_6205	Hs.433529	P62280	RPS11
1490_LGALS3_3958	Hs.531081	P17931	LGALS3 MAC2
150_YWHAG_7532	Hs.520974	P61981	YWHAG
151_ILDR1_286676	Hs.98484	Q86SU0	ILDR1
152_FAM162A_26355	Hs.584881	Q96A26	FAM162A C3orf28 E2IG5 DC16 FWP001
153_C1orf198_84886	Hs.520494	Q9H425	C1orf198
155_C11orf75_56935	Hs.438064	Q9NRQ5	SMCO4 C11orf75 FN5
156_ARF1_375	Hs.286221	P84077	ARF1
157_RPS13_6207	Hs.446588	P62277	RPS13
158_NUPR1_26471	Hs.513463	O60356	NUPR1 COM1
159_MGST2_4258	Hs.81874	Q99735	MGST2 GST2
16_ORAI1_84876	Hs.55148	Q96D31	ORAI1 CRACM1 TMEM142A
161_CDK2AP1_8099	Hs.725139	O14519	CDK2AP1 CDKAP1 DOC1
162_CEBPD_1052	Hs.440829	P49716	CEBPD
163_ATP13A3_79572	Hs.529609	Q9H7F0	ATP13A3 AFURS1
166_RPS17_6218	Hs.433427	P08708	RPS17 RPS17L
167_ATP5E_514	Hs.177530	P56381	ATP5F1E ATP5E
168_C16orf53_79447	Hs.702841	Q9BTK6	PAGR1 C16orf53 PA1
170_C15orf63_25764	Hs.730672	Q9NX55	HYPK C15orf63 HSPC136
172_GOLGA6L9_440295	Hs.630181	A6NEM1	GOLGA6L9 GOLGA6L20
175_IRF2BP2_359948	Hs.350268	Q7Z5L9	IRF2BP2
176_ORC6_23594	Hs.49760	Q9Y5N6	ORC6 ORC6L
177_RPL10A_4736	Hs.546269	P62906	RPL10A NEDD6
178_ZC3H11A_9877	Hs.532399	O75152	ZC3H11A KIAA0663 ZC3HDC11A
179_ATF4_468	Hs.496487	P18848	ATF4 CREB2 TXREB
18_RPL18_6141	Hs.515517	Q07020	RPL18
180_GLTSCR2_29997	Hs.421907	Q9NZM5	NOP53 GLT GLTSCR2 PICT1
182_PRNP_5621	Hs.472010	P04156	PRNP ALTPRP PRIP PRP
185_NGFRAP1_27018	Hs.448588	Q00994	BEX3 DXS6984E NADE NGFRAP1
19_NPIP_9284	Hs.676266	Q9UND3	NPIPA1 NPIP
190_ND5_4540	Hs.723616	P03915	MT-ND5 MTND5 NADH5 ND5
191_CMTM6_54918	Hs.380627	Q9NX76	CMTM6 CKLFSF6
195_NDUFB9_4715	Hs.15977	Q9Y6M9	NDUFB9 LYRM3 UQOR22
196_HNRNPM_4670	Hs.465808	P52272	HNRNPM HNRPM NAGR1
198_ATP9A_10079	Hs.649234	O75110	ATP9A ATPIIA KIAA0611
199_MAEA_10296	Hs.139896	Q7L5Y9	MAEA EMP HLC10 PIG5
2_AR_367	Hs.634882	P10275	AR DHTR NR3C4
200_BRI3_25798	Hs.567438	Q9NQX7	ITM2C BRI3 hucep-14 NPD018 PSEC0047
202_NACA_4666	Hs.505735	Q13765	NACA HSD48
203_TMEM87A_25963	Hs.730697	Q8NBN3	TMEM87A PSEC0094
207_FAU_2197	Hs.387208	P62861	FAU
208_TBCA_6902	Hs.291212	O75347	TBCA
209_RPL41_6171	Hs.157160	P62945	RPL41
21_GTF2I_2969	Hs.647041	P78347	GTF2I BAP135 WBSCR6
210_POTEG_404785	Hs.640191	Q6S5H5	POTEG A26C2 POTE14
211_RPS15_6209	Hs.370504	P62841	RPS15 RIG
212_ZRANB2_9406	Hs.194718	O95218	ZRANB2 ZIS ZNF265
213_HMGN2P46_283651	Hs.574240	Q86SG4	HMGN2P46 C15orf21
215_ATP6V1G1_9550	Hs.388654	O75348	ATP6V1G1 ATP6G ATP6G1 ATP6J

216_WDR6_11180	Hs.654815	Q9NNW5	WDR6
218_CHKA_1119	Hs.77221	P35790	CHKA CHK CKI
219_RPL36AL_6166	Hs.444749	Q969Q0	RPL36AL
22_EXOC3L2_90332	Hs.337557	Q2M3D2	EXOC3L2 XTP7
222_ACSS1_84532	Hs.529353	Q9NUB1	ACSS1 ACAS2L KIAA1846
224_RPL23A_6147	Hs.419463	P62750	RPL23A
226_RPS19_6223	Hs.438429	P39019	RPS19
2261_KLK2_3817		P20151	KLK2
230_RPS26_6231	Hs.567235	P62854	RPS26
231_B4GALT1_2683	Hs.272011	P15291	B4GALT1 GGTB2
233_COX7A2_1347	Hs.70312	P14406	COX7A2 COX7AL
234_ARPC3_10094	Hs.524741	O15145	ARPC3 ARC21
235_ATP2C1_27032	Hs.584884	P98194	ATP2C1 KIAA1347 PMR1L HUSSY-28
238_CASC3_22794	Hs.730662	O15234	CASC3 MLN51
239_DDR1_780	Hs.631988	Q08345	DDR1 CAK EDDR1 NEP NTRK4 PTK3A RTK6 TRK
241_RAB3D_9545	Hs.655274	O95716	RAB3D GOV RAB16
242_HMGB2_3148	Hs.434953	P26583	HMGB2 HMG2
244_RPL7_6129	Hs.571841	P18124	RPL7
245_HNRNPC_3183	Hs.508848	P07910	HNRNPC HNRPC
247_UBA52_7311	Hs.5308	P62987	UBA52 UBCEP2
248_OR51E2_81285	Hs.501758	Q9H255	OR51E2 PSGR
249_CCDC72_51372	Hs.356440	Q9Y2S6	TMA7 CCDC72 HSPC016 HSPC330
25_PEBP1_5037	Hs.433863	P30086	PEBP1 PBP PEBP
250_KPNB1_3837	Hs.532793	Q14974	KPNB1 NTF97
251_COX2_4513	Hs.197320	P35354	PTGS2 COX2
255_RANBP2_5903	Hs.199561	P49792	RANBP2 NUP358
257_HIST3H3_8290	Hs.248171	Q16695	HIST3H3 H3FT
258_C6orf62_81688	Hs.9676	Q9GZU0	C6orf62 XTP12 Nbla00237
259_ANAPC11_51529	Hs.534456	Q9NYG5	ANAPC11 HSPC214
26_RPL31_6160	Hs.469473	P62899	RPL31
260_EMP2_2013	Hs.531561	P54851	EMP2 XMP
261_APLP2_334	Hs.370247	Q06481	APLP2 APPL2
262_HSPD1_3329	Hs.727543	P10809	HSPD1 HSP60
263_RPL27_6155	Hs.523463	P61353	RPL27
266_UTRN_7402	Hs.133135	P46939	UTRN DMDL DRP1
268_ADM_133	Hs.370510	Q7Z4H4	ADM2 AM2
27_NBPF15_284565	Hs.656782	Q8N660	NBPF15 NBPF16
271_RPS4X_6191	Hs.118076	P62701	RPS4X CCG2 RPS4 SCAR
272_HBB_3043	Hs.523443	P68871	HBB
273_MAGED1_9500	Hs.5258	Q9Y5V3	MAGED1 NRAGE PP2250 PRO2292
274_SNRPD3_6634	Hs.356549	P62318	SNRPD3
275_RPL37A_6168	Hs.433701	P61513	RPL37A
276_TMBIM6_7009	Hs.730613	P55061	TMBIM6 BI1 TEGT
278_SSR2_6746	Hs.74564	P43308	SSR2 TRAPB HSD25
279_CTDSP2_10106	Hs.524530	O14595	CTDSP2 NIF2 OS4 SCP2
28_EEF1D_1936	Hs.333388	P29692	EEF1D EF1D
281_RPL29_6159	Hs.425125	P47914	RPL29
283_MZT2B_80097	Hs.469925	Q6NZ67	MZT2B FAM128B MOZART2B
284_DSP_1832	Hs.519873	P15924	DSP
286_NFIC_4782	Hs.170131	P08651	NFIC NFI

Supplemental material

BMJ Publishing Group Limited (BMJ) disclaims all liability and responsibility arising from any reliance placed on this supplemental material which has been supplied by the author(s)

J Immunother Cancer

287_USMG5_84833	Hs.500921	Q96IX5	ATP5MD DAPIT HCVFTP2 USMG5 PD04912
288_PUM1_9698	Hs.281707	Q14671	PUM1 KIAA0099 PUMH1
289_NDUFA8_4702	Hs.495039	P51970	NDUFA8
29_HSP90B1_7184	Hs.192374	P14625	HSP90B1 GRP94 TRA1
290_BRD2_6046	Hs.75243	P25440	BRD2 KIAA9001 RING3
291_CTBP2_1488	Hs.501345	P56545	CTBP2
292_CSNK1D_1453	Hs.631725	P48730	CSNK1D HCKID
293_RPL7A_6130	Hs.499839	P62424	RPL7A SURF-3 SURF3
295_ULK1_8408	Hs.47061	O75385	ULK1 KIAA0722
296_NDUFS5_4725	Hs.632385	O43920	NDUFS5
298_RPL24_6152	Hs.477028	P83731	RPL24
30_LOC100132247_100132247	Hs.720286		
300_GNL3_26354	Hs.313544	Q9BVP2	GNL3 E2IG3 NS
302_SRSF3_6428	Hs.405144	P84103	SRSF3 SFRS3 SRP20
303_RPL13AP3_645683	Hs.663461	Q6NVV1	RPL13AP3
304_ZNF706_51123	Hs.374485	Q9Y5V0	ZNF706 HSPC038 PNAS-113
305_NFE2L1_4779	Hs.514284	Q14494	NFE2L1 HBZ17 NRF1 TCF11
306_LBR_3930	Hs.435166	Q14739	LBR
309_TMC8_147138	Hs.592102	Q8IU68	TMC8 EVER2 EVIN2
31_MAT2A_4144	Hs.516157	P31153	MAT2A AMS2 MATA2
310_AKAP1_8165	Hs.522572	Q92667	AKAP1 AKAP149 PRKA1
315_SOX4_6659	Hs.643910	Q06945	SOX4
316_HIST1H1C_3006	Hs.7644	P16403	H1-2 H1F2 HIST1H1C
317_RPL13A_23521	Hs.523185	P40429	RPL13A
320_MLEC_9761	Hs.507074	Q14165	MLEC KIAA0152
321_SSB_6741	Hs.632535	P05455	SSB
322_ARF4_378	Hs.652183	P18085	ARF4 ARF2
324_CELF1_10658	Hs.595333	Q92879	CELF1 BRUNOL2 CUGBP CUGBP1 NAB50
327_AP3D1_8943	Hs.512815	O14617	AP3D1 PRO0039
328_C14orf2_9556	Hs.109052	P56378	ATP5MPL C14orf2 MP68 PRO1574
329_FOLH1_2346	Hs.654487	Q04609	FOLH1 FOLH NAALAD1 PSM PSMA GIG27
33_ANKK1_255239	Hs.448473	Q8NFD2	ANKK1 PKK2 SGK288
330_FKBP2_2286	Hs.227729	P26885	FKBP2 FKBP13
331_HIST1H2AD_3013	Hs.679229	P20671	H2AC7 H2AFG HIST1H2AD
332_RPL8_6132	Hs.178551	P62917	RPL8
333_HNRNPA3_220988	Hs.516539	P51991	HNRNPA3 HNRPA3
334_RALBP1_10928	Hs.528993	Q15311	RALBP1 RLIP1 RLIP76
336_STEAP1_26872	Hs.61635	Q9UHE8	STEAP1 PRSS24 STEAP
337_ATP1B3_483	Hs.477789	P54709	ATP1B3
339_SEPW1_6415	Hs.631549	P63302	SELENOW SELW SEPW1
34_PTPRF_5792	Hs.272062	P10586	PTPRF LAR
340_H2AFJ_55766	Hs.524280	Q9BTM1	H2AFJ
341_KRTCAP2_200185	Hs.516671	Q8N6L1	KRTCAP2 KCP2
343_TARDBP_23435	Hs.300624	Q13148	TARDBP TDP43
344_SEPT9_10801		Q9UHD8	SEPTIN9 KIAA0991 MSF SEPT9
346_WASH2P_375260	Hs.459573	Q6VEQ5	WASH2P FAM39B
347_TDG_6996	Hs.584809	Q13569	TDG
349_PARP1_142	Hs.177766	P09874	PARP1 ADPRT PPOL
35_MYO1C_4641	Hs.286226	Q12965	MYO1E MYO1C
350_RPL28_6158	Hs.652114	P46779	RPL28

Supplemental material

BMJ Publishing Group Limited (BMJ) disclaims all liability and responsibility arising from any reliance placed on this supplemental material which has been supplied by the author(s)

J Immunother Cancer

351_CCT4_10575	Hs.421509	P50991	CCT4 CCTD SRB
352_HP1BP3_50809	Hs.142442	Q5SSJ5	HP1BP3
353_GPI_2821	Hs.466471	Q9BRB3	PIGQ GPI1
354_SLC12A7_10723	Hs.172613	Q9Y666	SLC12A7 KCC4
355_CYB5R3_1727	Hs.561064	P00387	CYB5R3 DIA1
356_DNAJA4_55466	Hs.513053	Q8WW22	DNAJA4
361_EIF1_10209	Hs.150580	P41567	EIF1 SUI1
362_CYP1B1_1545	Hs.154654	Q16678	CYP1B1
363_EEF1B2_1933	Hs.421608	P24534	EEF1B2 EEF1B EF1B
364_TCF25_22980	Hs.415342	Q9BQ70	TCF25 KIAA1049 NULP1 FKSG26
365_SNRNP70_6625	Hs.467097	P08621	SNRNP70 RNPU1Z RPU1 SNRP70 U1AP1
367_TUBA1B_10376	Hs.524390	P68363	TUBA1B
369_KIAA1244_57221	Hs.194408	Q5TH69	ARFGEF3 BIG3 C6orf92 KIAA1244
37_RPL34_6164	Hs.438227	P49207	RPL34
370_NACA2_342538	Hs.591178	Q9H009	NACA2 NACAL
373_MTCH1_23787	Hs.485262	Q9NZJ7	MTCH1 PSAP CGI-64 UNQ1871/PRO4314
378_SNRPF_6636	Hs.105465	P62306	SNRPF PBSCF
379_ELP2_55250	Hs.8739	Q6IA86	ELP2 STATIP1
38_PDLIM5_10611	Hs.480311	Q96HC4	PDLIM5 ENH L9
380_HLA-G_3135	Hs.512152	P17693	HLA-G HLA-6.0 HLAG
382_UQCR10_29796	Hs.284292	Q9UDW1	UQCR10 UCRC HSPC119
383_TBC1D8_11138	Hs.442657	Q0IIM8	TBC1D8B
385_EIF3D_8664	Hs.55682	O15371	EIF3D EIF3S7
386_LRRC8A_56262	Hs.643600	Q8IWT6	LRRC8A KIAA1437 LRRC8 SWELL1 UNQ221/PR
387_RPS3A_6189	Hs.356572	P61247	RPS3A FTE1 MFTL
388_SND1_27044	Hs.122523	Q7KZF4	SND1 TDRD11
389_RPL6_6128	Hs.546283	Q02878	RPL6 TXREB1
390_IGFBP2_3485	Hs.438102	P18065	IGFBP2 BP2 IBP2
392_SPARC_6678	Hs.111779	P09486	SPARC ON
394_NDUFA4_4697	Hs.50098	O00483	NDUFA4
398_PDXDC1_23042	Hs.370781	Q6P996	PDXDC1 KIAA0251
40_TMPRSS2_7113	Hs.439309	O15393	TMPRSS2 PRSS10
400_CKB_1152	Hs.173724	P12277	CKB CKBB
401_RPN1_6184	Hs.518244	P04843	RPN1
404_ELL2_22936	Hs.192221	O00472	ELL2
408_HNRNPK_3190	Hs.522257	P61978	HNRNPK HNRPK
409_TPM1_7168	Hs.133892	P09493	TPM1 C15orf13 TMSA
41_NKX3-1_4824	Hs.55999	Q99801	NKX3-1 NKX3.1 NKX3A
410_C6orf115_58527	Hs.600861	Q9P1F3	ABRACL C6orf115 HSPC280 PRO2013
412_RPS4Y1_6192	Hs.282376	P22090	RPS4Y1 RPS4Y PRO2646
414_DSTN_11034	Hs.304192	P60981	DSTN ACTDP DSN
415_EPAS1_2034	Hs.468410	Q99814	EPAS1 BHLHE73 HIF2A MOP2 PASD2
416_CCDC47_57003	Hs.202011	Q96A33	CCDC47 GK001 MSTP041 PSEC0077
417_PNISR_25957	Hs.520287	Q8TF01	PNISR C6orf111 SFRS18 SRRP130 HSPC261 HSl
418_ALDH2_217	Hs.604551	P05091	ALDH2 ALDM
419_HK2_3099	Hs.591588	P52789	HK2
42_RPL35_11224	Hs.182825	P42766	RPL35
421_DNAJB2_3300	Hs.77768	P25686	DNAJB2 HSJ1 HSPF3
422_EIF3C_8663	Hs.567374	Q99613	EIF3C EIF3S8
427_SURF4_6836	Hs.512465	O15260	SURF4 SURF-4

Supplemental material

BMJ Publishing Group Limited (BMJ) disclaims all liability and responsibility arising from any reliance placed on this supplemental material which has been supplied by the author(s)

J Immunother Cancer

428_SPCS2_9789	Hs.282700	Q15005	SPCS2 KIAA0102 SPC25
43_PXN_5829	Hs.446336	P49023	PXN
433_CANX_821	Hs.567968	P27824	CANX
435_ZNF24_7572	Hs.514802	P17028	ZNF24 KOX17 ZNF191 ZSCAN3
437_PRR13_54458	Hs.426359	Q9NZ81	PRR13 TXR1 BM-041
438_AHCY_191	Hs.485365	P23526	AHCY SAHH
439_TAX1BP1_8887	Hs.34576	Q86VP1	TAX1BP1 T6BP PRO0105
440_NOP58_51602	Hs.471104	Q9Y2X3	NOP58 NOL5 NOP5 HSPC120
441_NSUN5P2_260294	Hs.510927	Q63ZY6	NSUN5P2 NSUN5C WBSCR20B WBSCR20C
442_PNRC1_10957	Hs.75969	Q12796	PNRC1 PROL2
443_BMPR1B_658	Hs.598475	O00238	BMPR1B
444_CBS_875	Hs.533013	P35520	CBS
445_MARCKS_4082	Hs.519909	P29966	MARCKS MACS PRKCSL
446_RPL26_6154	Hs.644794	P61254	RPL26
448_GOLGA4_2803	Hs.344151	Q13439	GOLGA4
449_GALNT11_63917	Hs.647109	Q8NCW6	GALNT11
45_MKNK2_2872	Hs.515032	Q9HBH9	MKNK2 GPRK7 MNK2
450_MRPS18B_28973	Hs.655329	Q9Y676	MRPS18B C6orf14 HSPC183 PTD017
452_CHSY1_22856	Hs.110488	Q86X52	CHSY1 CHSY CSS1 KIAA0990 UNQ756/PRO148
453_NCL_4691	Hs.79110	P19338	NCL
457_NEK9_91754	Hs.730635	Q8TD19	NEK9 KIAA1995 NEK8 NERCC
458_RBM8A_9939	Hs.591455	Q9Y5S9	RBM8A RBM8 HSPC114 MDS014
459_CLTC_1213	Hs.491351	Q00610	CLTC CLH17 CLTCL2 KIAA0034
460_NOTCH2_4853	Hs.487360	Q04721	NOTCH2
461_C7orf28B_221960	Hs.567779	P86790	CCZ1B C7orf28B
462_EIF3E_3646	Hs.405590	P60228	EIF3E EIF3S6 INT6
465_DHCR24_1718	Hs.498727	Q15392	DHCR24 KIAA0018
469_ASRGL1_80150	Hs.535326	Q7L266	ASRGL1 ALP CRASH
47_ARL6IP1_23204	Hs.634882	Q15041	ARL6IP1 ARL6IP ARMER KIAA0069
470_SCCPDH_51097	Hs.498397	Q8NBX0	SCCPDH CGI-49
473_RPL5_6125	Hs.532359	P46777	RPL5 MSTP030
474_RPL18A_6142	Hs.337766	Q02543	RPL18A
475_PDHA1_5160	Hs.530331	P08559	PDHA1 PHE1A
476_EIF3H_8667	Hs.492599	O15372	EIF3H EIF3S3
477_SRSF5_6430	Hs.632326	Q13243	SRSF5 HRS SFRS5 SRP40
478_VDAC1_7416	Hs.519320	P21796	VDAC1 VDAC
48_RPS6_6194	Hs.408073	P62753	RPS6 OK/SW-cl.2
481_ATP5O_539	Hs.409140	P48047	ATP5PO ATP5O ATPO
483_EML4_27436	Hs.730709	Q9HC35	EML4 C2orf2 EMAPL4
485_TSPAN1_10103	Hs.38972	O60635	TSPAN1
486_SRPR_6734	Hs.368376	P08240	SRPRA SRPR
487_CTSF_8722	Hs.11590	Q9UBX1	CTSF
488_MYL12B_103910	Hs.464472	O14950	MYL12B MRLC2 MYLC2B
489_MTMR4_9110	Hs.514373	Q9NYA4	MTMR4 KIAA0647 ZFYVE11
49_U2AF1_7307	Hs.365116	Q8WU68	U2AF1L4 U2AF1-RS3 U2AF1L3
490_ABCC5_10057	Hs.728765	O15440	ABCC5 MRP5
491_KDELR2_11014	Hs.654552	P33947	KDELR2 ERD2.2
493_HOXB13_10481	Hs.66731	Q92826	HOXB13
494_MT2A_4502	Hs.647371	P02795	MT2A CES1 MT2
499_TCEAL4_79921	Hs.194329	Q96EI5	TCEAL4 NPD017

500_F11R_50848	Hs.517293	Q9Y624	F11R JAM1 JCAM UNQ264/PRO301
502_NBPF10_100132406	Hs.714127	Q6P3W6	NBPF10
503_KIF5C_3800	Hs.660699	O60282	KIF5C KIAA0531 NKHC2
504_IER2_9592	Hs.501629	Q9BTL4	IER2 ETR101 PIP92
506_SPOCK1_6695	Hs.596136	Q08629	SPOCK1 SPOCK TIC1 TICN1
507_H1F0_3005	Hs.226117	P07305	H1-0 H1F0 H1FV
509_PILRB_29990	Hs.632314	Q9UKJ0	PILRB FDFACT PP1551
51_SLC45A3_85414	Hs.278695	Q96JT2	SLC45A3 PCANAP6 PRST
511_SLC25A5_292	Hs.632282	P05141	SLC25A5 ANT2
512_HIST1H2BK_85236	Hs.437275	O60814	H2BC12 H2BFT HIRIP1 HIST1H2BK
513_ZMIZ1_57178	Hs.193118	Q9ULJ6	ZMIZ1 KIAA1224 RAI17 ZIMP10
514_NR2F2_7026	Hs.347991	P24468	NR2F2 ARP1 TFCOUP2
515_ACO2_50	Hs.643610	Q99798	ACO2
516_TACSTD2_4070	Hs.23582	P09758	TACSTD2 GA733-1 M1S1 TROP2
517_NME3_4832	Hs.514065	Q13232	NME3
519_NBPF11_200030	Hs.515947	Q86T75	NBPF11 NBPF24
52_RPS20_6224	Hs.8102	P60866	RPS20
520_PTGES3_10728	Hs.50425	Q15185	PTGES3 P23 TEBP
521_YTHDF2_51441	Hs.532286	Q9Y5A9	YTHDF2 HGRG8
523_TRMT5_57570	Hs.380159	Q32P41	TRMT5 KIAA1393 TRM5
524_ACAA1_30	Hs.643487	P09110	ACAA1 ACAA PTHIO
525_TAF7_6879	Hs.438838	Q15545	TAF7 TAF2F TAFII55
526_PDIA3_2923	Hs.591095	P30101	PDIA3 ERP57 ERP60 GRP58
527_PALM2-AKAP2_445815	Hs.591908	B1ALY0	PALM2AKAP2
53_PABPC1_26986	Hs.387804	P11940	PABPC1 PAB1 PABP1 PABPC2
531_SMARCA4_6597	Hs.327527	P51532	SMARCA4 BAF190A BRG1 SNF2B SNF2L4
532_ACTN1_87	Hs.356285	P12814	ACTN1
534_MRPS24_64951	Hs.284286	Q96EL2	MRPS24 HSPC335
535_MKRN1_23608	Hs.728819	Q9UHC7	MKRN1 RNF61
536_MANF_7873	Hs.436446	P55145	MANF ARMET ARP
537_DGKD_8527	Hs.471675	Q16760	DGKD KIAA0145
538_THRAP3_9967	Hs.160211	Q9Y2W1	THRAP3 BCLAF2 TRAP150
539_MAML1_9794	Hs.631951	Q92585	MAML1 KIAA0200
54_P4HB_5034	Hs.464336	P07237	P4HB ERBA2L PDI PDIA1 PO4DB
540_CSTB_1476	Hs.695	P04080	CSTB CST6 STFB
543_RHOU_58480	Hs.647774	Q7L0Q8	RHOU ARHU CDC42L1 G28K WRCH1 SB128
544_MGST3_4259	Hs.191734	O14880	MGST3
545_MGEA5_10724	Hs.500842	O60502	OGA HEXC KIAA0679 MEA5 MGEA5
547_MTA1_9112	Hs.525629	Q13330	MTA1
548_SCYL1_57410	Hs.238839	Q96KG9	SCYL1 CVAK90 GKLP NTKL TAPK TEIF TRAP HT(
549_REPIN1_29803	Hs.647086	Q9BWE0	REPIN1 RIP60 ZNF464
551_GNG10_2790	Hs.534196	P50151	GNG10 GNGT10
552_ADAR_103	Hs.12341	P55265	ADAR ADAR1 DSRAD G1P1 IFI4
553_METTL7A_25840	Hs.728181	Q9H8H3	METTL7A PRO0066 UNQ1902/PRO4348
555_RAD21_5885	Hs.81848	O60216	RAD21 HR21 KIAA0078 NXP1 SCC1
556_POGZ_23126	Hs.489873	Q7Z3K3	POGZ KIAA0461 SUHW5 ZNF280E ZNF635 Nbl
557_CTDSP1_58190	Hs.444468	Q9GZU7	CTDSP1 NIF3 NLIIF SCP1
56_ALPK1_80216	Hs.652825	Q96QP1	ALPK1 KIAA1527 LAK
561_DYNC1LI2_1783	Hs.369068	O43237	DYNC1LI2 DNCLI2 LIC2
564_HIST2H2AC_8338	Hs.408067	Q16777	HIST2H2AC H2AFQ

Supplemental material

BMJ Publishing Group Limited (BMJ) disclaims all liability and responsibility arising from any reliance placed on this supplemental material which has been supplied by the author(s)

J Immunother Cancer

565_LRIG1_26018	Hs.518055	Q96JA1	LRIG1 LIG1
566_MEAF6_64769	Hs.17118	Q9HAF1	MEAF6 C1orf149 CENP-28 EAF6
567_YWHAB_7529	Hs.643544	P31946	YWHAB
568_CCNI_10983	Hs.518827	Q14094	CCNI
569_NAP1L1_4673	Hs.524599	P55209	NAP1L1 NRP
571_CMTM4_146223	Hs.643961	Q8IZR5	CMTM4 CKLFSF4
572_DDIT4_54541	Hs.523012	Q9NX09	DDIT4 REDD1 RTP801
574_SLC19A2_10560	Hs.30246	O60779	SLC19A2 THT1 TRMA
576_H3F3B_3021	Hs.180877	P84243	H3-3A H3.3A H3F3 H3F3A PP781; H3-3B H3.3B
58_RPL12_6136	Hs.408054	P30050	RPL12
580_HMGB1_3146	Hs.434102	P09429	HMGB1 HMG1
581_PDCD6IP_10015	Hs.475896	Q8WUM4	PDCD6IP AIP1 ALIX KIAA1375
583_RPL9_6133	Hs.412370	P32969	RPL9 OK/SW-cl.103; RPL9P7; RPL9P8; RPL9P9
584_TUBA1C_84790	Hs.652390	Q9BQE3	TUBA1C TUBA6
585_RPS24_6229	Hs.284286	P62847	RPS24
587_BTF3_689	Hs.591768	P78410	BTN3A2 BT3.2 BTF3 BTF4
588_TPT1_7178	Hs.374596	P13693	TPT1
589_FDPS_2224	Hs.335918	P14324	FDPS FPS KIAA1293
59_MLPH_79083	Hs.102406	Q9BV36	MLPH SLAC2A
590_PSMA1_5682	Hs.102798	P25786	PSMA1 HC2 NU PROS30 PSC2
592_NET1_10276	Hs.25155	Q7Z628	NET1 ARHGEF8
593_NUDT9_53343	Hs.149500	Q9BW91	NUDT9 NUDT10 PSEC0099 UNQ3012/PRO977
596_RPS23_6228	Hs.527193	P62266	RPS23
598_GALNT7_51809	Hs.548088	Q86SF2	GALNT7
599_COX7A2L_9167	Hs.339639	O14548	COX7A2L COX7AR COX7RP
6_EPCAM_4072	Hs.542050	P16422	EPCAM GA733-2 M1S2 M4S1 MIC18 TACSTD1
60_RPL36A_6173	Hs.432485	P83881	RPL36A RPL44 GIG15 MIG6
602_REEP3_221035	Hs.499833	Q6NUK4	REEP3 C10orf74
603_PDCD7_10081	Hs.458596	Q8N8D1	PDCD7
604_RPL10L_140801	Hs.308332	Q96L21	RPL10L
605_YTHDF1_54915	Hs.11747	Q9BYJ9	YTHDF1 C20orf21
606_UBL5_59286	Hs.534477	Q9BZL1	UBL5
607_C20orf30_29058	Hs.472024	Q96A57	TMEM230 C20orf30 HSPC274 UNQ2432/PRO4
608_CCDC6_8030	Hs.591360	Q16204	CCDC6 D10S170 TST1
609_HNRNPD_3184	Hs.480073	Q14103	HNRNPD AUF1 HNRPD
610_USP9X_8239	Hs.77578	Q93008	USP9X DFFRX FAM USP9
611_KIAA1429_25962	Hs.202238	Q69YN4	VIRMA KIAA1429 MSTP054
612_ARHGAP1_392	Hs.138860	Q07960	ARHGAP1 CDC42GAP RHOGAP1
613_FNBP4_23360	Hs.6834	Q8N3X1	FNBP4 FBP30 KIAA1014
614_SNX3_8724	Hs.12102	O60493	SNX3
616_GRP_2922	Hs.153444	O43739	CYTH3 ARNO3 GRP1 PSCD3
618_FKBP5_2289	Hs.407190	Q13451	FKBP5 AIG6 FKBP51
619_NSUN2_54888	Hs.481526	Q08J23	NSUN2 SAKI TRM4
62_RPL39_6170	Hs.558387	P62891	RPL39
622_SNRPD1_6632	Hs.464734	P62316	SNRPD2 SNRPD1
624_PHB2_11331	Hs.504620	Q99623	PHB2 BAP REA
626_GOLGA3_2802	Hs.507333	Q08378	GOLGA3
628_NFIB_4781	Hs.644095	O00712	NFIB
629_RBM5_10181	Hs.439480	P52756	RBM5 H37 LUCA15
630_AHCYL1_10768	Hs.485365	O43865	AHCYL1 DCAL IRBIT XPVKONA

Supplemental material

BMJ Publishing Group Limited (BMJ) disclaims all liability and responsibility arising from any reliance placed on this supplemental material which has been supplied by the author(s)

J Immunother Cancer

631_HEXIM1_10614	Hs.730687	O94992	HEXIM1 CLP1 EDG1 HIS1 MAQ1
632_NOS1_4842	Hs.466662	P29475	NOS1
633_USP54_159195	Hs.657355	Q70EL1	USP54 C10orf29
634_MRPL41_64975	Hs.44017	Q8IXM3	MRPL41 BMRP MRPL27 RPML27 PIG3
635_GUCY1A3_2982	Hs.24258	Q02108	GUCY1A1 GUC1A3 GUCSA3 GUCY1A3
638_RYBP_23429	Hs.7910	Q8N488	RYBP DEDAF YEAF1
639_HECTD1_25831	Hs.708017	Q9ULT8	HECTD1 KIAA1131
64_COX6C_1345	Hs.351875	P09669	COX6C
640_VPS35_55737	Hs.454528	Q96QK1	VPS35 MEM3 TCCCTA00141
641_TMSB4X_7114	Hs.437277	P62328	TMSB4X TB4X THYB4 TMSB4
642_ERH_2079	Hs.509791	P84090	ERH
644_WASF2_10163	Hs.469244	Q9Y6W5	WASF2 WAVE2
646_FASTK_10922	Hs.647094	Q14296	FASTK
647_GOLGB1_2804	Hs.213389	Q14789	GOLGB1
649_TCP1_6950	Hs.363137	P17987	TCP1 CCT1 CCTA
65_ZKSCAN1_7586	Hs.615360	P17029	ZKSCAN1 KOX18 ZNF139 ZNF36
650_SQLE_6713	Hs.71465	Q14534	SQLE ERG1
653_NUFIP2_57532	Hs.462598	Q7Z417	NUFIP2 KIAA1321 PIG1
654_RPS3_6188	Hs.356572	P23396	RPS3 OK/SW-cl.26
656_ANK3_288	Hs.499725	Q12955	ANK3
657_LRPAP1_4043	Hs.533136	P30533	LRPAP1 A2MRAP
658_CASC4_113201	Hs.512867	Q6P4E1	CASC4 UNQ2573/PRO6308
660_GRB10_2887	Hs.164060	Q13322	GRB10 GRBIR KIAA0207
661_EDF1_8721	Hs.174050	O60869	EDF1
662_AUTS2_26053	Hs.21631	Q8WXX7	AUTS2 KIAA0442
663_ZFAND6_54469	Hs.730626	Q6FIF0	ZFAND6 AWP1 ZA20D3 HT032
665_SLC2A4RG_56731	Hs.435126	Q9NR83	SLC2A4RG HDBP1
666_RRAGA_10670	Hs.702275	Q7L523	RRAGA
667_RNF130_55819	Hs.484363	Q86XS8	RNF130
669_IFT57_55081	Hs.412196	Q9NWB7	IFT57 DERP8 ESRRBL1 HIPPI
672_PTP4A1_7803	Hs.227777	Q93096	PTP4A1 PRL1 PTPCAAX1
674_HIST1H2BL_8340	Hs.137594	Q99880	H2BC13 H2BFC HIST1H2BL
675_SOCS2_8835	Hs.485572	O14508	SOCS2 CIS2 SSI2 STATI2
676_EIF3A_8661	Hs.523299	P56537	EIF6 EIF3A ITGB4BP OK/SW-cl.27
677_ZNF598_90850	Hs.343828	Q86UK7	ZNF598
679_SELS_55829	Hs.32148	Q9BQE4	SELENOS SELS VIMP AD-015 SBBI8
68_GNAS_2778	Hs.125898	Q5JWF2	GNAS GNAS1
681_RPSA_3921	Hs.449909	P08865	RPSA LAMBR LAMR1
682_ARFGAP3_26286	Hs.685225	Q9NP61	ARFGAP3 ARFGAP1
683_MRPL3_11222	Hs.205163	P09001	MRPL3 MRL3 RPML3
692_ANAPC5_51433	Hs.7101	Q9UJX4	ANAPC5 APC5
693_ZMAT2_153527	Hs.350194	Q96NC0	ZMAT2
694_GCN1L1_10985	Hs.298716	Q92616	GCN1 GCN1L1 KIAA0219
696_ECI2_10455	Hs.15250	O75521	ECI2 DRS1 HCA88 PECI
697_N4BP2L2_10443	Hs.507680	Q92802	N4BP2L2 CG005 PFAAP5
698_SF1_7536	Hs.502829	Q13285	NR5A1 AD4BP FTZF1 SF1
699_RGPD5_84220	Hs.469630	Q99666	RGPD5 RANBP2L1 RGP5 RGP7 RGPD7; RGPD6
70_RPL32_6161	Hs.265174	P62910	RPL32 PP9932
700_CBX1_10951	Hs.77254	P83916	CBX1 CBX
702_ZNF395_55893	Hs.435535	Q9H8N7	ZNF395 HDBP2 PBF

Supplemental material

BMJ Publishing Group Limited (BMJ) disclaims all liability and responsibility arising from any reliance placed on this supplemental material which has been supplied by the author(s)

J Immunother Cancer

704_XRCC6_2547	Hs.292493	P12956	XRCC6 G22P1
706_CYHR1_50626	Hs.459379	Q6ZMK1	CYHR1 KIAA0496
707_MORF4L1_10933	Hs.374503	Q9UBU8	MORF4L1 MRG15 FWP006 HSPC008 HSPC061
708_CYTH1_9267	Hs.191215	Q15438	CYTH1 D17S811E PSCD1
709_NAMPT_10135	Hs.489615	P43490	NAMPT PBEF PBEF1
71_SERF2_10169	Hs.424126	P84101	SERF2 FAM2C
711_ENY2_56943	Hs.492555	Q9NPA8	ENY2 DC6
712_HIST1H2AK_8330	Hs.558421	P0C0S8	H2AC11 H2AFP HIST1H2AG; H2AC13 H2AFC H
713_SERBP1_26135	Hs.730604	Q8NC51	SERBP1 PAIRBP1 CGI-55
714_MYH9_4627	Hs.474751	P35579	MYH9
716_GTF3C6_112495	Hs.418520	Q969F1	GTF3C6 C6orf51 CDA020 NPD020
718_HIST1H4C_8364	Hs.46423	P62805	H4C1 H4/A H4FA HIST1H4A; H4C2 H4/I H4FI H
719_FAM156A_29057	Hs.653131	Q8NDB6	FAM156A TMEM29 PP12994 PRO0659; FAM1
720_SNRPC_6631	Hs.1063	P09234	SNRPC
721_HADH_3033	Hs.438289	Q99714	HSD17B10 ERAB HADH2 MRPP2 SCHAD SDR5(
724_CCT3_7203	Hs.491494	P49368	CCT3 CCTG TRIC5
726_HIPK2_28996	Hs.397465	Q9H2X6	HIPK2
727_JUN_3725	Hs.696684	P05412	JUN
729_HSPA8_3312	Hs.180414	P11142	HSPA8 HSC70 HSP73 HSPA10
73_SORD_6652	Hs.878	Q00796	SORD
730_ACAD9_28976	Hs.567482	Q9H845	ACAD9
731_F5_2153	Hs.352638	P12259	F5
732_NUP62_23636	Hs.574492	P37198	NUP62
734_MRPL51_51258	Hs.55847	Q4U2R6	MRPL51 MRP64 CDA09 HSPC241
735_ATP6V1A_523	Hs.477155	P38606	ATP6V1A ATP6A1 ATP6V1A1 VPP2
736_PMPCB_9512	Hs.184211	O75439	PMPCB MPPB
738_SPATS2L_26010	Hs.120323	Q9NUQ6	SPATS2L DNAPTP6 SP1224
740_PA2G4_5036	Hs.524498	Q9UQ80	PA2G4 EBP1
741_DDX5_1655	Hs.279806	P17844	DDX5 G17P1 HELR HLR1
744_C21orf59_56683	Hs.5811	P57076	CFAP298 C21orf48 C21orf59
746_S100A10_6281	Hs.143873	P60903	S100A10 ANX2LG CAL1L CLP11
747_TSPAN8_7103	Hs.170563	P19075	TSPAN8 TM4SF3
748_C22orf28_51493	Hs.474643	Q9Y3I0	RTCB C22orf28 HSPC117
749_STEAP2_261729	Hs.489051	Q8NFT2	STEAP2 PCANAP1 STAMP1 UNQ6507/PRO232(
75_RPS15A_6210	Hs.370504	P62244	RPS15A OK/SW-cl.82
750_NACAP1_83955	Hs.567608	Q9BZK3	NACA4P NACAP1 FKSG17
751_TRAM1_23471	Hs.491988	Q9Y6Q9	NCOA3 AIB1 BHLHE42 RAC3 TRAM1
752_BCAP31_10134	Hs.522817	P51572	BCAP31 BAP31 DXS1357E
754_AZGP1_563	Hs.546239	P25311	AZGP1 ZAG ZNGP1
755_EHF_26298	Hs.653859	Q9NZC4	EHF ESE3 ESE3B ESEJ
757_BAG1_573	Hs.377484	Q99933	BAG1 HAP
758_C12orf23_90488	Hs.257664	Q8WUH6	TMEM263 C12orf23
759_PSMD4_5710	Hs.505059	P55036	PSMD4 MCB1
76_RPL30_6156	Hs.400295	P62888	RPL30
760_TALDO1_6888	Hs.438678	P37837	TALDO1 TAL TALDO TALDOR
761_MCM3_4172	Hs.179565	P25205	MCM3
763_SRP14_6727	Hs.533732	P37108	SRP14
764_ATP5J2_9551	Hs.521056	P56134	ATP5MF ATP5J2 ATP5JL
765_ANKRD36_375248	Hs.541894	Q96IX9	ANKRD36BP1 ANKRD26L1
766_RPS4Y2_140032	Hs.367761	Q8TD47	RPS4Y2 RPS4Y2P

Supplemental material

BMJ Publishing Group Limited (BMJ) disclaims all liability and responsibility arising from any reliance placed on this supplemental material which has been supplied by the author(s)

J Immunother Cancer

767_DDX50_79009	Hs.522984	Q9BQ39	DDX50
768_NUCKS1_64710	Hs.213061	Q9H1E3	NUCKS1 NUCKS JC7
769_PRDX6_9588	Hs.120	P30041	PRDX6 AOP2 KIAA0106
77_SP100_6672	Hs.369056	P23497	SP100
770_ODC1_4953	Hs.467701	P11926	ODC1
771_HNRNPR_10236	Hs.373763	O43390	HNRNPR HNRPR
772_MARS_4141	Hs.632707	P56192	MARS
773_PHF8_23133	Hs.133352	Q9UPP1	PHF8 KIAA1111 ZNF422
775_KIAA2013_90231	Hs.520094	Q8IYS2	KIAA2013
776_PLA2G16_11145	Hs.502775	P53816	PLAAT3 HRASLS3 HREV107 PLA2G16
778_FAM120AOS_158293	Hs.350364	Q5T036	FAM120AOS C9orf10OS
779_POLR2L_5441	Hs.441072	P62875	POLR2L
78_RPL11_6135	Hs.719951	P62913	RPL11
781_ATP1A1_476	Hs.371889	P05023	ATP1A1
782_MRPL20_55052	Hs.730767	Q9BYC9	MRPL20
783_RAMP1_10267	Hs.471783	O60894	RAMP1
784_FBL_2091	Hs.299002	Q9UKA2	FBXL4 FBL4 FBL5
786_SNRPD2_6633	Hs.515472	P62316	SNRPD2 SNRPD1
787_ERRFI1_54206	Hs.605445	Q9UJM3	ERRFI1 MIG6
788_IVNS1ABP_10625	Hs.497183	Q9Y6Y0	IVNS1ABP ARA3 FLARA3 KIAA0850 KLHL39 NS
790_STK24_8428	Hs.508514	Q9Y6E0	STK24 MST3 STK3
791_HIST1H2BF_8343	Hs.182137	P62807	H2BC4 H2BFL HIST1H2BC; H2BC6 H2BFH HIST
795_UQCRC2_7385	Hs.528803	P22695	UQCRC2
797_MARCH6_10299		O60337	MARCH6 KIAA0597 RNF176 TEB4
799_MAPRE1_22919	Hs.472437	Q15691	MAPRE1
80_RPL27A_6157	Hs.523463	P46776	RPL27A
800_FAM129A_116496	Hs.518662	Q9BZQ8	NIBAN1 C1orf24 FAM129A NIBAN GIG39
801_GRSF1_2926	Hs.309763	Q12849	GRSF1
803_LDHA_3939	Hs.2795	P00338	LDHA PIG19
805_WSB2_55884	Hs.728135	Q9NYS7	WSB2
806_CSDE1_7812	Hs.69855	O75534	CSDE1 D1S155E KIAA0885 NRU UNR
807_SNRPG_6637	Hs.516076	P62308	SNRPG PBSCG
809_PDS5A_23244	Hs.331431	Q29RF7	PDS5A KIAA0648 PDS5 PIG54
81_RPS8_6202	Hs.512675	P62241	RPS8 OK/SW-cl.83
811_H3F3C_440093	Hs.448697	Q6NXT2	H3F3C
814_CASP9_842	Hs.329502	P55211	CASP9 MCH6
816_ZFAND5_7763	Hs.406096	O76080	ZFAND5 ZA20D2 ZNF216
818_ILF3_3609	Hs.465885	Q12906	ILF3 DRBF MPHOSPH4 NF90
819_ZFP36_7538	Hs.503093	P26651	ZFP36 G0S24 NUP475 RNF162A TIS11A TTP
821_RBM39_9584	Hs.282901	Q14498	RBM39 HCC1 RNPC2
822_RPS27L_51065	Hs.108957	Q71UM5	RPS27L
823_UBE2E3_10477	Hs.470804	Q969T4	UBE2E3 UBCE4 UBCH9
826_RSRC2_65117	Hs.432996	Q7L4I2	RSRC2
827_PRR11_55771	Hs.631750	Q96HE9	PRR11
828_HEBP1_50865	Hs.642618	Q9NRV9	HEBP1 HBP
830_ZNF664_144348	Hs.524828	Q8N3J9	ZNF664 ZFOC1 ZNF176
831_CCT7_10574	Hs.368149	Q99832	CCT7 CCTH NIP7-1
832_RPL3_6122	Hs.438227	P39023	RPL3 OK/SW-cl.32
833_ZMPSTE24_10269	Hs.132642	O75844	ZMPSTE24 FACE1 STE24
834_SRSF4_6429	Hs.469970	Q08170	SRSF4 SFRS4 SRP75

836_TBRG1_84897	Hs.436410	Q3YBR2	TBRG1 NIAM
837_BBX_56987	Hs.124366	Q8WY36	BBX HBP2
839_IL13RA1_3597	Hs.496646	P78552	IL13RA1 IL13R IL13RA
840_HIST1H2AM_8336	Hs.134999	P0C0S8	H2AC11 H2AFP HIST1H2AG; H2AC13 H2AFC HI
841_ASNS_440	Hs.489207	P08243	ASNS TS11
844_FNBP1L_54874	Hs.134060	Q5T0N5	FNBP1L C1orf39 TOCA1
847_TMC5_79838	Hs.115838	Q6UXY8	TMC5 UNQ8238/PRO33604
849_BASP1_10409	Hs.201641	P80723	BASP1 NAP22
85_RPL38_6169	Hs.380953	P63173	RPL38
852_RAI1_10743	Hs.55148	Q7Z5J4	RAI1 KIAA1820
853_NBR1_4077	Hs.277721	Q14596	NBR1 1A13B KIAA0049 M17S2 MIG19
854_SORL1_6653	Hs.368592	Q92673	SORL1 C11orf32
855_PDCD4_27250	Hs.711490	Q53EL6	PDCD4 H731
856_HES1_3280	Hs.250666	Q14469	HES1 BHLHB39 HL HRY
857_RPL15_6138	Hs.381219	P61313	RPL15 EC45 TCBAP0781
859_KIAA1522_57648	Hs.591502	Q9P206	KIAA1522
861_PNN_5411	Hs.409965	Q9H307	PNN DRS MEMA
865_PSME1_5720	Hs.75348	Q06323	PSME1 IFI5111
866_MYL12A_10627	Hs.190086	P19105	MYL12A MLCB MRLC3 RLC
867_KHDRBS1_10657	Hs.445893	Q07666	KHDRBS1 SAM68
868_MPZL1_9019	Hs.493919	O95297	MPZL1 PZR UNQ849/PRO1787
869_COX7B_1349	Hs.522699	P24311	COX7B
87_NBEAL1_65065	Hs.408054	Q6ZS30	NBEAL1 ALS2CR16 ALS2CR17
870_CBX3_11335	Hs.381189	Q13185	CBX3
872_RASD1_51655	Hs.25829	Q9Y272	RASD1 AGS1 DEXRAS1
873_SHROOM3_57619	Hs.702168	Q8TF72	SHROOM3 KIAA1481 SHRML MSTP013
874_C15orf24_56851	Hs.160565	Q9NPA0	EMC7 C11orf3 C15orf24 HT022 UNQ905/PRO:
876_SON_6651	Hs.517262	P18583	SON C21orf50 DBP5 KIAA1019 NREBP HSPC31
877_KCTD3_51133	Hs.335139	Q9Y597	KCTD3
879_CREB3L4_148327	Hs.372924	Q8TEY5	CREB3L4 AIBZIP CREB4 JAL
88_RPL22_6146	Hs.515329	P35268	RPL22
883_UBE2C_11065	Hs.93002	O00762	UBE2C UBCH10
885_TBCD_6904	Hs.464391	Q9BTW9	TBCD KIAA0988 SSD1 TFCD PP1096
887_DNAJC10_54431	Hs.516632	Q8IXB1	DNAJC10 ERDJ5 UNQ495/PRO1012
888_CKS1B_1163	Hs.374378	P61024	CKS1B CKS1 PNAS-143 PNAS-16
889_CSNK1E_1454	Hs.474833	P49674	CSNK1E
890_RRAGC_64121	Hs.532461	Q9HB90	RRAGC
891_PTPLAD1_51495	Hs.512973	Q9P035	HACD3 BIND1 PTPLAD1
893_UPF1_5976	Hs.515266	Q92900	UPF1 KIAA0221 RENT1
894_PPP1R16A_84988	Hs.521937	Q96I34	PPP1R16A MYPT3
896_PTCD3_55037	Hs.323489	Q96EY7	PTCD3 MRPS39 TRG15
899_RNF103_7844	Hs.469199	O00237	RNF103 ZFP103
9_RAX2_84839	Hs.532691	Q96IS3	RAX2 QRX RAXL1
90_TXNIP_10628	Hs.533977	Q9H3M7	TXNIP VDUP1
903_AHSA2_130872	Hs.655602	Q719I0	AHSA2P AHSA2
905_MKL2_57496	Hs.49143	Q9ULH7	MRTFB KIAA1243 MKL2
906_GTF3A_2971	Hs.445977	Q92664	GTF3A
907_ACADVL_37	Hs.437178	P49748	ACADVL VLCAD
910_KIAA1191_57179	Hs.730636	Q96A73	KIAA1191 P33MONOX
912_EIF2B1_1967	Hs.728874	Q14232	EIF2B1 EIF2BA

915_SMS_6611	Hs.727552	Q86VZ5	SGMS1 MOB SMS1 TMEM23
916_SUMO2_6613	Hs.546298	P61956	SUMO2 SMT3B SMT3H2
918_MT1G_4495	Hs.433391	P13640	MT1G MT1K MT1M
919_HADHB_3032	Hs.515848	P55084	HADHB MSTP029
92_WDR45L_56270	Hs.132161	Q5MNZ6	WDR45B WDR45L WIPI3
921_RANBP9_10048	Hs.708182	Q96P70	IPO9 IMP9 KIAA1192 RANBP9 HSPC273
922_CEP95_90799	Hs.569713	Q96GE4	CEP95 CCDC45 CEP45
923_MRPS6_64968	Hs.302742	P82932	MRPS6 C21orf101 RPMS6
924_IRX3_79191	Hs.499205	P78415	IRX3 IRXB1
928_LOC653061_653061	Hs.547454		
929_SPARCL1_8404	Hs.62886	Q14515	SPARCL1
93_PABPC3_5042	Hs.458280	Q9H361	PABPC3 PABP3 PABPL3
930_CEBPB_1051	Hs.517106	P17676	CEBPB TCF5 PP9092
932_ATP6V0B_533	Hs.596514	Q99437	ATP6V0B ATP6F
933_VCP_7415	Hs.529782	P55072	VCP
935_HIPK3_10114	Hs.709696	Q9H422	HIPK3 DYRK6 FIST3 PKY
936_SESN3_143686	Hs.120633	P58005	SESN3 SEST3
937_MYL6_4637	Hs.632717	P60660	MYL6
938_HMGN1_3150	Hs.356285	P05114	HMGN1 HMG14
939_RNF220_55182	Hs.456557	Q5VTB9	RNF220 C1orf164
94_SMN1_6606	Hs.535788	Q16637	SMN1 SMN SMNT; SMN2 SMNC
940_LIMCH1_22998	Hs.335163	Q9UPQ0	LIMCH1 KIAA1102
941_PSMC1_5700	Hs.356654	P62191	PSMC1
942_DNAJA1_3301	Hs.445203	P31689	DNAJA1 DNAJ2 HDJ2 HSJ2 HSPF4
946_NKTR_4820	Hs.529509	P30414	NKTR
947_HSD17B12_51144	Hs.132513	Q53GQ0	HSD17B12 SDR12C1
948_IMMT_10989	Hs.148559	Q16891	IMMT HMP MIC60 MINOS2 PIG4 PIG52
949_DNAJB6_10049	Hs.593923	O75190	DNAJB6 HSJ2 MRJ MSJ1
95_AHNAK_79026	Hs.502756	Q8IVF2	AHNAK2 C14orf78 KIAA2019
950_LOC100287195_100287195	Hs.528369		
951_ENTPD6_955	Hs.500375	O75354	ENTPD6 CD39L2 IL6ST2
954_FAM177A1_283635	Hs.446357	Q8N128	FAM177A1 C14orf24
955_TCEA1_6917	Hs.491745	P23193	TCEA1 GTF2S TFIIS
956_RBM14_10432	Hs.714949	Q96PK6	RBM14 SIP
957_COPB2_9276	Hs.75724	P35606	COPB2
958_SAT2_112483	Hs.10846	Q96QD8	SLC38A2 ATA2 KIAA1382 SAT2 SNAT2
959_NCOR2_9612	Hs.137510	Q9Y618	NCOR2 CTG26
96_ND1_4535	Hs.511386	P03886	MT-ND1 MTND1 NADH1 ND1
960_SEPT2_4735		Q15019	SEPTIN2 DIFF6 KIAA0158 NEDD5 SEPT2
961_GGA1_26088	Hs.499158	Q9UJY5	GGA1
963_MUT_4594	Hs.485527	P22033	MMUT MUT
965_DAZAP1_26528	Hs.222510	Q96EP5	DAZAP1
966_TARS_6897	Hs.481860	P26639	TARS1 TARS
967_FAM111A_63901	Hs.150651	Q96PZ2	FAM111A KIAA1895
968_CXCR4_7852	Hs.593413	P61073	CXCR4
969_C8orf4_56892	Hs.591849	Q9NR00	TCIM C8orf4 TC1
972_AK2_204	Hs.470907	P54819	AK2 ADK2
973_TTC19_54902	Hs.462316	Q6DKK2	TTC19
974_EIF3L_51386	Hs.446852	Q9Y262	EIF3L EIF3EIP EIF3S6IP HSPC021 HSPC025 MST
976_FOXP1_27086	Hs.431498	Q9H334	FOXP1 HSPC215

977_SECISBP2_79048	Hs.59804	Q96T21	SECISBP2 SBP2
978_CHERP_10523	Hs.631627	Q8IWX8	CHERP DAN26 SCAF6
981_HIST3H2A_92815	Hs.26331	Q7L7L0	HIST3H2A
982_MRPL32_64983	Hs.50252	Q6P1L8	MRPL14 MRPL32 RPML32
983_PURB_5814	Hs.728785	Q96QR8	PURB
985_CALD1_800	Hs.490203	Q05682	CALD1 CAD CDM
987_DDX47_51202	Hs.719938	Q9H0S4	DDX47
989_HSD17B4_3295	Hs.406861	P51659	HSD17B4 EDH17B4 SDR8C1
99_RPS18_6222	Hs.655329	P62269	RPS18 D6S218E
990_AKAP9_10142	Hs.651221	Q99996	AKAP9 AKAP350 AKAP450 KIAA0803
991_TSFM_10102	Hs.632704	P43897	TSFM
994_GAR1_54433	Hs.69851	Q9NY12	GAR1 NOLA1
995_EED_8726	Hs.503510	O75530	EED
997_ZNF275_10838	Hs.348963	Q9NSD4	ZNF275
998_SLC38A10_124565	Hs.352240	Q9HBR0	SLC38A10 PP1744
999_MRP63_78988	Hs.458367	Q9BQC6	MRPL57 MRP63
ADT14		Q9NZN5	ARHGEF12 KIAA0382 LARG
ADT2		P35609	ACTN2
ADT20		Q9UNZ2	NSFL1C UBXN2C
ADT26		P35749	MYH11 KIAA0866
ADT28		A0A024R7P5	LOC388524 hCG_20807
ADT3		Q99743	NPAS2 BHLHE9 MOP4 PASD4
ADT6		Q13368	MPP3 DLG3
ADT9		Q15714	TSC22D1 KIAA1994 TGFB1I4 TSC22 hucep-2
ANO1_AS1_T062911_G014510_1_447_1019_573			
ANO1_AS1_T062911_G014510_2_398_895_498			
BOLA3_AS1_T191973_G044207_1_1427_1822_396			
CAT1367_T060449_G014057_1_30_1331_1302			
CAT1367_T060449_G014057_2_532_807_276			
CAT1449.1_T070828_G016390_1_238_720_483			
CAT1449.1_T070828_G016390_2_401_652_252			
CAT151.3_T027960_G006287_2_15387_15731_345			
CAT1651_T102861_G024234_1_1199_1891_693			
CAT1686_T107057_G025268_1_5122_5934_813			
CAT1917.2_T144453_G033626_1_2303_2959_657			
CAT1942_T149369_G034642_1_6407_7270_864			
CAT1968.2_T153055_G035480_2_2275_2736_462			
CAT239_T189457_G043567_1_3047_3727_681			
CAT297_T196839_G045377_1_2510_3112_603			
CAT446.1_T250066_G057497_1_562_1254_693			
CAT583_T271074_G062826_1_2272_2871_600			
CAT668.2_T283555_G066082_1_5822_6478_657			
CAT668.2_T283555_G066082_2_6783_7376_594			
CTA11		Q9UBF1	MAGEC2 HCA587 MAGEE1
CTA13		Q9UNA0	ADAMTS5 ADAMTS11 ADMP2
CTA15		Q8NEN9	PDZD8 PDZK8
CTA16		Q969F0	FATE1 FATE
CTA18		Q13136	PPFIA1 LIP1
CTA2		Q16385	SSX2 SSX2A; SSX2B
CTA21		P43366	MAGEB1 MAGEL1 MAGEXP

Supplemental material

BMJ Publishing Group Limited (BMJ) disclaims all liability and responsibility arising from any reliance placed on this supplemental material which has been supplied by the author(s)

J Immunother Cancer

CTA22	O15479	MAGEB2
CTA24	Q16384	SSX1
CTA27	Q9UNF1	MAGED2 BCG1
CTA28	Q9UHG2	PCSK1N
CTA5	O60224	SSX4 SSX4A; SSX4B
CTA6	Q9GZY0	NXF2 TAPL2; NXF2B
CTA8	Q9HD64	XAGE1A GAGED2 XAGE1; XAGE1B; XAGE1C; XA
FAM83H_AS1.5_T353728_G083462_1_2453_3277_825		
FBXL19_AS1_T130509_G030577_1_4499_4918_420		
LINC00675.4_T141809_G033025_1_1138_1524_387		
PCA10	P01619	IGKV3-20
PCA13	Q9H4A3	WNK1 HSN2 KDP KIAA0344 PRKWNK1
PCA14	Q86UV5	USP48 USP31
PCA19	Q15435	PPP1R7 SDS22
PCA22	O15031	PLXNB2 KIAA0315
PCA27	P68104	EEF1A1 EEF1A EF1A LENG7
PCA29	Q14149	MORC3 KIAA0136 NXP2 ZCWCC3
PCA6	P29144	TPP2
PCAT1_T351126_G082910_1_3108_3569_462		
PCAT1_T351126_G082910_2_1371_1655_285		
PRCAT104.1_T230582_G053084_2_4907_5623_717		
PRCAT104.3_T230574_G053084_2_6009_6725_717		
PRCAT104.4_T230577_G053084_1_1393_2109_717		
PRCAT104.5_T230585_G053084_2_4999_5715_717		
PRCAT104.7_T230583_G053084_2_4930_5646_717		
PRCAT11.3_T317393_G074313_1_1665_2435_771		
PRCAT139_T035222_G008006_2_2852_3289_438		
PRCAT182_T137385_G032197_1_4841_5419_579		
PRCAT188.2_T382727_G090657_1_4263_4976_714		
PRCAT188.2_T382727_G090657_2_1887_2474_588		
PRCAT236_T273012_G063396_1_1305_2057_753		
PRCAT28.1_T183157_G042036_1_3585_4718_1134		
PRCAT28.1_T183157_G042036_2_4136_5131_996		
PRCAT28.4_T183159_G042036_1_1382_2515_1134		
PRCAT28.4_T183159_G042036_2_1933_2928_996		
PRCAT282_T344692_G081083_2_2771_2995_225		
PRCAT41_T315818_G074087_2_4464_4820_357		
PRO10	P40121	CAPG AFCP MCP
PRO11	P23280	CA6
PRO14	Q02224	CENPE
PRO16	Q9ULV8	CBLC CBL3 RNF57
PRO18	Q12802	AKAP13 BRX HT31 LBC
PRO23	Q7Z7E8	UBE2Q1 NICE5 UBE2Q PRO3094
PRO25	Q9NP31	SH2D2A SCAP TSAD VRAP
PRO29	O75521	ECI2 DRS1 HCA88 PECI
PRO3	P05067	APP A4 AD1
PRO30	Q9HCK8	CHD8 HELSNF1 KIAA1564
PRO31	Q9UNE7	STUB1 CHIP PP1131
PRO37	Q9BXL7	CARD11 CARMA1
PRO38	P15311	EZR VIL2

Supplemental material

BMJ Publishing Group Limited (BMJ) disclaims all liability and responsibility arising from any reliance placed on this supplemental material which has been supplied by the author(s)

J Immunother Cancer

PRO40   Q92791   P3H4 LEPREL4 NOL55 SC65
SPATA41_T123512_G029083_1_801_1718_918
SPATA41_T123512_G029083_2_2954_3229_276

IST1H4B; H4C3 H4/G H4FG HIST1H4C; H4C4 H4/B H4FB HIST1H4D; H4C5 H4/J H4FJ HIST1H4E; H4C6 H4/(

IST1H2AI; H2AC15 H2AFD HIST1H2AK; H2AC16 H2AFI HIST1H2AL; H2AC17 H2AFN HIST1H2AM

Supplemental material

BMJ Publishing Group Limited (BMJ) disclaims all liability and responsibility arising from any reliance placed on this supplemental material which has been supplied by the author(s)

J Immunother Cancer

Supplemental material

BMJ Publishing Group Limited (BMJ) disclaims all liability and responsibility arising from any reliance placed on this supplemental material which has been supplied by the author(s)

J Immunother Cancer

IST1H2AI; H2AC15 H2AFD HIST1H2AK; H2AC16 H2AFI HIST1H2AL; H2AC17 H2AFN HIST1H2AM

IST1H4B; H4C3 H4/G H4FG HIST1H4C; H4C4 H4/B H4FB HIST1H4D; H4C5 H4/J H4FJ HIST1H4E; H4C6 H4/G

IST1H2AI; H2AC15 H2AFD HIST1H2AK; H2AC16 H2AFI HIST1H2AL; H2AC17 H2AFN HIST1H2AM

C H4FC HIST1H4F; H4C8 H4/H H4FH HIST1H4H; H4C9 H4/M H4FM HIST1H4I; H4C11 H4/E H4FE HIST1H4J;

H4FC HIST1H4F; H4C8 H4/H H4FH HIST1H4H; H4C9 H4/M H4FM HIST1H4I; H4C11 H4/E H4FE HIST1H4J;

Supplemental material

BMJ Publishing Group Limited (BMJ) disclaims all liability and responsibility arising from any reliance placed on this supplemental material which has been supplied by the author(s)

J Immunother Cancer

H4C12 H4/D H4FD HIST1H4K; H4C13 H4/K H4FK HIST1H4L; H4C14 H4/N H4F2 H4FN HIST2H4 HIST2H4A;

Supplemental material

BMJ Publishing Group Limited (BMJ) disclaims all liability and responsibility arising from any reliance
placed on this supplemental material which has been supplied by the author(s)

J Immunother Cancer

H4C12 H4/D H4FD HIST1H4K; H4C13 H4/K H4FK HIST1H4L; H4C14 H4/N H4F2 H4FN HIST2H4 HIST2H4A;

Supplemental material

BMJ Publishing Group Limited (BMJ) disclaims all liability and responsibility arising from any reliance
placed on this supplemental material which has been supplied by the author(s)

J Immunother Cancer

Supplemental material

BMJ Publishing Group Limited (BMJ) disclaims all liability and responsibility arising from any reliance placed on this supplemental material which has been supplied by the author(s)

J Immunother Cancer

H4C15 H4/O H4FO HIST2H4B; H4-16 HIST4H4

Supplemental material

BMJ Publishing Group Limited (BMJ) disclaims all liability and responsibility arising from any reliance placed on this supplemental material which has been supplied by the author(s)

J Immunother Cancer

Supplemental material

BMJ Publishing Group Limited (BMJ) disclaims all liability and responsibility arising from any reliance
placed on this supplemental material which has been supplied by the author(s)

J Immunother Cancer

H4C15 H4/O H4FO HIST2H4B; H4-16 HIST4H4

Antibody Profiling of Prostate Cancer Patients Between Disease Stages and Following Treatment

Tun Lee Ng and Michael A. Newton

July 07, 2020

Contents

1 Introduction

This supplemental analysis consists of two major sections:

- Section I focuses on characterizing antibody responses to a wide variety of proteins in prostate cancer patients at different stages of the disease.

- Section II focuses on analyzing whether treatments induces different changes in antibody repertoires in individuals over time.

2 Section I: Antibody Responses between Disease Stages

2.1 Preamble

In this section, we consider a study that involved healthy subjects and patients with different stages of prostate cancer

- `new_dx`: newly diagnosed,
- `nmCSPC`: non-metastatic castration-sensitive
- `mCSPC`: metastatic castration-sensitive,
- `nmCRPC`: non-metastatic castration-resistant,
- `mCRPC`: metastatic castration-resistant

Each patient's serum was assayed in a number of replicates, `rep`, which were 1, 2, or 3, for peptide-specific IgG responses using a microarray: 16-mer peptides spanning the amino acid sequences of these 1611 gene products, and overlapping by 12 amino acids, were used to generate the microarray comprising 177,604 peptides. We also considered peptides with fluorescence intensity of at least 2^{12}, and a sliding-window p-value of less than 0.05 (indicating high signal in adjacent peptides), in at least 2 of the 3 technical replicates to be called positive.

We remove patients with `rep` $= 1$. The criterion for a positive call on a peptide for a patient was that they had to meet the signal (fluorescence level) threshold in at least two of the technical replicates. Since this is not possible for patients without technical replicates, we exclude them for consistency.

Note that there were 6 patients who were measured at two different stages of prostate cancer. We removed their earlier-stage records, and finally arrive at 94 distinct patients.

Patient Counts by Disease Stages
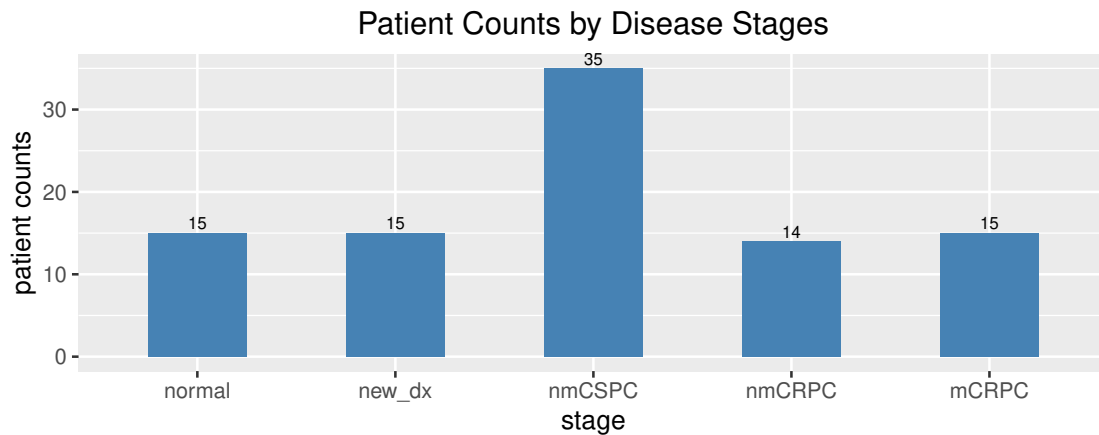
We will utilize both binary calls data and fluorescence levels data to **investigate if patients at different stages of prostate cancer exhibit different antibody responses to certain peptide chains or proteins**. We take $\log_2$ transformation on the fluorescence levels prior to subsequent steps in our analysis.

2.2 Normalization of Fluorescence Data

In order to verify normalization of the fluorescence level, we also plot the boxplots of median (across replicates) $\log_2$ fluorescence level of all peptides for each patient.

Supplemental material

BMJ Publishing Group Limited (BMJ) disclaims all liability and responsibility arising from any reliance placed on this supplemental material which has been supplied by the author(s)

J Immunother Cancer

Boxplots of Peptide Fluorescence Levels for All Patients
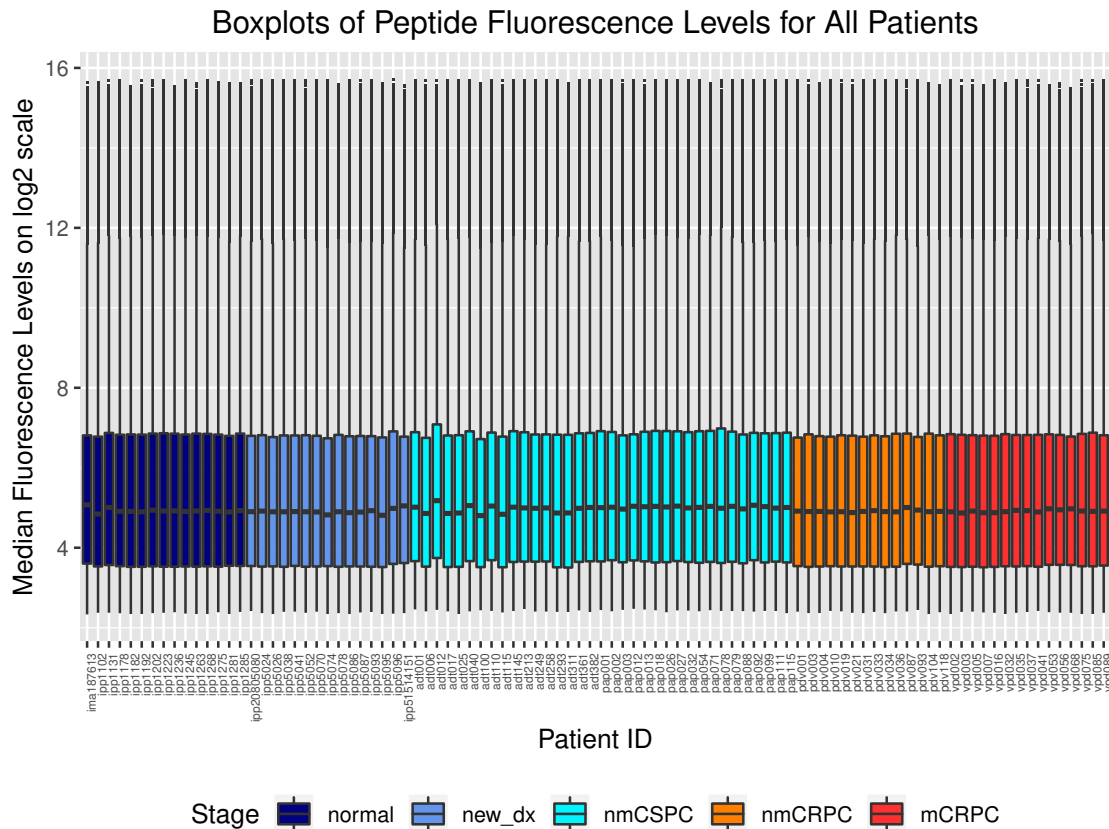
It appears that the fluorescence levels of the peptides are normalized accordingly.

2.3 Reproducibility of Replicates

We have assessed the issue of replicate reproducibility by looking at (Pearson) correlation coefficients between patients' fluorescence levels. Another approach is to measure how much variation the technical replicates are contributing to the overall variation in the data. Everytime when the fluorescence levels were measured (with replicates) for patient's stage effects, there are two sources of random variation at play, namely

- patient/subject `random effect`: this reflects the biological variation of a patient (as opposed to the `fixed effect` term, which would be the cancer stage effect in this experiment)
- (residual) random error: measuring replicates of a patient is itself a source of technical variation.

Specifically,

$$y_{ijk} = \mu + \beta_i + b_j + \epsilon_{ijk},$$

where

- y_{ijk} denotes the $\log_2$ fluorescence level of a replicate,
- μ denotes the grand mean/intercept,
- β_i denotes the fixed effect term, ie. cancer stage, with i indexing the patients' cancer stage,
- b_j denotes the random effect term, ie. individual patient, with j indexing the patients,
- ϵ_{ijk} denotes the (residual) random error of the model, with k indexing the replicates.

3

This is the linear mixed-effects model, which we deploy using the R package `lme4` [Bates et al., 2015]. The model estimates the two sources of variation: $\hat{\sigma}_b^2$ (biological variation) and $\hat{\sigma}_\epsilon^2$ (technical variation). Ideally, biological variation should dominate technical variation since the replicates' variance $\hat{\sigma}_\epsilon^2$ should be minimal. Hence, we are interested in the estimated proportion of random-effect variance to total variance

$$\frac{\hat{\sigma}_b^2}{\hat{\sigma}_b^2 + \hat{\sigma}_\epsilon^2},$$

and we would like to see if this ratio is close to one. For each of the 177,604 peptides, we deploy this mixed-effect model, and plot the histogram of the estimated proportions of variances.

Histogram of peptide–level proportion of random–effect variance to total variance
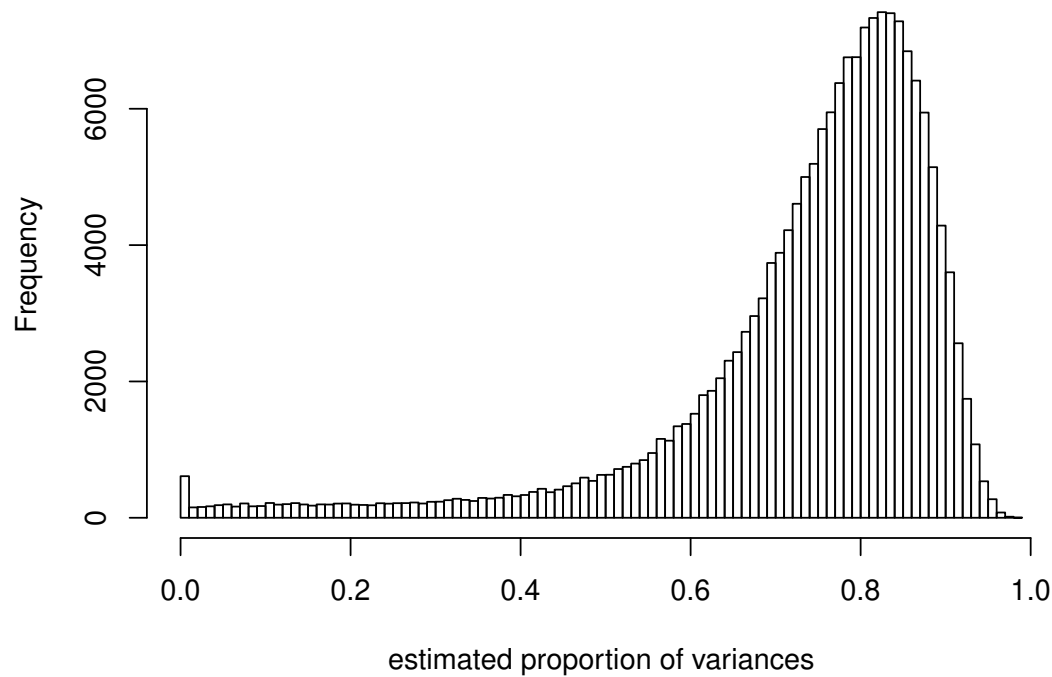
As expected, the histogram amasses at values near one, indicating that most of the variation in the ($\log_2$) fluorescence data is attributable to the biological variation of the patients and not the technical replicates themselves, which also suggests reproducibility of the replicates.

2.4 Tests on Binary Calls

The binary calls on a peptide of a patient are conservative – out of 177,604 peptides, only 37919 of them have at least one call among all patients. To verify that positive calls are associated with stronger signals (remember that `call = 1` if fluorescence levels meet a certain signal threshold in at least two of the replicates), we plot the boxplot of $\log_2$ fluorescence levels for all peptides across all patients, comparing between those that are associated with positive calls and those with zero-calls. Boxplots are plotted with their width reflecting the sample size in each group (positive or zero call).

4

Boxplots of Fluorescence Levels per Peptide per Patient
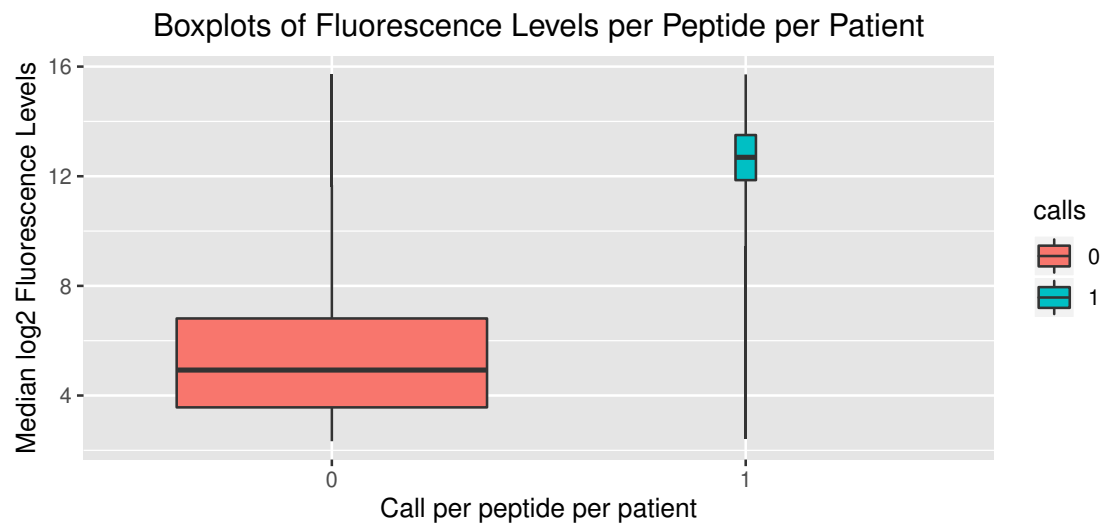
For each of these 37919 peptides, we run a logistic regression based on these binary calls of the patients in order **to determine if calls are significantly different among patients of different cancer stages**.

Specifically, for each of these 37919 peptides, we fit the following model:

$$\text{logit}\left(y_{ij}^{\text{calls}}\right) = \mu + \beta_i + \epsilon_{ij},$$

where

- y_{ij}^{calls} denotes the binary call of the peptide of a patient: 1 if the fluorescence levels meet the signal threshold in at least two replicates of the patient, and 0 otherwise,
- μ denotes the grand mean/intercept,
- β_i denotes the cancer stage,
- ϵ_{ij} denotes the random error of the model, with j indexing the patients,

and compute the deviance p-values: (null_deviance - residual_deviance) $\sim \chi^2$ with 4 degrees of freedom. We plot the histogram of the 37919 p-values.

Logistic Regression Deviance p–values

5
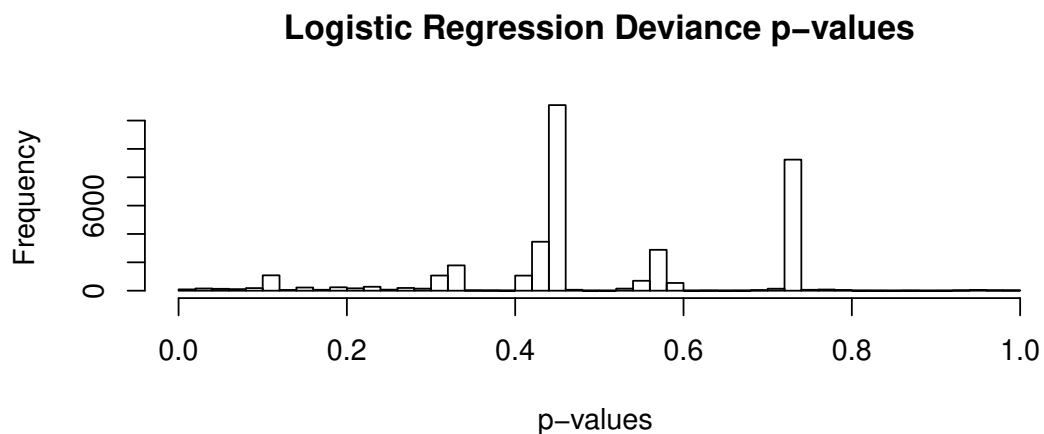
It appears that there are hardly any signals of different calls pattern among patients of different cancer stages, which corroborates with the results in the main manuscript. As expected, after correcting for false discovery rate, no peptides appear to be significant.

2.5 Tests on Fluorescence Levels

We hypothesized that while the overall number of peptides recognized may not change with disease stages, the composition of peptides recognized may be different. In this section, we will instead utilize the fluorescence data to investigate our hypothesis.

We are aware that the $\log_2$ fluorescence data among the prostate cancer patients of different disease stages may violate the assumptions in the normal-theory one-way analysis of variance (ANOVA). For one, the variation of fluorescence levels among patients of different stages may not be similar, as illustrated by the boxplots of the peptide *1324_KIAA1430_57587;185* as an example.

Peptide ID: 1324_KIAA1430_57587;185
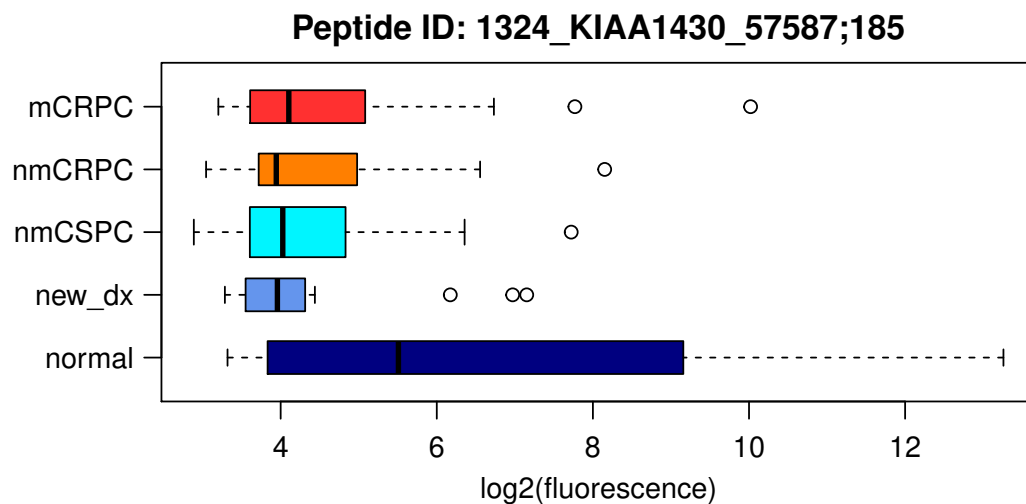
Presence of outliers may also distort inference by the ANOVA. An example would be the peptide *459_CLTC_1213;1421*.

Peptide ID: 459_CLTC_1213;1421

6
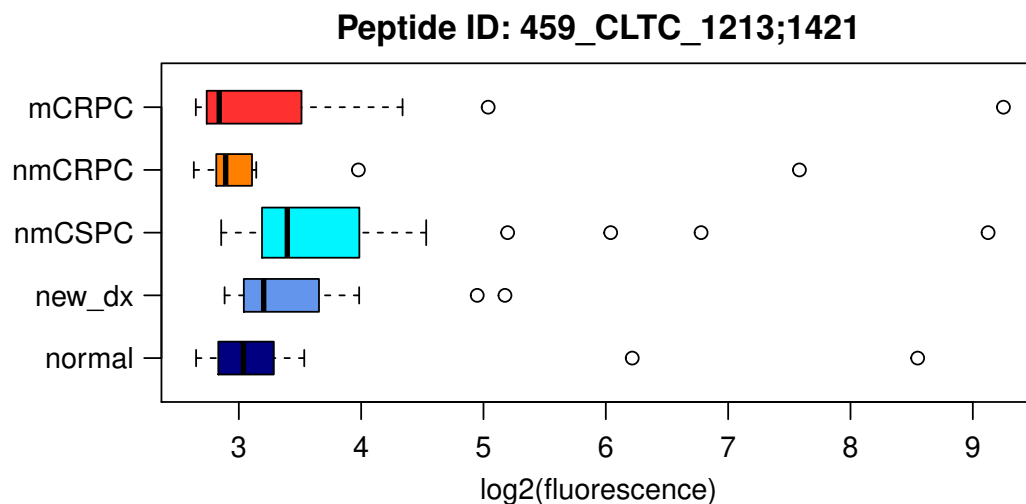
To avoid making any distributional assumptions on the fluorescence levels, we adopt the nonparamteric Kruskal-Wallis test [McDonald, 2014] on each of the 177,604 peptides to test:

H_0: The antibody responce levels (in terms of $\log_2$ fluorescence levels) for each disease stage are stochastically equal, ie. Once the fluorescence levels from all groups are ranked, the probability of an observation from one group being higher than an observation from another group is 0.5.
H_1: The antibody responce levels for at least one disease stage are stochastically dominant than those of other groups in the study.

Note that this is not a test of medians of the fluorescence levels since we are not making any distributional assumptions (shape and spread) on the fluorescence levels [McDonald, 2014].

After getting p-values for all the peptides, we plot the p-value histogram.

p–values distribution for 177604 peptides
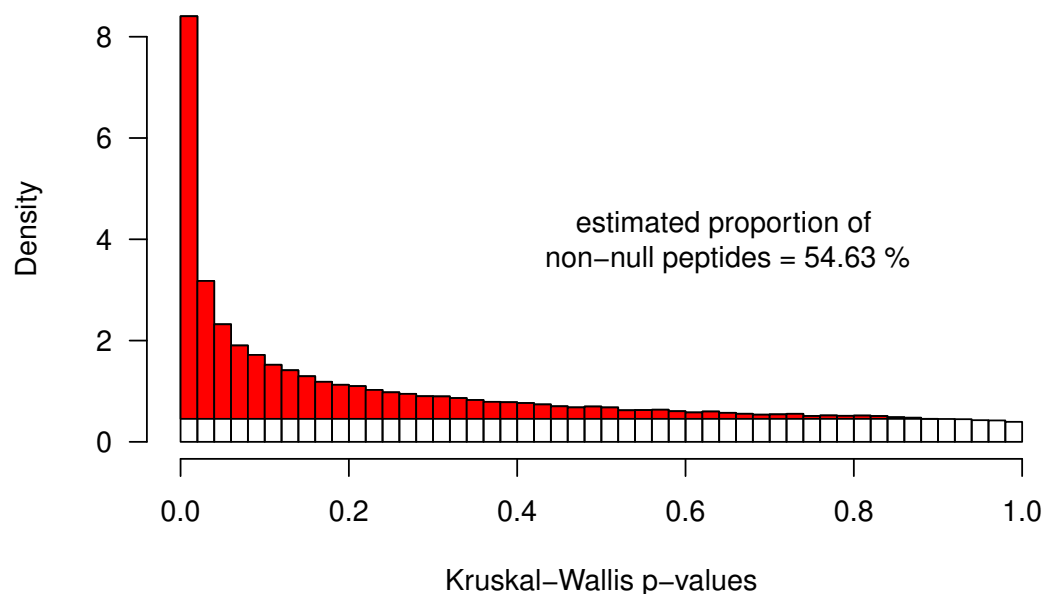
If cancer-stage effect is not present in our peptide array data, then the p-values from the Kruskal-Wallis tests would have a uniform distribution between 0 and 1, and we expect to see a rather flat-shaped histogram of p-values.

However, the p-values histogram exhibits large counts of significant p-values (p-values close to zero), and the shape of histogram flattens off exponentially with larger p-values. Such a large count of significant p-values may not be explained by false discovery alone, and that perhaps cancer-stage effect is indeed present in some of the peptides in our profile. The red-shaded regions of the histogram represents the estimated proportion of non-null peptides in the data based on Storey's q-values [Storey and Tibshirani, 2003] calculation obtained via the R package `fdrtool` [Strimmer, 2008].

We apply the Benjamini-Hochberg (BH) method [Benjamini and Hochberg, 1995] on the Kruskal-Wallis p-values to control for false discovery rate (FDR). The peptide counts at various BH FDR thresholds are tabulated below.

We could obtain a graphical representation to illustrate how the $\log_2$ fluorescence levels differ across different

7

FDR threshold	0.01	0.02	0.03	0.04	0.05	0.06	0.07	0.08	0.09	0.1
Peptide counts	522	3499	7301	10826	13729	16515	18940	21401	23640	25828

cancer stages for these peptides via the Principal Component Analysis (PCA). For each peptide, we remove the grand mean (row mean) of the $\log_2$ fluorescence levels for all patients before performing PCA on the residuals. If there is no cancer-stage effect, we expect these residual $\log_2$ fluorescence to be random noises. Any observed (clustering) patterns among these residual data points reveal the effects of various stages of prostate cancer.

For purpose of uniformity, we also use the same color scheme to distinguish the different stages of cancer patients (notice how the spectrum of colors changes with severity of the cancer stages):

- navy for healthy subjects
- cornflower_blue for `new_dx` newly diagnosed patients
- turquoise for `nmCSPC` patients
- light_pink for `mCSPC` patients – these patients have no technical replicates and are excluded from this analysis
- dark_orange for `nmCSPC` patients
- dark_red for `mCSPC` patients
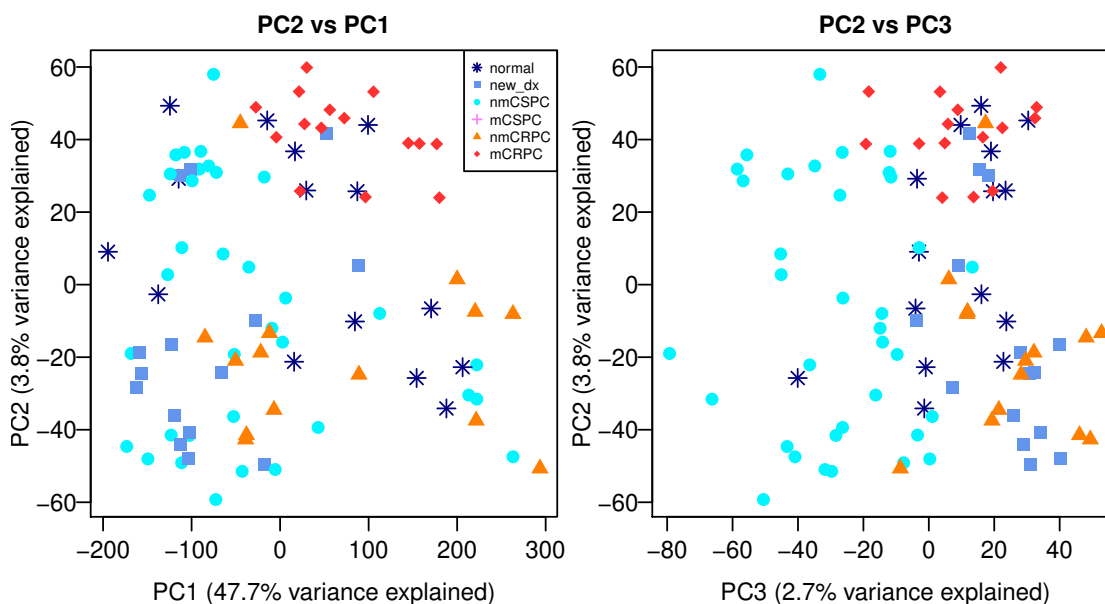
From the "*PC2 vs PC1*" plot, we observe that all mCRPC points are clustered at the topright of the panel, whereas newly-diagnosed and nmCRPC observations hover at the bottom of panel. The percentage of variance explained for each principal component (PC) is shown on the axis. Note that the first principal component manages to capture most of the variation in the data.

8

2.6 Pairwise Comparisons

Based on the Kruskal-Wallis tests, we identified 13729 peptides for which at least one group of patients stochastically dominates patients from the other disease stages at 5% BH FDR. Among these "interesting" peptides, we are interested in making some further pairwise comparisons between the groups of patients. In particular, we would like to analyze if antibody responses are different between cancer patients and healthy subjects. Besides that, the PCA plot has revealed that the mCRPC (worst-case scenario) patients are clustered away from the other patients and it may be interesting to compare how the antibody profiles of the mCRPC (worst-case-scenario) patients could be different from the other subjects. In addition, we would like to make pairwise comparison between consecutive groups of patients in terms of disease severity, namely:

- between mCRPC and nmCRPC patients
- between nmCRPC and nmCSPC patients
- between nmCSPC and newly-diagnosed patients
- between newly-diagnosed and healthy subjects

For each of the 13729 peptides, we will perform a two-sided Wilcoxon-Rank-Sum (henceforth known as Wilcoxon) test [Winner, 2004] for each of the 6 contrasts as mentioned above, to test the following hypothesis:

H_0: The antibody responses of both groups of patients are stochastically equal.
H_1: The antibody responses of both groups of patients are NOT stochastically equal.

Exact p-values are computed for each Wilcoxon test whenever possible – if there are ties in the fluorescence levels, then normal approximation is used to obtain the p-values. After getting the 13729 p-values for each of the 6 contrasts, we plot their p-value density histograms at the same scale.

Density Histograms of the 13729 Wilcoxon p−values
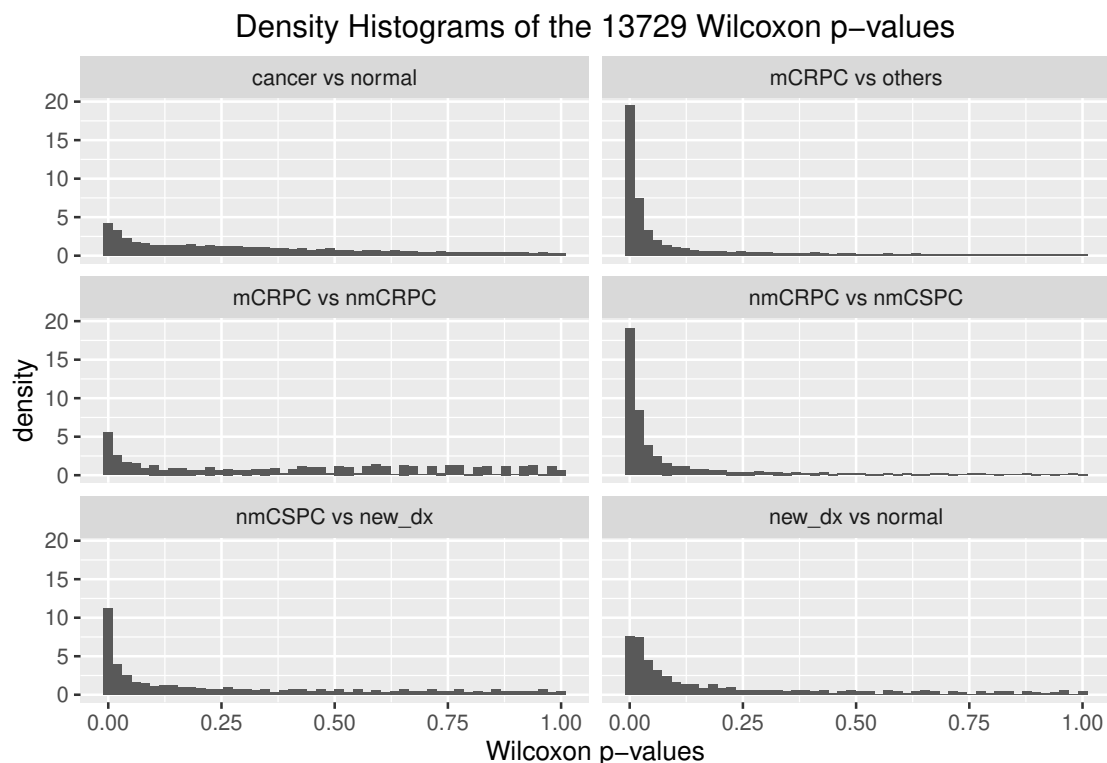
The BH procedure is also performed **on the 13729 Wilcoxon p-values separately for each contrast** to control FDR within each contrast (at 5%). On top of that, we also require at least a two-fold difference between the medians of the two groups' fluorescence levels, ie. the absolute difference of the medians of the

9

Supplemental material

BMJ Publishing Group Limited (BMJ) disclaims all liability and responsibility arising from any reliance placed on this supplemental material which has been supplied by the author(s)

J Immunother Cancer

$\log_2$ fluorescence ≥ 1. We graph the number of peptides that fulfill these two secondary cut-offs.

Peptide Counts at 5% BH FDR based on Wilcoxon p–values with at least two–fold difference in medians of fluorescence
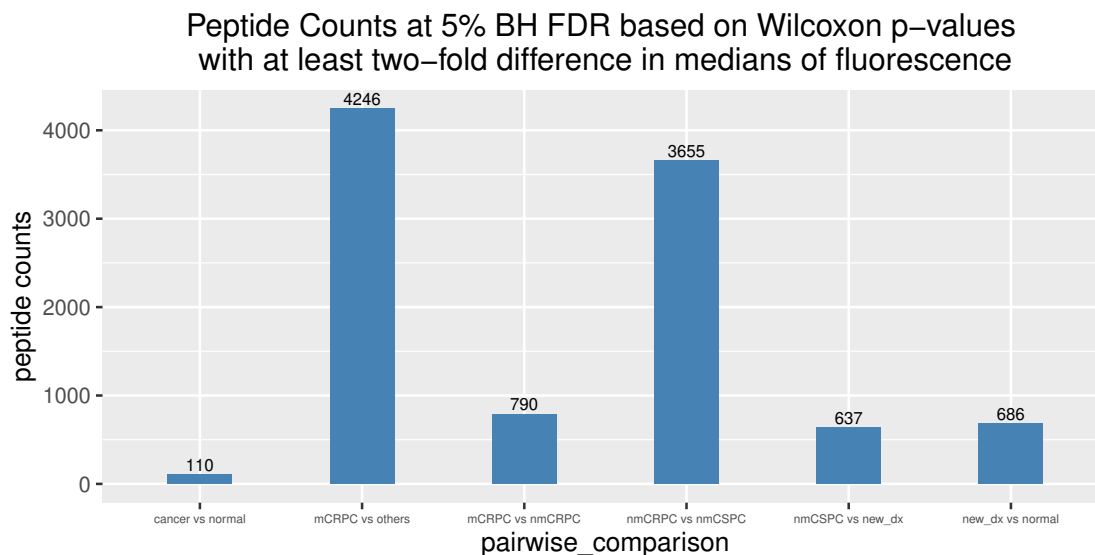
The volcano plots for these contrasts are also obtained. Each volcano plot has 13729 points, which are the peptides identified by the omnibus Kruskal-Wallis tests at 5% BH FDR. The Wilcoxon p-values of each contrast are plotted at $-\log_{10}$ scale. The peptides which meet the secondary cutoffs for each contrast are colored red. The vertical blue dashed lines refer to the two-fold difference in medians. The horizontal blue dashed line refers to the minimum $-\log_{10}$ (p-value) at which the peptides meet the secondary 5% BH FDR cutoff based on the Wilcoxon p-values.

From the bar chart of peptide counts and volcano plots of the pairwise comparisons of consecutive groups, it appears that as disease stage worsens, some peptides exhibit significantly higher median fluorescence levels (especially from nmCSPC to nmCRPC) whereas many peptides also display lower median fluorescence levels (especially from nmCRPC to mCRPC). Overall, if we compare the worst-case-scenario mCRPC against the other stages, many peptides exhibit significantly different (could be higher or lower) median fluorescence. Such changes across disease stages may explain why fewer significant peptides show up when we compare all cancer patients against healthy subjects.

The lists of significant/interesting peptides are also exported to the spreadsheet "*09_Significant_Peptides.xlsx*". Specifically, the "*Kruskal-Wallis*" sheet contains the 13729 peptides at 5% BH FDR based on the Kruskal-Wallis tests on all 177,604 peptides. The other contrast sheets (for example, the "*cancer vs normal*" sheet) contain the lists of peptides at 5% BH FDR (based on the Wilcoxon tests on the 13729 peptides) which also exhibit at least a two-fold difference in medians of the two groups.

Supplemental material

BMJ Publishing Group Limited (BMJ) disclaims all liability and responsibility arising from any reliance placed on this supplemental material which has been supplied by the author(s)

J Immunother Cancer

Volcano plot of contrast: cancer vs normal

110 signif peptides

Volcano plot of contrast: mCRPC vs others

4246 signif peptides

Volcano plot of contrast: mCRPC vs nmCRPC

790 signif peptides

Volcano plot of contrast: nmCRPC vs nmCSPC

3655 signif peptides

Volcano plot of contrast: nmCSPC vs new_dx

637 signif peptides

Volcano plot of contrast: new_dx vs normal

686 signif peptides

2.7   Visualization

We are interested in peptides that meet the secondary cutoffs (at least a two-fold difference in medians and 5% BH FDR based on the Wilcoxon p-values) in at least one of the 6 contrasts. Out of the 13729 peptides at

11

Supplemental material

BMJ Publishing Group Limited (BMJ) disclaims all liability and responsibility arising from any reliance placed on this supplemental material which has been supplied by the author(s)

J Immunother Cancer

5% BH FDR based on the Kruskal-Wallis p-values, only 6708 of them also meet the secondary cutoff. We shall use these 6708 peptides to illustrate the effects of cancer stages via heatmap.

We remove the gand mean of each row of $\log_2$ fluorescence. The fluorescence residuals are then winsorized at -2 and 2, which correspond to roughly bottom 12% and top 15% of the residuals. We then use these winsorized fluorescence residuals to plot the heatmap without any row-wise scaling. The color scheme of the heatmap is specified as navy for -2 which gradually transitions to firebrick for 2.

From the heatmap, we observe a clear pattern. The bottom part of the heatmap consists of peptides that show higher fluorescence levels consistently among all mCRPC patients compared to other groups of patients. Interestingly, there seem to be equal number of healthy subjects who display either higher or lower antibody responses in these peptides. Meanwhile, the upper part of the heatmap consists of peptides that show lower antibody responses consistenly among mCRPC as well as nmCRPC patients.

We also could also reproduce the PCA plot for these unwinsorized fluorescence residuals of these 6708 peptides. Interestingly, they largely preserve the clustering pattern that we observe in the previous PCA plot when we use all the 13729 peptides at 5% BH FDR based on the Kruskal-Wallis p-values.

12

Supplemental material

BMJ Publishing Group Limited (BMJ) disclaims all liability and responsibility arising from any reliance placed on this supplemental material which has been supplied by the author(s)

J Immunother Cancer
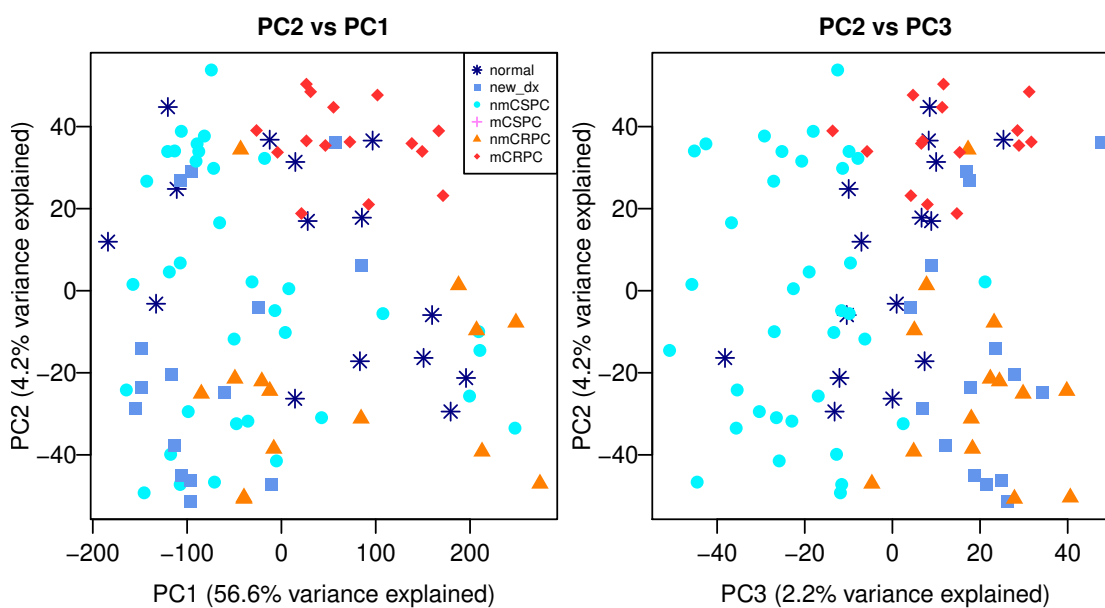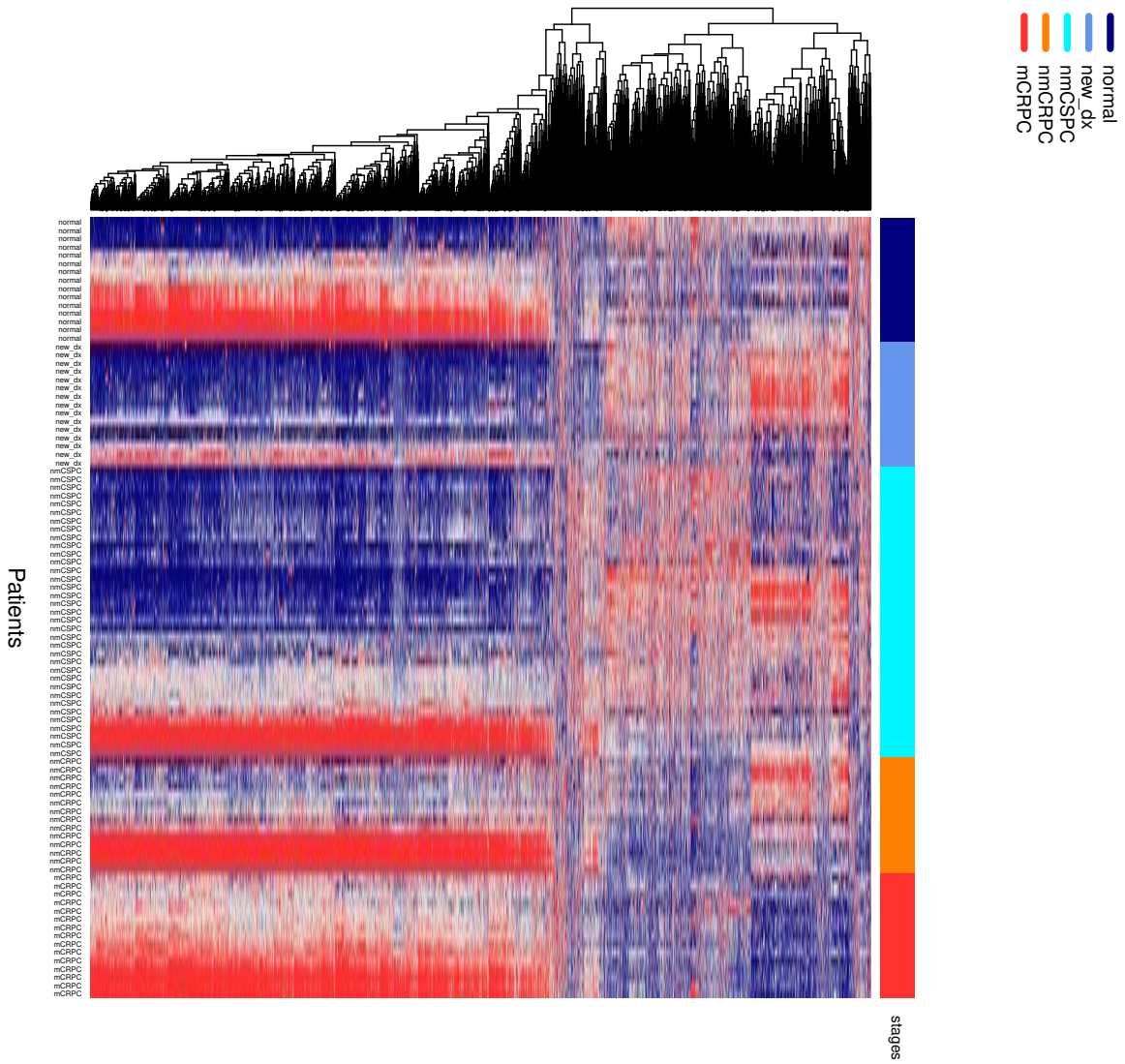
2.8 Gene-Set-Analyses

Here, we shall perform the gene-set analysis based on the interesting/significant peptides identified by the Wilcoxon-BH-FDR and absolute-difference-of-medians cutoffs for each contrast or pairwise comparison. Recall

13

that the 177604 peptides correspond to 1611 proteins, and 1463 of these proteins have matching genes in "*uniprot_gene_entrez.csv*". In this analysis, we deem a protein to be significant if it has at least one significant associated peptide.

Specifically, we investigate if there are any pre-specified gene-sets that are enriched for the genes associated with the list of significant peptides for each contrast or pairwise comparison. These pre-determined gene-sets are defined based on their functional categories or biological properties, such as the Gene Ontology (GO) annotations. Enriched gene-sets could reflect the biological signals in the peptide microarray data. The gene-set-analysis is performed with the R package `allez` [Newton et al., 2018]. We shall consider gene-sets containing at least 2 interesting/significant genes (`n.cell` = 2) with Bonferroni-corrected enrichment p-values not exceeding 5% (`nominal.alpha` = 0.05) . We also limit our analysis to those GO gene-sets which contain at least 5 genes (`n.low` = 5) and at most 300 genes (`n.upp` = 300).

We present our gene-set-analysis results for each contrast in the following subsections.

2.8.1 Cancer vs Normal

Recall that we identified 110 interesting/significant peptides for this contrast. Based on these peptides, the gene-set-analysis yields the following waterfall plot.
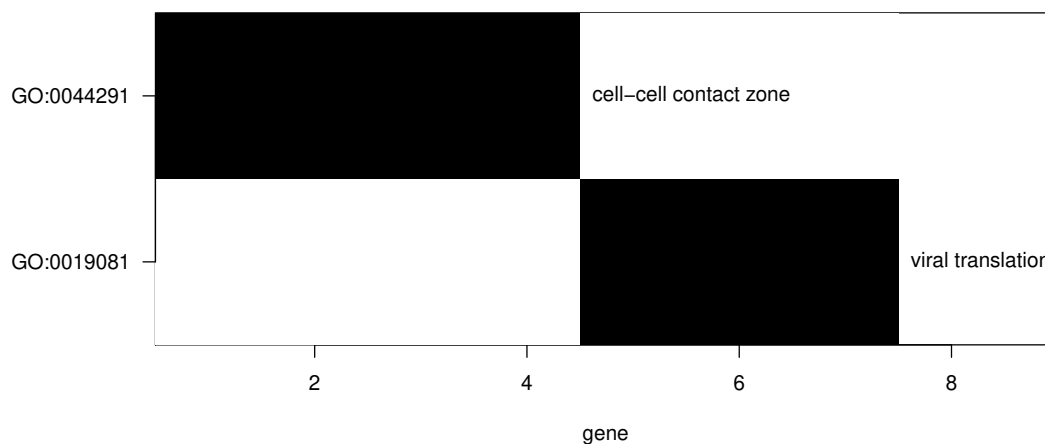
The waterfall plot was constructed by finding the significant (Bonferroni-corrected p-value < 0.05) GO term having the largest overlap with genes associated with proteins that have at least one significant peptide with at least one call among all patients (cell-cell contact zone GO:0044291) and placing it in the top row of the figure. We next removed these genes from the list and found the significant GO term having the highest overlap with the remainder of the list (viral translation GO: 0019081). This process is repeated, and genes identified by this sequential process are counted along the x-axis, and the overlap between the GO terms can be visually assessed. Shading under the 'waterfall' component of the graph indicates genes that were annotated to previously named categories.

We also tabulate the enriched/overrepresented GO terms. The last column of the table shows the genes associated with proteins that have at least one significant peptide in the contrast or pairwise comparison.

Term	Ontology	set.mean	set.size	z.score	in.genes
viral translation	BP	0.5000	3/6	4.2446	EIF3A; EIF3D; EIF3L
T-tubule	CC	0.5000	3/6	4.2446	ANK3; ATP1A1; AHNAK
cell-cell contact zone	CC	0.4444	4/9	4.5363	ANK3; ATP1A1; AFDN; AHNAK

14

2.8.2 mCRPC vs others

Recall that we identified 4246 interesting/significant peptides for this contrast. Based on these peptides, the gene-set-analysis yields the following waterfall plot.

Interpretation for the waterfall plot remains the same as above. We also tabulate the enriched/overrepresented GO terms. The last column of the table shows the genes associated with proteins that have at least one significant peptide in the contrast or pairwise comparison.

Term	Ontology	set.mean	set.size	z.score	in.genes
chromatin	CC	0.9333	70/75	4.6899	ACTB; AR; CEBPB; DHX9; EZH2; MSH6; H1F0; HIST1H1C; HIST1H2AD; H3F3A; H3F3B; HDAC1; HMGB2; HMGN1; HMGN2; HNRNPC; HNRNPK; HSF1; EIF3E; JUN; JUNB; JUND; MCM7; PRM2; RAD21; RAN; RBBP4; RBBP7; UPF1; SMARCA1; SMARCA4; SMARCC2; TCF3; KAT6A; HIST3H3; HIST1H2AK; HIST1H2AM; HIST2H2AC; HIST1H2BL; HIST1H2BF; HIST1H2BH; HIST1H4C; HIST1H4L; EED; HIST1H2AG; MTA1; MAGED1; H2AFY; NCOR2; IST1; MORF4L1; CBX3; POGZ; PDS5A; TARDBP; SUZ12; NOP53; BICRA; HP1BP3; PHF10; H2AFJ; FAM111A; NUCKS1; HIST1H2AH; HIST1H2BK; HIST3H2A; H2AFV; HIST2H2AB; H3F3C; HIST2H2AA4
chromosome	CC	0.8655	103/119	4.3386	ACTB; PARP1; AR; BCL6; CEBPB; CENPE; DHX9; DYNC1LI2; FBL; EZH2; XRCC6; MSH6; H1F0; HIST1H1C; HIST1H2AD; H3F3A; H3F3B; HDAC1; HMGB1; HMGB2; HMGN1; HMGN2; HNRNPC; HNRNPK; HSF1; EIF3E; JUN; JUNB; JUND; MCM3; MCM7; SEPTIN2; NKX3-1; PAFAH1B1; PHF2; PPP1CC; PRM2; PURB; RAD21; RAN; RBBP4; RBBP7; UPF1; RPA1; CLIP1; SMARCA1; SMARCA4; SMARCC2; SP100; SSB; SSRP1; TCF3; VCP; KAT6A; USP11; HIST3H3; HIST1H2AK; HIST1H2AM; HIST2H2AC; HIST1H2BL; HIST1H2BF; HIST1H2BH; HIST1H4C; HIST1H4L; EED; HIST1H2AG; MTA1; MAGED1; H2AFY; NCOR2; IST1; ARPC3; ARPC2; PCGF3; P3H4; MORF4L1; CBX3; POGZ; PDS5A; TARDBP; SUZ12; SPIDR; ORC6; REPIN1; NOP53; BICRA; HP1BP3; PHF10; H2AFJ; NSFL1C; THOC2; FAM111A; NUCKS1; MEAF6; HIST1H2AH; HIST1H2BK; HIST3H2A; H2AFV; TOP1MT; ANAPC16; HIST2H2AB; H3F3C; HIST2H2AA4

15

Supplemental material

BMJ Publishing Group Limited (BMJ) disclaims all liability and responsibility arising from any reliance placed on this supplemental material which has been supplied by the author(s)

J Immunother Cancer

(continued)

| Term	Ontology	set.mean	set.size	z.score	in.genes
transcription regulator activity	MF	0.8571	114/133	4.3918	ACTN1; ACTN2; PARP1; AR; ATF4; BCL6; ZFP36L1; ZFP36L2; C1QBP; CEBPB; CEBPD; CTBP2; DDX1; DHX9; EPAS1; EZH2; GOLGB1; GTF2I; GTF3A; HDAC1; HMGB1; HMGB2; FOXA1; HNRNPK; HES1; HSF1; HSPA1A; DNAJB1; ID1; RBPJ; JUN; JUNB; JUND; MAFG; KMT2A; NFIA; NFE2L1; NFIB; NFIC; NFIL3; NKX3-1; NONO; CNOT2; NPAS2; NPM1; YBX1; PA2G4; PHF2; PURB; SMARCA1; SMARCA4; SMARCC2; SOX4; SP3; SP100; SREBF1; SSRP1; SSX1; TAF7; TCF3; TDG; NR2F2; TSG101; SF1; ZNF24; VEZF1; KAT6A; EDF1; TSC22D1; MTA1; ZRANB2; MAGED1; IER2; NCOR2; MAML1; THRAP3; SAP18; RBM14; N4BP2L2; TADA3; HOXB13; SUB1; FOXJ3; TCF25; POGZ; WWC1; RYBP; TARDBP; EHF; NUPR1; SND1; HIPK2; BICRA; GMNN; LEF1; TDP2; ARID4B; YEATS2; ZNF395; SLC2A4RG; ENY2; BBX; MRTFB; ZNF462; ZNF350; NUCKS1; NIBAN2; IRX3; TBL1XR1; RAX2; ZNF664; CREB3L4; ZNF525; ZFP62
positive regulation of RNA metabolic process	BP	0.8519	138/162	4.7482	ACTN1; ACTN2; PARP1; AGT; APP; AR; ARF4; ATF4; BMPR1B; ZFP36L1; ZFP36L2; CEBPB; CEBPD; CTBP2; DDX3X; DDX5; DHX9; DVL1; EPAS1; FLT3LG; XRCC6; HDAC1; HMGB1; HMGB2; HMGN1; FOXA1; HNRNPD; HNRNPK; HES1; HSF1; HSPA1A; HSPA8; RBPJ; ILF3; INSIG1; JUN; JUNB; JUND; EPCAM; MAFG; MARS; MDK; MAP3K5; KMT2A; MYO6; NCL; NFIA; NFE2L1; NFIB; NFIC; NFIL3; NKX3-1; NOS1; NPAS2; NPM1; YBX1; PFKM; PHF2; PPP3CA; PPP3R1; MAP2K3; RAN; UPF1; RPS27A; SRSF5; TRA2B; SMARCA1; SMARCA4; SMARCC2; SNRNP70; SOX4; SP3; SP100; SREBF1; TAF7; TCEA1; TCF3; NR2F2; TSG101; UBA52; ZNF24; VEZF1; KAT6A; TAF15; OGT; KHSRP; EDF1; MTA1; MAGED1; PRDX6; IER2; MORF4L2; MICAL2; PUM1; BCLAF1; MAML1; THRAP3; NAMPT; HNRNPR; RBM14; TADA3; CAMKK2; RAI1; GCN1; FOXJ3; PHF8; WWC1; RYBP; TARDBP; NUP62; AUTS2; EHF; GNL3; NUPR1; PABPC1; HIPK2; BICRA; LEF1; WAC; YTHDF2; RTRAF; ARID4B; BANP; CHD7; ENY2; ZMIZ1; MRTFB; MAVS; CHD8; NUCKS1; NIBAN2; PAGR1; TBL1XR1; LBH; ING5; RAX2; CREB3L4; IRF2BP2
positive regulation of transcription, DNA-templated	BP	0.8478	117/138	4.2336	PARP1; AGT; APP; AR; ARF4; ATF4; BMPR1B; CEBPB; CEBPD; CTBP2; DDX3X; DHX9; DVL1; EPAS1; FLT3LG; XRCC6; HDAC1; HMGB1; HMGB2; HMGN1; FOXA1; HNRNPD; HNRNPK; HES1; HSF1; RBPJ; ILF3; INSIG1; JUN; JUNB; JUND; EPCAM; MAFG; MARS; MDK; MAP3K5; KMT2A; MYO6; NCL; NFIA; NFE2L1; NFIB; NFIC; NFIL3; NKX3-1; NOS1; NPAS2; NPM1; YBX1; PFKM; PHF2; PPP3CA; PPP3R1; MAP2K3; RAN; RPS27A; SMARCA1; SMARCA4; SMARCC2; SOX4; SP3; SP100; SREBF1; TAF7; TCF3; NR2F2; UBA52; ZNF24; VEZF1; KAT6A; TAF15; OGT; EDF1; MAGED1; IER2; MORF4L2; MICAL2; BCLAF1; MAML1; THRAP3; NAMPT; RBM14; TADA3; CAMKK2; RAI1; GCN1; FOXJ3; PHF8; WWC1; RYBP; TARDBP; NUP62; AUTS2; EHF; GNL3; HIPK2; BICRA; LEF1; WAC; RTRAF; ARID4B; BANP; CHD7; ENY2; ZMIZ1; MRTFB; MAVS; CHD8; NUCKS1; NIBAN2; PAGR1; TBL1XR1; LBH; ING5; RAX2; CREB3L4; IRF2BP2
positive regulation of RNA biosynthetic process	BP	0.8472	122/144	4.3183	ACTN1; ACTN2; PARP1; AGT; APP; AR; ARF4; ATF4; BMPR1B; CEBPB; CEBPD; CTBP2; DDX3X; DHX9; DVL1; EPAS1; FLT3LG; XRCC6; HDAC1; HMGB1; HMGB2; HMGN1; FOXA1; HNRNPD; HNRNPK; HES1; HSF1; RBPJ; ILF3; INSIG1; JUN; JUNB; JUND; EPCAM; MAFG; MARS; MDK; MAP3K5; KMT2A; MYO6; NCL; NFIA; NFE2L1; NFIB; NFIC; NFIL3; NKX3-1; NOS1; NPAS2; NPM1; YBX1; PFKM; PHF2; PPP3CA; PPP3R1; MAP2K3; RAN; RPS27A; SMARCA1; SMARCA4; SMARCC2; SOX4; SP3; SP100; SREBF1; TAF7; TCF3; NR2F2; TSG101; UBA52; ZNF24; VEZF1; KAT6A; TAF15; OGT; EDF1; MTA1; MAGED1; IER2; MORF4L2; MICAL2; BCLAF1; MAML1; THRAP3; NAMPT; RBM14; TADA3; CAMKK2; RAI1; GCN1; FOXJ3; PHF8; WWC1; RYBP; TARDBP; NUP62; AUTS2; EHF; GNL3; NUPR1; HIPK2; BICRA; LEF1; WAC; RTRAF; ARID4B; BANP; CHD7; ENY2; ZMIZ1; MRTFB; MAVS; CHD8; NUCKS1; NIBAN2; PAGR1; TBL1XR1; LBH; ING5; RAX2; CREB3L4; IRF2BP2

16

Supplemental material

BMJ Publishing Group Limited (BMJ) disclaims all liability and responsibility arising from any reliance placed on this supplemental material which has been supplied by the author(s)

J Immunother Cancer

(continued)

Term	Ontology	set.mean	set.size	z.score	in.genes
positive regulation of nucleic acid-templated transcription	BP	0.8472	122/144	4.3183	ACTN1; ACTN2; PARP1; AGT; APP; AR; ARF4; ATF4; BMPR1B; CEBPB; CEBPD; CTBP2; DDX3X; DHX9; DVL1; EPAS1; FLT3LG; XRCC6; HDAC1; HMGB1; HMGB2; HMGN1; FOXA1; HNRNPD; HNRNPK; HES1; HSF1; RBPJ; ILF3; INSIG1; JUN; JUNB; JUND; EPCAM; MAFG; MARS; MDK; MAP3K5; KMT2A; MYO6; NCL; NFIA; NFE2L1; NFIB; NFIC; NFIL3; NKX3-1; NOS1; NPAS2; NPM1; YBX1; PFKM; PHF2; PPP3CA; PPP3R1; MAP2K3; RAN; RPS27A; SMARCA1; SMARCA4; SMARCC2; SOX4; SP3; SP100; SREBF1; TAF7; TCF3; NR2F2; TSG101; UBA52; ZNF24; VEZF1; KAT6A; TAF15; OGT; EDF1; MTA1; MAGED1; IER2; MORF4L2; MICAL2; BCLAF1; MAML1; THRAP3; NAMPT; RBM14; TADA3; CAMKK2; RAI1; GCN1; FOXJ3; PHF8; WWC1; RYBP; TARDBP; NUP62; AUTS2; EHF; GNL3; NUPR1; HIPK2; BICRA; LEF1; WAC; RTRAF; ARID4B; BANP; CHD7; ENY2; ZMIZ1; MRTFB; MAVS; CHD8; NUCKS1; NIBAN2; PAGR1; TBL1XR1; LBH; ING5; RAX2; CREB3L4; IRF2BP2
DNA binding	MF	0.8378	155/185	4.6798	ACTB; ADAR; PARP1; APLP2; APP; AR; ATF4; BCL6; ZFP36L1; ZFP36L2; CEBPB; CEBPD; CUX1; DDX1; DDX3X; DHX9; EPAS1; EZH2; XRCC6; GOLGB1; MSH6; GTF2I; GTF3A; H1F0; HIST1H1C; H3F3A; H3F3B; HDAC1; HMGB1; HMGB2; HMGN1; HMGN2; FOXA1; HNRNPC; HNRNPD; HNRNPK; HES1; HSF1; HSPD1; RBPJ; ILF3; JUN; JUNB; JUND; MCM3; MCM7; KMT2A; NACA; NCL; NFIA; NFE2L1; NFIB; NFIC; NFIL3; NKX3-1; NONO; NPAS2; NPM1; YBX1; PA2G4; PNN; PRM2; PURB; RAD23B; RBBP4; UPF1; RPA1; RPL6; RPL7; RPS15; RPS27; SET; SMARCA1; SMARCA4; SMARCC2; SON; SOX4; SP3; SP100; SREBF1; SSRP1; TAF7; TCEA1; TCF3; TDG; NR2F2; TSG101; ZNF24; VEZF1; ZFAND5; KAT6A; TAF15; HIST1H2BL; HIST1H2BF; HIST1H2BH; HIST1H4C; HIST1H4L; KHSRP; DDX3Y; EDF1; EED; TAF1C; MTA1; H2AFY; IER2; BCLAF1; THRAP3; DNAJB6; AKAP9; RBM5; SRRM1; ZMPSTE24; HOXB13; RAI1; SUB1; FOXJ3; TCF25; SMG1; RYBP; TARDBP; SUZ12; LSM14A; EHF; NUPR1; REPIN1; HP1BP3; SIDT2; LEF1; CXXC5; TDP2; SRRT; XRN1; ZFAND6; BANP; IFT57; STRBP; CHD7; ZNF395; SLC2A4RG; BBX; SCYL1; CHD8; ZNF350; NUCKS1; IRX3; TBL1XR1; RAX2; HIST3H2A; GTF3C6; TOP1MT; ZNF664; CREB3L4; ZMAT2; ZNF525; H3F3C
positive regulation of gene expression	BP	0.8223	162/197	4.3466	ACTB; ADAR; PARP1; AGT; ANK3; APP; AR; ARF4; ATF4; BMPR1B; C1QBP; CEBPB; CEBPD; CTBP2; DDX3X; DDX5; DHX9; DVL1; EPAS1; FLT3LG; XRCC6; HDAC1; HMGB1; HMGB2; HMGN1; FOXA1; HNRNPC; HNRNPD; HNRNPK; HES1; HSF1; HSPA1A; HSPA8; ID1; RBPJ; ILF3; INSIG1; EIF3E; JUN; JUNB; JUND; KRAS; LDLR; LIMS1; EPCAM; MAFG; MARS; MDK; MAP3K5; KMT2A; AFDN; MYH9; MYO1C; MYO6; NCL; NFIA; NFE2L1; NFIB; NFIC; NFIL3; NKX3-1; NOS1; NPAS2; NPM1; YBX1; PFKM; PHF2; PPP3CA; PPP3R1; MAP2K3; RAN; RPL5; RPL26; RPL30; RPS4X; RPS7; RPS27A; SRSF5; TRA2B; SMARCA1; SMARCA4; SMARCC2; SNRNP70; SOX4; SP3; SP100; SREBF1; TAF7; TCF3; NR2F2; UBA52; EZR; ZNF24; VEZF1; KAT6A; TAF15; OGT; EIF3C; EIF3D; EDF1; TAF1C; HGS; RPL23; MAGED1; H2AFY; PRDX6; IER2; NCOR2; MORF4L2; MICAL2; BCLAF1; EIF4A3; MAML1; THRAP3; NAMPT; ZMPSTE24; RBM14; TADA3; SYNCRIP; CAMKK2; RAI1; GCN1; PKP3; FOXJ3; PHF8; WWC1; RYBP; TARDBP; SF3B1; NUP62; AUTS2; EHF; GNL3; PABPC1; HIPK2; BICRA; RPS27L; LEF1; WAC; YTHDF2; RTRAF; ARID4B; YTHDF1; BANP; DNAJA4; CHD7; ENY2; ZMIZ1; MRTFB; MAVS; CHD8; NUCKS1; NIBAN2; SECISBP2; PAGR1; TBL1XR1; LBH; ING5; RAX2; NIBAN1; CREB3L4; IRF2BP2

(continued)

Term	Ontology	set.mean	set.size	z.score	in.genes
negative regulation of gene expression	BP	0.7950	221/278	4.2448	A2M; ADAR; PARP1; APP; AR; ATF4; BCL6; ZFP36L1; ZFP36L2; C1QBP; CAST; CEBPB; CEBPD; CTBP2; DDX3X; DDX5; DHX9; EZH2; XRCC6; H1F0; HIST1H1C; H3F3A; H3F3B; HDAC1; HMGB1; HMGB2; FOXA1; HNRNPC; HNRNPD; HNRNPK; HES1; HSF1; HSPA1A; HSPA8; DNAJB1; ID1; RBPJ; ILF3; EIF3E; JUN; RPSA; LDLR; LIMS1; CAPRIN1; NCL; RPL10A; NFIB; NFIC; NFIL3; NKX3-1; NONO; CNOT2; NOTCH2; NPM1; YBX1; PA2G4; PHF2; PPP3CA; PRNP; PSMA1; PSMA6; PSMB6; PSMC1; PSMD1; PSMD3; PSMD4; PSME1; PURB; RAN; RANBP2; RBBP4; RBBP7; UPF1; RNH1; RPL3; RPL5; RPL6; RPL7; RPL7A; RPL8; RPL9; RPL12; RPL13; RPL15; RPL17; RPL18; RPL18A; RPL19; RPL21; RPL22; RPL23A; RPL24; RPL26; RPL27; RPL30; RPL27A; RPL28; RPL29; RPL31; RPL32; RPL34; RPL37; RPL37A; RPL38; RPL39; RPL41; RPL36A; RPLP0; RPS2; RPS3A; RPS4X; RPS4Y1; RPS6; RPS7; RPS8; RPS10; RPS11; RPS12; RPS13; RPS14; RPS15; RPS15A; RPS17; RPS18; RPS19; RPS20; RPS23; RPS24; RPS25; RPS26; RPS27; RPS27A; SET; SRSF4; SRSF7; SMARCA4; SMARCC2; SP3; SP100; SREBF1; SSB; TAF7; TCF3; TDG; TMBIM6; NR2F2; TSG101; UBA52; EZR; ZNF24; CSDE1; KAT6A; FXR1; USP9X; HIST1H4C; HIST1H4L; KHSRP; EED; RPL14; RPL23; MAGED1; TMEM59; H2AFY; NCOR2; PUM1; BCLAF1; EIF4A3; POM121; RBM8A; THRAP3; DNAJB6; HNRNPR; ZMPSTE24; SAP18; N4BP2L2; HOXB13; SYNCRIP; HEXIM1; CELF1; SRSF10; PKP3; RPL35; PHB2; CBX3; CASC3; TCF25; SMG1; PHF8; WWC1; NEDD4L; RYBP; TARDBP; SUZ12; RPL13A; NUP62; RPL36; SERBP1; PABPC1; SND1; EIF2AK1; PDCD4; HIPK2; SNX12; NOP53; GMNN; ZNF706; LEF1; YTHDF2; CXXC5; SRRT; PTRH2; RASD1; UIMC1; XRN1; YEATS2; CHD8; ZNF350; NIBAN2; SECISBP2; TBL1XR1; LBH

2.8.3 mCRPC vs nmCRPC

Recall that we identified 790 interesting/significant peptides for this contrast. Based on these peptides, the gene-set-analysis yields the following waterfall plot.
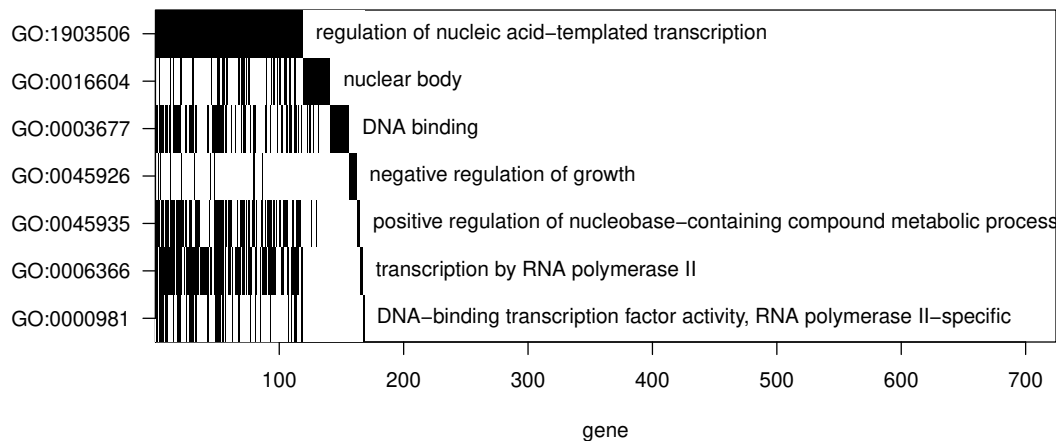
Interpretation for the waterfall plot remains the same as above. We also tabulate the enriched/overrepresented GO terms. The last column of the table shows the genes associated with proteins that have at least one significant peptide in the contrast or pairwise comparison.

Term	Ontology	set.mean	set.size	z.score	in.genes
negative regulation of growth	BP	0.7143	15/21	4.3829	AGT; BCL6; DDX3X; DNAJB2; HSPA1A; MT1E; MT1G; MT1H; MT1X; MT2A; NOTCH2; RBBP7; SMARCA4; RAI1; WWC1

18

Supplemental material

BMJ Publishing Group Limited (BMJ) disclaims all liability and responsibility arising from any reliance placed on this supplemental material which has been supplied by the author(s)

J Immunother Cancer

(continued)

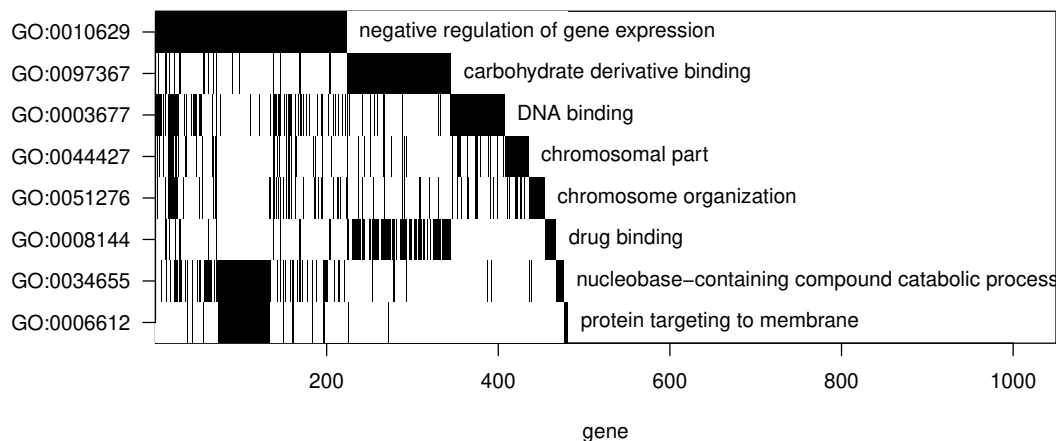| Term	Ontology	set.mean	set.size	z.score	in.genes
DNA-binding transcription factor activity, RNA polymerase II-specific	MF	0.5200	39/75	4.6219	PARP1; AR; BCL6; ZFP36L1; ZFP36L2; CEBPB; KLF6; EPAS1; FOXA1; HES1; HSF1; JUN; KMT2A; NFIA; NFIC; NONO; NPAS2; YBX1; PURB; SMARCC2; SOX4; SP3; SP100; SREBF1; TCF3; VEZF1; TSC22D1; NCOR2; HOXB13; SUB1; POGZ; EHF; YEATS2; BBX; ZNF462; ZNF350; NUCKS1; ZNF525; ZFP62
nuclear body	CC	0.4854	50/103	4.6676	ADD1; AR; DDX3X; EPAS1; MKNK2; HSF1; HSPA1A; NBR1; NONO; PNN; PKN2; BRD2; RPA1; SRSF5; SNRPC; SON; SP3; SP100; TCF3; SF1; KAT6A; AKAP17A; TRIP12; NCOR2; PUM1; BCLAF1; MAML1; THRAP3; HIPK3; NAMPT; SRRM1; RBM14; ATXN2L; CASC3; FNBP4; SUZ12; MORC3; SRRM2; PNISR; VIRMA; GNL3; HIPK2; HP1BP3; WAC; UIMC1; BANP; SLC2A4RG; THOC2; NUFIP2; ZNF350
positive regulation of RNA metabolic process	BP	0.4568	74/162	5.1325	ACTN1; PARP1; AGT; AR; ZFP36L1; ZFP36L2; CEBPB; KLF6; CTBP2; DDX3X; DVL1; EPAS1; XRCC6; HMGN1; FOXA1; HES1; HSF1; HSPA1A; HSPA8; ILF3; JUN; KMT2A; NFIA; NFIC; NPAS2; YBX1; PFKM; MAP2K3; RAN; SRSF5; SMARCA4; SMARCC2; SOX4; SP3; SP100; SREBF1; TCEA1; TCF3; VEZF1; KAT6A; OGT; KHSRP; MAGED1; MICAL2; PUM1; BCLAF1; MAML1; THRAP3; NAMPT; RBM14; CAMKK2; RAI1; GCN1; PHF8; WWC1; RYBP; NUP62; AUTS2; EHF; GNL3; PABPC1; HIPK2; BICRA; WAC; YTHDF2; RTRAF; BANP; CHD7; MRTFB; MAVS; NUCKS1; PAGR1; TBL1XR1; LBH
positive regulation of transcription, DNA-templated	BP	0.4565	63/138	4.6850	PARP1; AGT; AR; CEBPB; KLF6; CTBP2; DDX3X; DVL1; EPAS1; XRCC6; HMGN1; FOXA1; HES1; HSF1; ILF3; JUN; KMT2A; NFIA; NFIC; NPAS2; YBX1; PFKM; MAP2K3; RAN; SMARCA4; SMARCC2; SOX4; SP3; SP100; SREBF1; TCF3; VEZF1; KAT6A; OGT; MAGED1; MICAL2; BCLAF1; MAML1; THRAP3; NAMPT; RBM14; CAMKK2; RAI1; GCN1; PHF8; WWC1; RYBP; NUP62; AUTS2; EHF; GNL3; HIPK2; BICRA; WAC; RTRAF; BANP; CHD7; MRTFB; MAVS; NUCKS1; PAGR1; TBL1XR1; LBH
transcription regulator activity	MF	0.4511	60/133	4.4458	ACTN1; PARP1; AR; BCL6; ZFP36L1; ZFP36L2; C1QBP; CEBPB; KLF6; CTBP2; EPAS1; GOLGB1; FOXA1; HES1; HSF1; HSPA1A; DNAJB1; JUN; KMT2A; NFIA; NFIC; NONO; NPAS2; YBX1; PURB; SMARCA4; SMARCC2; SOX4; SP3; SP100; SREBF1; TCF3; SF1; VEZF1; KAT6A; TSC22D1; MAGED1; NCOR2; MAML1; THRAP3; RBM14; HOXB13; SUB1; POGZ; WWC1; RYBP; EHF; HIPK2; BICRA; GMNN; YEATS2; SLC2A4RG; BBX; MRTFB; ZNF462; ZNF350; NUCKS1; TBL1XR1; ZNF525; ZFP62
positive regulation of RNA biosynthetic process	BP	0.4444	64/144	4.4587	ACTN1; PARP1; AGT; AR; CEBPB; KLF6; CTBP2; DDX3X; DVL1; EPAS1; XRCC6; HMGN1; FOXA1; HES1; HSF1; ILF3; JUN; KMT2A; NFIA; NFIC; NPAS2; YBX1; PFKM; MAP2K3; RAN; SMARCA4; SMARCC2; SOX4; SP3; SP100; SREBF1; TCF3; VEZF1; KAT6A; OGT; MAGED1; MICAL2; BCLAF1; MAML1; THRAP3; NAMPT; RBM14; CAMKK2; RAI1; GCN1; PHF8; WWC1; RYBP; NUP62; AUTS2; EHF; GNL3; HIPK2; BICRA; WAC; RTRAF; BANP; CHD7; MRTFB; MAVS; NUCKS1; PAGR1; TBL1XR1; LBH
positive regulation of nucleic acid-templated transcription	BP	0.4444	64/144	4.4587	ACTN1; PARP1; AGT; AR; CEBPB; KLF6; CTBP2; DDX3X; DVL1; EPAS1; XRCC6; HMGN1; FOXA1; HES1; HSF1; ILF3; JUN; KMT2A; NFIA; NFIC; NPAS2; YBX1; PFKM; MAP2K3; RAN; SMARCA4; SMARCC2; SOX4; SP3; SP100; SREBF1; TCF3; VEZF1; KAT6A; OGT; MAGED1; MICAL2; BCLAF1; MAML1; THRAP3; NAMPT; RBM14; CAMKK2; RAI1; GCN1; PHF8; WWC1; RYBP; NUP62; AUTS2; EHF; GNL3; HIPK2; BICRA; WAC; RTRAF; BANP; CHD7; MRTFB; MAVS; NUCKS1; PAGR1; TBL1XR1; LBH
regulation of transcription by RNA polymerase II	BP	0.4352	84/193	4.9595	PARP1; AR; BCL6; ZFP36L1; ZFP36L2; C1QBP; CEBPB; KLF6; CTBP2; CUX1; DDX3X; EPAS1; XRCC6; HMGN1; FOXA1; HES1; HSF1; HSPA1A; DNAJB1; JUN; MAGEA1; KMT2A; NFIA; NFIC; NONO; NPAS2; YBX1; PFKM; PSMA6; PSMB6; PSMD1; PSMD3; PSMD4; PSME1; PURB; RBBP7; BRD2; SMARCA4; SMARCC2; SOX4; SP3; SP100; SREBF1; TCF3; VEZF1; USP9X; OGT; TSC22D1; RPL23; MAGED1; NCOR2; MICAL2; MAML1; THRAP3; NAMPT; RBM14; HOXB13; HEXIM1; SUB1; GCN1; POGZ; WWC1; NEDD4L; RYBP; SUZ12; AUTS2; EHF; GNL3; PDCD4; HIPK2; NOP53; CXXC5; RTRAF; CHD7; YEATS2; BBX; MRTFB; MAVS; ZNF350; NUCKS1; PAGR1; TBL1XR1; ZNF525; ZFP62

19

(continued)

Term	Ontology	set.mean	set.size	z.score	in.genes
transcription by RNA polymerase II	BP	0.4272	91/213	4.9729	PARP1; AR; BCL6; ZFP36L1; ZFP36L2; BTF3; C1QBP; CEBPB; KLF6; CTBP2; CUX1; DDX3X; DVL1; EPAS1; XRCC6; HMGN1; FOXA1; HES1; HSF1; HSPA1A; DNAJB1; JUN; MAGEA1; KMT2A; NFIA; NFIC; NONO; NOTCH2; NPAS2; YBX1; PFKM; PSMA6; PSMB6; PSMD1; PSMD3; PSMD4; PSME1; PURB; RBBP7; BRD2; SMARCA4; SMARCC2; SOX4; SP3; SP100; SREBF1; TCEA1; TCF3; VEZF1; USP9X; OGT; TSC22D1; TAF1C; RPL23; MAGED1; NCOR2; MICAL2; MAML1; THRAP3; NAMPT; RBM14; HOXB13; HEXIM1; SUB1; GCN1; POGZ; WWC1; NEDD4L; RYBP; SUZ12; AUTS2; EHF; GNL3; PDCD4; HIPK2; NOP53; CXXC5; PCF11; SRRT; RTRAF; CHD7; YEATS2; BBX; MRTFB; MAVS; ZNF350; NUCKS1; PAGR1; TBL1XR1; ZNF525; ZFP62
positive regulation of nucleobase-containing compound metabolic process	BP	0.4254	77/181	4.4664	ACTN1; PARP1; AGT; AR; ZFP36L1; ZFP36L2; CCT6A; CEBPB; KLF6; CTBP2; DDX3X; EPAS1; XRCC6; HMGN1; FOXA1; HES1; HSF1; HSPA1A; HSPA8; ILF3; JUN; KMT2A; NFIA; NFIC; NPAS2; YBX1; PFKM; MAP2K3; RAN; SRSF5; SMARCA4; SMARCC2; SOX4; SP3; SP100; SREBF1; TCEA1; TCF3; VEZF1; KAT6A; USP9X; OGT; KHSRP; MAGED1; MICAL2; PUM1; BCLAF1; MAML1; THRAP3; NAMPT; RBM14; CAMKK2; RAI1; GCN1; PHF8; WWC1; RYBP; NUP62; AUTS2; EHF; GNL3; PABPC1; HIPK2; BICRA; WAC; YTHDF2; RTRAF; UIMC1; BANP; CHD7; MRTFB; MAVS; NUCKS1; PAGR1; TBL1XR1; LBH
DNA binding	MF	0.4162	77/185	4.2259	ADAR; PARP1; AR; BCL6; ZFP36L1; ZFP36L2; CEBPB; KLF6; CUX1; DDX3X; EPAS1; XRCC6; GOLGB1; HMGN1; FOXA1; HES1; HSF1; ILF3; JUN; MCM3; KMT2A; NACA; NFIA; NFIC; NONO; NPAS2; YBX1; NUCB2; PNN; PURB; RAD23B; RPA1; SET; SMARCA4; SMARCC2; SON; SOX4; SP3; SP100; SREBF1; TCEA1; TCF3; VEZF1; ZFAND5; KAT6A; KHSRP; DDX3Y; TAF1C; BCLAF1; THRAP3; DNAJB6; AKAP9; RBM5; SRRM1; HOXB13; RAI1; SUB1; SMG1; RYBP; SUZ12; LSM14A; EHF; REPIN1; HP1BP3; CXXC5; SRRT; ZFAND6; BANP; STRBP; CHD7; SLC2A4RG; BBX; SCYL1; ZNF350; NUCKS1; TBL1XR1; ZNF525
regulation of transcription, DNA-templated	BP	0.4021	117/291	4.9447	PARP1; AGT; AR; BCL6; ZFP36L1; ZFP36L2; C1QBP; CEBPB; KLF6; CTBP2; CUX1; DDX3X; DVL1; EPAS1; XRCC6; GOLGB1; HMGN1; FOXA1; HES1; HSF1; HSPA1A; HSPA8; DNAJB1; ILF3; JUN; MAGEA1; KMT2A; NFIA; NFIC; NONO; NOTCH2; NPAS2; YBX1; PFKM; MAP2K3; PSMA6; PSMB6; PSMD1; PSMD3; PSMD4; PSME1; PURB; RAN; RBBP7; BRD2; SET; SMARCA4; SMARCC2; SOX4; SP3; SP100; SREBF1; TCEA1; TCF3; VEZF1; KAT6A; AKAP17A; USP9X; OGT; KHSRP; TSC22D1; TAX1BP1; TAF1C; RPL23; MAGED1; NCOR2; MICAL2; BCLAF1; MAML1; THRAP3; DNAJB6; NAMPT; PCGF3; RBM14; HOXB13; HEXIM1; CAMKK2; RAI1; SUB1; GCN1; PHB2; TAB2; POGZ; PHF8; WWC1; NEDD4L; RYBP; SUZ12; NUP62; AUTS2; EHF; GNL3; PDCD4; HIPK2; NOP53; BICRA; HP1BP3; GMNN; WAC; CXXC5; SRRT; RTRAF; UIMC1; BANP; CHD7; YEATS2; SLC2A4RG; BBX; MRTFB; MAVS; ZNF350; NUCKS1; PAGR1; TBL1XR1; LBH; ZNF525; ZFP62
regulation of nucleic acid-templated transcription	BP	0.3980	119/299	4.8548	ACTN1; PARP1; AGT; AR; BCL6; ZFP36L1; ZFP36L2; C1QBP; CEBPB; KLF6; CTBP2; CUX1; DDX3X; DVL1; EPAS1; XRCC6; GOLGB1; HMGN1; FOXA1; HES1; HSF1; HSPA1A; HSPA8; DNAJB1; ILF3; JUN; MAGEA1; KMT2A; NFIA; NFIC; NONO; NOTCH2; NPAS2; YBX1; PFKM; MAP2K3; PSMA6; PSMB6; PSMD1; PSMD3; PSMD4; PSME1; PURB; RAN; RBBP7; BRD2; SET; SMARCA4; SMARCC2; SOX4; SP3; SP100; SREBF1; TCEA1; TCF3; SF1; VEZF1; KAT6A; AKAP17A; USP9X; OGT; KHSRP; TSC22D1; TAX1BP1; TAF1C; RPL23; MAGED1; NCOR2; MICAL2; BCLAF1; MAML1; THRAP3; DNAJB6; NAMPT; PCGF3; RBM14; HOXB13; HEXIM1; CAMKK2; RAI1; SUB1; GCN1; PHB2; TAB2; POGZ; PHF8; WWC1; NEDD4L; RYBP; SUZ12; NUP62; AUTS2; EHF; GNL3; PDCD4; HIPK2; NOP53; BICRA; HP1BP3; GMNN; WAC; CXXC5; SRRT; RTRAF; UIMC1; BANP; CHD7; YEATS2; SLC2A4RG; BBX; MRTFB; MAVS; ZNF350; NUCKS1; PAGR1; TBL1XR1; LBH; ZNF525; ZFP62

(continued)

Term	Ontology	set.mean	set.size	z.score	in.genes
regulation of RNA biosynthetic process	BP	0.3980	119/299	4.8548	ACTN1; PARP1; AGT; AR; BCL6; ZFP36L1; ZFP36L2; C1QBP; CEBPB; KLF6; CTBP2; CUX1; DDX3X; DVL1; EPAS1; XRCC6; GOLGB1; HMGN1; FOXA1; HES1; HSF1; HSPA1A; HSPA8; DNAJB1; ILF3; JUN; MAGEA1; KMT2A; NFIA; NFIC; NONO; NOTCH2; NPAS2; YBX1; PFKM; MAP2K3; PSMA6; PSMB6; PSMD1; PSMD3; PSMD4; PSME1; PURB; RAN; RBBP7; BRD2; SET; SMARCA4; SMARCC2; SOX4; SP3; SP100; SREBF1; TCEA1; TCF3; SF1; VEZF1; KAT6A; AKAP17A; USP9X; OGT; KHSRP; TSC22D1; TAX1BP1; TAF1C; RPL23; MAGED1; NCOR2; MICAL2; BCLAF1; MAML1; THRAP3; DNAJB6; NAMPT; PCGF3; RBM14; HOXB13; HEXIM1; CAMKK2; RAI1; SUB1; GCN1; PHB2; TAB2; POGZ; PHF8; WWC1; NEDD4L; RYBP; SUZ12; NUP62; AUTS2; EHF; GNL3; PDCD4; HIPK2; NOP53; BICRA; HP1BP3; GMNN; WAC; CXXC5; SRRT; RTRAF; UIMC1; BANP; CHD7; YEATS2; SLC2A4RG; BBX; MRTFB; MAVS; ZNF350; NUCKS1; PAGR1; TBL1XR1; LBH; ZNF525; ZFP62

2.8.4 nmCRPC vs nmCSPC

Recall that we identified 3655 interesting/significant peptides for this contrast. Based on these peptides, the gene-set-analysis yields the following waterfall plot.

Interpretation for the waterfall plot remains the same as above. We also tabulate the enriched/overrepresented GO terms. The last column of the table shows the genes associated with proteins that have at least one significant peptide in the contrast or pairwise comparison.

Term	Ontology	set.mean	set.size	z.score	in.genes
chromatin	CC	0.9333	70/75	4.8602	ACTB; AR; CEBPB; DHX9; EZH2; MSH6; H1F0; HIST1H1C; HIST1H2AD; H3F3A; H3F3B; HDAC1; HMGB2; HMGN1; HMGN2; HNRNPC; HNRNPK; HSF1; EIF3E; JUN; JUNB; JUND; MCM7; MYC; PRM2; RAD21; RAN; RBBP4; RBBP7; UPF1; SMARCA1; SMARCA4; SMARCC2; TCF3; TCP1; KAT6A; HIST3H3; HIST1H2AK; HIST1H2AM; HIST2H2AC; HIST1H2BL; HIST1H2BF; HIST1H2BH; HIST1H4C; HIST1H4L; EED; HIST1H2AG; MTA1; MAGED1; H2AFY; NCOR2; MORF4L1; PARK7; CBX3; POGZ; PDS5A; SUZ12; NOP53; BICRA; HP1BP3; PHF10; H2AFJ; FAM111A; NUCKS1; HIST1H2AH; HIST1H2BK; HIST3H2A; H2AFV; H3F3C; HIST2H2AA4

Supplemental material

BMJ Publishing Group Limited (BMJ) disclaims all liability and responsibility arising from any reliance placed on this supplemental material which has been supplied by the author(s)

J Immunother Cancer

(continued)

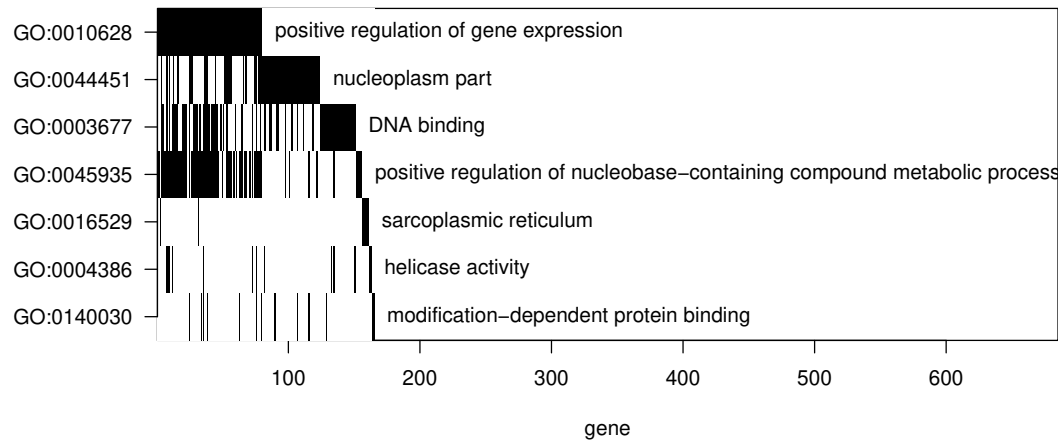| Term	Ontology	set.mean	set.size	z.score	in.genes
nuclear-transcribed mRNA catabolic process, nonsense-mediated decay	BP	0.9059	77/85	4.6352	EIF3E; RPSA; RPL10A; UPF1; RPL3; RPL5; RPL6; RPL7; RPL7A; RPL8; RPL9; RPL10; RPL12; RPL13; RPL15; RPL17; RPL18; RPL18A; RPL19; RPL21; RPL22; RPL23A; RPL24; RPL26; RPL27; RPL30; RPL27A; RPL28; RPL29; RPL31; RPL32; RPL34; RPL35A; RPL37; RPL37A; RPL38; RPL39; RPL41; RPL36A; RPLP0; RPS2; RPS3; RPS3A; RPS4Y1; RPS6; RPS7; RPS8; RPS10; RPS11; RPS12; RPS13; RPS14; RPS15; RPS15A; RPS16; RPS17; RPS18; RPS19; RPS20; RPS23; RPS24; RPS25; RPS26; RPS27A; UBA52; RPL14; RPL23; EIF4A3; RBM8A; RPL35; CASC3; SMG1; RPL13A; RPL36; PABPC1; MAGOHB; SECISBP2
SRP-dependent cotranslational protein targeting to membrane	BP	0.8987	71/79	4.3187	RPSA; RPL10A; RPL3; RPL5; RPL6; RPL7; RPL7A; RPL8; RPL9; RPL10; RPL12; RPL13; RPL15; RPL17; RPL18; RPL18A; RPL19; RPL21; RPL22; RPL23A; RPL24; RPL26; RPL27; RPL30; RPL27A; RPL28; RPL29; RPL31; RPL32; RPL34; RPL35A; RPL37; RPL37A; RPL38; RPL39; RPL41; RPL36A; RPLP0; RPS2; RPS3; RPS3A; RPS4Y1; RPS6; RPS7; RPS8; RPS10; RPS11; RPS12; RPS13; RPS14; RPS15; RPS15A; RPS16; RPS17; RPS18; RPS19; RPS20; RPS23; RPS24; RPS25; RPS26; RPS27A; SRP14; SRPRA; UBA52; RPL14; RPL23; RPL35; TRAM1; RPL13A; RPL36
protein targeting to membrane	BP	0.8953	77/86	4.4486	AKT2; ANK3; RPSA; MYO1C; RPL10A; PRNP; RPL3; RPL5; RPL6; RPL7; RPL7A; RPL8; RPL9; RPL10; RPL12; RPL13; RPL15; RPL17; RPL18; RPL18A; RPL19; RPL21; RPL22; RPL23A; RPL24; RPL26; RPL27; RPL30; RPL27A; RPL28; RPL29; RPL31; RPL32; RPL34; RPL35A; RPL37; RPL37A; RPL38; RPL39; RPL41; RPL36A; RPLP0; RPS2; RPS3; RPS3A; RPS4Y1; RPS6; RPS7; RPS8; RPS10; RPS11; RPS12; RPS13; RPS14; RPS15; RPS15A; RPS16; RPS17; RPS18; RPS19; RPS20; RPS23; RPS24; RPS25; RPS26; RPS27A; SRP14; SRPRA; UBA52; RPL14; RPL23; RPL35; CHP1; TRAM1; RPL13A; RPL36; RAB3IP
nuclear-transcribed mRNA catabolic process	BP	0.8750	84/96	4.2762	ZFP36L2; DDX5; EIF3E; RPSA; RPL10A; CNOT2; UPF1; RPL3; RPL5; RPL6; RPL7; RPL7A; RPL8; RPL9; RPL10; RPL12; RPL13; RPL15; RPL17; RPL18; RPL18A; RPL19; RPL21; RPL22; RPL23A; RPL24; RPL26; RPL27; RPL30; RPL27A; RPL28; RPL29; RPL31; RPL32; RPL34; RPL35A; RPL37; RPL37A; RPL38; RPL39; RPL41; RPL36A; RPLP0; RPS2; RPS3; RPS3A; RPS4Y1; RPS6; RPS7; RPS8; RPS10; RPS11; RPS12; RPS13; RPS14; RPS15; RPS15A; RPS16; RPS17; RPS18; RPS19; RPS20; RPS23; RPS24; RPS25; RPS26; RPS27A; SSB; UBA52; CSDE1; RPL14; RPL23; EIF4A3; RBM8A; THRAP3; RPL35; CASC3; SMG1; RPL13A; RPL36; PABPC1; XRN1; MAGOHB; SECISBP2
chromosomal part	CC	0.8727	96/110	4.5488	ACTB; PARP1; AR; BCL6; CEBPB; CENPE; DDB1; DHX9; DYNC1LI2; EZH2; XRCC6; MSH6; H1F0; HIST1H1C; HIST1H2AD; H3F3A; H3F3B; HDAC1; HMGB2; HMGN1; HMGN2; HNRNPC; HNRNPK; HSF1; EIF3E; JUN; JUNB; JUND; MCM3; MCM7; MYC; NKX3-1; PAFAH1B1; PHF2; PPP1CC; PPP2CB; PRM2; PURB; RAD21; RAN; RBBP4; RBBP7; UPF1; CLIP1; SEC13; SMARCA1; SMARCA4; SMARCC2; SP100; SSB; TCF3; TCP1; VCP; KAT6A; HIST3H3; HIST1H2AK; HIST1H2AM; HIST2H2AC; HIST1H2BL; HIST1H2BF; HIST1H2BH; HIST1H4C; HIST1H4L; EED; HIST1H2AG; MTA1; MAGED1; H2AFY; NCOR2; ARPC3; ARPC2; P3H4; MORF4L1; PARK7; CBX3; POGZ; PDS5A; SUZ12; ORC6; REPIN1; NOP53; BICRA; HP1BP3; GAR1; PHF10; H2AFJ; THOC2; FAM111A; NUCKS1; MEAF6; HIST1H2AH; HIST1H2BK; HIST3H2A; H2AFV; H3F3C; HIST2H2AA4
chromosome organization	BP	0.8525	104/122	4.3118	ACTB; PARP1; BCL6; CENPE; DDB1; DDX1; DDX3X; DHX9; EZH2; XRCC6; H1F0; HIST1H1C; H3F3A; H3F3B; HDAC1; HMGB1; HMGB2; HMGN1; HNRNPC; HNRNPD; HSP90AA1; IGF2; KPNB1; MCM7; KMT2A; MYC; NAP1L1; NOS1; NPM1; PHF2; PRM2; RAD21; RAD23B; RAN; RBBP4; RBBP7; UPF1; BRD2; RPS27A; SET; SMARCA1; SMARCA4; SMARCC2; SP100; SREBF1; TAF7; TCP1; TDG; UBA52; KAT6A; HIST3H3; HIST1H2BL; HIST1H2BF; HIST1H2BH; HIST1H4C; HIST1H4L; OGT; COPS3; EED; TRIP12; H2AFY; ZMPSTE24; PCGF3; RBM14; TADA3; CCT7; CCT4; CCT2; P3H4; MORF4L1; PHB2; CBX3; SMG1; POGZ; PHF8; PDS5A; TSPYL4; SUN1; RYBP; SUZ12; NUP62; BRD1; AUTS2; GNL3; HP1BP3; LEF1; UIMC1; ARID4B; GAR1; XRN1; BANP; PHF10; NOP10; CHD7; YEATS2; ENY2; CHD8; ZNF462; NUCKS1; MEAF6; HDAC10; ING5; TSPYL5; HIST3H2A

22

(continued)

Term	Ontology	set.mean	set.size	z.score	in.genes
drug binding	MF	0.8521	121/142	4.6789	ABAT; ACTB; ACTG1; AKT2; ASNS; ATP1A1; ATP1B1; ATP6V1A; ATP6AP1; ATP5PO; BMPR1B; DDR1; CBS; CENPE; CHKA; CSNK1D; CSNK1E; CYP1B1; DDX1; DDX3X; DDX5; DHX9; CYB5R3; DYNC1LI2; FKBP2; FKBP5; XRCC6; MKNK2; MSH6; HBB; HK2; HMGB2; DNAJA1; HSPA1A; HSPA8; HSP90AA1; HSPD1; IARS; IGF1R; ILF2; ITPK1; KIF5C; MARS; MAT2A; MCM3; MCM7; MAP3K5; MT2A; MMUT; MYH9; MYH11; MYO1C; MYO6; NKTR; NME3; NOS1; PDPK1; PFKM; PGK1; PPP3CA; PPP3R1; PKN2; MAP2K3; PSMC1; RARS; UPF1; SGK1; SMARCA1; SMARCA4; TARS; TCP1; TDG; HSP90B1; VCP; CXCR4; PIP4K2B; ULK1; STK24; DGKD; DDX3Y; EIF4A3; THRAP3; FARSB; ABCC5; ATP9A; HIPK3; NAMPT; UBE2E3; CCT7; CCT4; CCT2; CAMKK2; HSPH1; FASTK; SNRNP200; SMG1; KIF13B; ATP2C1; EIF2AK1; HIPK2; DDX47; IP6K2; RTCB; RIPK4; DNAJA4; UBE2Q1; CHD7; MCCC1; ATP8B2; SCYL1; CHD8; WNK1; UBE2Z; DDX50; ATP13A3; MYO19; ALPK1; ACSS1; NEK9; ANKK1; NRBP2
nucleobase-containing compound catabolic process	BP	0.8293	136/164	4.4069	ACAT1; AHCY; ZFP36L2; ENTPD6; DDX5; DHX9; GPI; H1F0; HINT1; HK2; HMGB1; HMGB2; HNRNPC; HNRNPD; HPRT1; HSF1; HSPA1A; HSPA8; HSPB1; EIF3E; KPNB1; RPSA; LDHA; RPL10A; CNOT2; NPM1; YBX1; PDE4C; PFKM; PGK1; PSMA1; PSMA6; PSMB6; PSMB7; PSMC1; PSMD1; PSMD3; PSMD4; PSME1; RANBP2; UPF1; RNH1; RPL3; RPL5; RPL6; RPL7; RPL7A; RPL8; RPL9; RPL10; RPL12; RPL13; RPL15; RPL17; RPL18; RPL18A; RPL19; RPL21; RPL22; RPL23A; RPL24; RPL26; RPL27; RPL30; RPL27A; RPL28; RPL29; RPL31; RPL32; RPL34; RPL35A; RPL37; RPL37A; RPL38; RPL39; RPL41; RPL36A; RPLP0; RPS2; RPS3; RPS3A; RPS4Y1; RPS6; RPS7; RPS8; RPS10; RPS11; RPS12; RPS13; RPS14; RPS15; RPS15A; RPS16; RPS17; RPS18; RPS19; RPS20; RPS23; RPS24; RPS25; RPS26; RPS27A; SEC13; SET; SSB; TDG; UBA52; VCP; CSDE1; OGT; KHSRP; RPL14; RPL23; PUM1; EIF4A3; RBM8A; THRAP3; HNRNPR; SYNCRIP; PKP3; RPL35; CASC3; SMG1; RPL13A; NUP62; RPL36; SERBP1; NUPR1; PABPC1; SND1; SIDT2; YTHDF2; XRN1; DDIT4; MAGOHB; SECISBP2
cellular nitrogen compound catabolic process	BP	0.8242	136/165	4.2752	ACAT1; AHCY; ZFP36L2; ENTPD6; DDX5; DHX9; GPI; H1F0; HINT1; HK2; HMGB1; HMGB2; HNRNPC; HNRNPD; HPRT1; HSF1; HSPA1A; HSPA8; HSPB1; EIF3E; KPNB1; RPSA; LDHA; RPL10A; CNOT2; NPM1; YBX1; PDE4C; PFKM; PGK1; PSMA1; PSMA6; PSMB6; PSMB7; PSMC1; PSMD1; PSMD3; PSMD4; PSME1; RANBP2; UPF1; RNH1; RPL3; RPL5; RPL6; RPL7; RPL7A; RPL8; RPL9; RPL10; RPL12; RPL13; RPL15; RPL17; RPL18; RPL18A; RPL19; RPL21; RPL22; RPL23A; RPL24; RPL26; RPL27; RPL30; RPL27A; RPL28; RPL29; RPL31; RPL32; RPL34; RPL35A; RPL37; RPL37A; RPL38; RPL39; RPL41; RPL36A; RPLP0; RPS2; RPS3; RPS3A; RPS4Y1; RPS6; RPS7; RPS8; RPS10; RPS11; RPS12; RPS13; RPS14; RPS15; RPS15A; RPS16; RPS17; RPS18; RPS19; RPS20; RPS23; RPS24; RPS25; RPS26; RPS27A; SEC13; SET; SSB; TDG; UBA52; VCP; CSDE1; OGT; KHSRP; RPL14; RPL23; PUM1; EIF4A3; RBM8A; THRAP3; HNRNPR; SYNCRIP; PKP3; RPL35; CASC3; SMG1; RPL13A; NUP62; RPL36; SERBP1; NUPR1; PABPC1; SND1; SIDT2; YTHDF2; XRN1; DDIT4; MAGOHB; SECISBP2
heterocycle catabolic process	BP	0.8242	136/165	4.2752	ACAT1; AHCY; ZFP36L2; ENTPD6; DDX5; DHX9; GPI; H1F0; HINT1; HK2; HMGB1; HMGB2; HNRNPC; HNRNPD; HPRT1; HSF1; HSPA1A; HSPA8; HSPB1; EIF3E; KPNB1; RPSA; LDHA; RPL10A; CNOT2; NPM1; YBX1; PDE4C; PFKM; PGK1; PSMA1; PSMA6; PSMB6; PSMB7; PSMC1; PSMD1; PSMD3; PSMD4; PSME1; RANBP2; UPF1; RNH1; RPL3; RPL5; RPL6; RPL7; RPL7A; RPL8; RPL9; RPL10; RPL12; RPL13; RPL15; RPL17; RPL18; RPL18A; RPL19; RPL21; RPL22; RPL23A; RPL24; RPL26; RPL27; RPL30; RPL27A; RPL28; RPL29; RPL31; RPL32; RPL34; RPL35A; RPL37; RPL37A; RPL38; RPL39; RPL41; RPL36A; RPLP0; RPS2; RPS3; RPS3A; RPS4Y1; RPS6; RPS7; RPS8; RPS10; RPS11; RPS12; RPS13; RPS14; RPS15; RPS15A; RPS16; RPS17; RPS18; RPS19; RPS20; RPS23; RPS24; RPS25; RPS26; RPS27A; SEC13; SET; SSB; TDG; UBA52; VCP; CSDE1; OGT; KHSRP; RPL14; RPL23; PUM1; EIF4A3; RBM8A; THRAP3; HNRNPR; SYNCRIP; PKP3; RPL35; CASC3; SMG1; RPL13A; NUP62; RPL36; SERBP1; NUPR1; PABPC1; SND1; SIDT2; YTHDF2; XRN1; DDIT4; MAGOHB; SECISBP2

23

(continued)

Term	Ontology	set.mean	set.size	z.score	in.genes
DNA binding	MF	0.8216	152/185	4.4818	ACTB; ADAR; PARP1; APLP2; APP; AR; ATF4; BCL6; ZFP36L2; CEBPB; CUX1; DDB1; DDX1; DDX3X; DHX9; EEF1D; EPAS1; EZH2; XRCC6; GOLGB1; MSH6; GTF2I; GTF3A; H1F0; HIST1H1C; H3F3A; H3F3B; HDAC1; HMGB1; HMGB2; HMGN1; HMGN2; HNRNPC; HNRNPD; HNRNPK; HSF1; HSPD1; RBPJ; ILF2; ILF3; JUN; JUNB; JUND; MCM3; MCM7; KMT2A; MYC; NACA; NCL; NFIA; NFE2L1; NFIB; NFIC; NFIL3; NKX3-1; NONO; NPAS2; NPM1; YBX1; NUCB2; PA2G4; PCBP1; PNN; PRM2; PURB; RAD23B; RBBP4; UPF1; RPL6; RPL7; RPS3; RPS15; SET; SMARCA1; SMARCA4; SMARCC2; SON; SOX4; SP3; SP100; SREBF1; SSRP1; TAF7; TCEA1; TCF3; TDG; NR2F2; ZNF24; ZKSCAN1; VEZF1; ZFAND5; KAT6A; TAF15; HIST1H2BL; HIST1H2BF; HIST1H2BH; HIST1H4C; HIST1H4L; KHSRP; DDX3Y; EDF1; EED; TAF1C; MTA1; H2AFY; BCLAF1; THRAP3; DNAJB6; AKAP9; RBM5; SRRM1; ZMPSTE24; HOXB13; KHDRBS1; RAI1; ZNF275; FOXJ3; TCF25; SMG1; RYBP; SUZ12; LSM14A; EHF; NUPR1; FOXP1; REPIN1; IRX4; HP1BP3; SIDT2; LEF1; CXXC5; TDP2; SRRT; XRN1; ZFAND6; BANP; STRBP; CHD7; ZNF395; BBX; SCYL1; CHD8; ZNF350; NUCKS1; IRX3; TBL1XR1; HIST3H2A; ZNF664; CREB3L4; ZMAT2; ZNF525; H3F3C
carbohydrate derivative binding	MF	0.8192	145/177	4.2962	ACTB; ACTG1; AKT2; APLP2; APP; ARF1; ARF4; ASNS; ATP1A1; ATP1B1; ATP6V1A; ATP6AP1; BMPR1B; DDR1; CENPE; CHKA; CSNK1D; CSNK1E; CTSB; DDX1; DDX3X; DDX5; DHX9; CYB5R3; DYNC1LI2; DPYSL3; EEF1A1; EIF5; XRCC6; GNAQ; GNAS; MKNK2; MSH6; GUCY1A1; HK2; HMGB1; DNAJA1; HSPA1A; HSPA8; HSP90AA1; HSPD1; IARS; IGF1R; ILF2; ITPK1; KIF5C; KRAS; LRPAP1; MARS; MAT2A; MCM3; MCM7; MDK; MAP3K5; MYH9; MYH11; MYO1C; MYO6; NME3; NOS1; PAFAH1B1; PDPK1; PFKM; PGK1; PRKAR2A; PKN2; MAP2K3; PRNP; PSMA1; PSMC1; PTPRF; RAB5A; RAN; RAP1B; RARS; UPF1; RPL22; RPL29; SGK1; SMARCA1; SMARCA4; SRPRA; TARS; TCP1; TDG; HSP90B1; VCP; DAP3; MANF; PIP4K2B; ULK1; STK24; DGKD; DDX3Y; ADGRG1; EIF4A3; MFN2; THRAP3; FARSB; ABCC5; ATP9A; HIPK3; ECI2; UBE2E3; CCT7; CCT4; CCT2; CAMKK2; RRAGA; HSPH1; FASTK; RAB35; ADAMTS5; SNRNP200; SMG1; KIF13B; GTPBP4; GNL3; ATP2C1; EIF2AK1; HIPK2; SAR1B; HSD17B12; DDX47; IP6K2; RTCB; RIPK4; DNAJA4; UBE2Q1; CHD7; MCCC1; ATP8B2; SCYL1; CHD8; RRAGC; WNK1; UBE2Z; DDX50; ATP13A3; MYO19; ALPK1; ACSS1; NEK9; ANKK1; NRBP2
negative regulation of gene expression	BP	0.8022	223/278	4.9399	A2M; ADAR; PARP1; APP; AR; ATF4; BCL6; ZFP36L2; CAST; CEBPB; CTBP2; DDX3X; DDX5; DHX9; EIF4EBP2; EZH2; XRCC6; H1F0; HIST1H1C; H3F3A; H3F3B; HDAC1; HMGB1; HMGB2; HNRNPC; HNRNPD; HNRNPK; HSF1; HSPA1A; HSPA8; HSPB1; DNAJB1; IGF2; RBPJ; ILF3; EIF3E; JUN; RPSA; LDLR; LIMS1; CAPRIN1; MYC; NCL; RPL10A; NFIB; NFIC; NFIL3; NKX3-1; NONO; CNOT2; NOTCH2; NPM1; YBX1; PA2G4; PHF2; PPP3CA; PRNP; PSMA1; PSMA6; PSMB6; PSMB7; PSMC1; PSMD1; PSMD3; PSMD4; PSME1; PURB; RAN; RANBP2; RBBP4; RBBP7; UPF1; RNH1; RPL3; RPL5; RPL6; RPL7; RPL7A; RPL8; RPL9; RPL10; RPL12; RPL13; RPL15; RPL17; RPL18; RPL18A; RPL19; RPL21; RPL22; RPL23A; RPL24; RPL26; RPL27; RPL30; RPL27A; RPL28; RPL29; RPL31; RPL32; RPL34; RPL35A; RPL37; RPL37A; RPL38; RPL39; RPL41; RPL36A; RPLP0; RPS2; RPS3; RPS3A; RPS4Y1; RPS6; RPS7; RPS8; RPS10; RPS11; RPS12; RPS13; RPS14; RPS15; RPS15A; RPS16; RPS17; RPS18; RPS19; RPS20; RPS23; RPS24; RPS25; RPS26; RPS27A; SEC13; SET; SRSF4; SRSF7; SMARCA4; SMARCC2; SP3; SP100; SREBF1; SSB; TAF7; TCF3; TDG; TMBIM6; NR2F2; TXN; UBA52; ZNF24; CSDE1; KAT6A; FXR1; USP9X; HIST1H4C; HIST1H4L; KHSRP; EED; RPL14; RPL23; MAGED1; TMEM59; H2AFY; NCOR2; PUM1; BCLAF1; EIF4A3; RBM8A; THRAP3; DNAJB6; HNRNPR; ZMPSTE24; SAP18; CNPY2; N4BP2L2; HOXB13; SYNCRIP; HEXIM1; KHDRBS1; CELF1; SRSF10; PKP3; RPL35; PARK7; PHB2; CBX3; CASC3; TCF25; SMG1; PHF8; WWC1; NEDD4L; RYBP; SUZ12; RPL13A; NUP62; RPL36; SERBP1; PABPC1; SND1; FOXP1; EIF2AK1; PDCD4; HIPK2; NOP53; ZNF706; LEF1; YTHDF2; CXXC5; SRRT; PTRH2; UIMC1; XRN1; MAGOHB; YEATS2; VPS35; CHD8; ZNF350; NIBAN2; SECISBP2; TBL1XR1; HDAC10

Supplemental material

BMJ Publishing Group Limited (BMJ) disclaims all liability and responsibility arising from any reliance placed on this supplemental material which has been supplied by the author(s)

J Immunother Cancer

2.8.5 nmCSPC vs new_dx

Recall that we identified 637 interesting/significant peptides for this contrast. Based on these peptides, the gene-set-analysis yields the following waterfall plot.

Interpretation for the waterfall plot remains the same as above. We also tabulate the enriched/overrepresented GO terms. The last column of the table shows the genes associated with proteins that have at least one significant peptide in the contrast or pairwise comparison.

Term	Ontology	set.mean	set.size	z.score	in.genes
sarcoplasmic reticulum	CC	1.0000	7/7	4.3065	ANK3; HK2; NOS1; SRI; MANF; CHERP; RASD1
promoter-specific chromatin binding	MF	1.0000	9/9	4.8866	DDX5; DHX9; EZH2; HDAC1; HSF1; NFE2L1; H2AFY; SUZ12; CHD7
helicase activity	MF	0.7222	13/18	4.2777	DDX1; DDX3X; DDX5; DHX9; EIF4A1; XRCC6; MCM7; UPF1; SMARCA4; DDX3Y; CHD7; CHD8; DDX50
modification-dependent protein binding	MF	0.7222	13/18	4.2777	MSH6; DNAJB2; KMT2A; PHF2; BRD2; SMARCA4; TAF7; TAB2; PHF8; SUZ12; UIMC1; CHD8; ING5
chromatin binding	MF	0.5283	28/53	4.2125	AR; BCL6; CTBP2; DDX1; DDX5; DHX9; EZH2; MSH6; HDAC1; HNRNPD; HSF1; JUN; NFIA; NFE2L1; NONO; YBX1; UPF1; BRD2; SMARCA4; SP3; MTA1; H2AFY; PHF8; SUZ12; AUTS2; HP1BP3; CHD7; CHD8
nucleoplasm part	CC	0.5109	70/137	6.5131	ADD1; AR; DDX1; DDX3X; DHX9; EZH2; HDAC1; HSF1; HSPA1A; NBR1; KMT2A; MYO1C; MYO6; HNRNPM; NONO; PNN; PKN2; RBBP7; BRD2; RPA1; SON; SP3; SP100; TAF7; TDG; TPP2; U2AF1; SF1; KAT6A; AKAP17A; MTA1; TRIP12; RBM39; NCOR2; PUM1; BCLAF1; THRAP3; HIPK3; ALYREF; SRRM1; SAP18; RBM14; TADA3; UBOX5; ELL2; FNBP4; SF3B1; SUZ12; MORC3; SRRM2; BRD1; PNISR; VIRMA; GNL3; HP1BP3; ARL6IP4; PCF11; NOP58; UIMC1; NXF2; ZMIZ1; THOC2; CHD8; ZNF350; MEAF6; PAGR1; TBL1XR1; LAS1L; HDAC10; ING5
nuclear body	CC	0.5049	52/103	5.4300	ADD1; AR; DDX1; DDX3X; DHX9; HSF1; HSPA1A; NBR1; MYO1C; HNRNPM; NONO; PNN; PKN2; BRD2; RPA1; SON; SP3; SP100; TDG; TPP2; U2AF1; SF1; KAT6A; AKAP17A; TRIP12; RBM39; NCOR2; PUM1; BCLAF1; THRAP3; HIPK3; ALYREF; SRRM1; SAP18; RBM14; UBOX5; FNBP4; SF3B1; SUZ12; MORC3; SRRM2; BRD1; PNISR; VIRMA; GNL3; HP1BP3; ARL6IP4; NOP58; UIMC1; ZMIZ1; THOC2; ZNF350
DNA binding	MF	0.4216	78/185	4.7975	ADAR; AR; ATF4; BCL6; CUX1; DDX1; DDX3X; DHX9; EEF1D; EZH2; XRCC6; GOLGB1; MSH6; GTF2I; GTF3A; HDAC1; HNRNPD; HES1; HSF1; ILF2; ILF3; JUN; JUNB; LBR; MCM7; KMT2A; NACA; NCL; NFIA; NFE2L1; NFIC; NONO; YBX1; PNN; PURB; UPF1; RPA1; RPS27; SMARCA4; SON; SP3; SP100; TAF7; TDG; NR2F2; ZFP36; ZNF24; ZKSCAN1; VEZF1; KAT6A; TAF15; DDX3Y; TAF1C; MTA1; H2AFY; BCLAF1; THRAP3; AKAP9; SRRM1; KHDRBS1; SMG1; RYBP; SUZ12; REPIN1; IRX4; HP1BP3; SRRT; IFT57; CHD7; BBX; SCYL1; CHD8; ZNF350; ZSCAN18; TBL1XR1; ZNF587; ZNF664; ZNF525

25

Supplemental material

BMJ Publishing Group Limited (BMJ) disclaims all liability and responsibility arising from any reliance placed on this supplemental material which has been supplied by the author(s)

J Immunother Cancer

(continued)

Term	Ontology	set.mean	set.size	z.score	in.genes
positive regulation of RNA metabolic process	BP	0.4136	67/162	4.2046	AGT; AR; ATF4; CDKN1C; CTBP2; DDX3X; DDX5; DHX9; FLT3LG; XRCC6; HDAC1; HNRNPD; HES1; HSF1; HSPA1A; HSPA8; IGF2; ILF2; ILF3; JUN; JUNB; KMT2A; MYO6; NCL; NFIA; NFE2L1; NFIC; NOS1; YBX1; PHF2; UPF1; TRA2B; SMARCA4; SP3; SP100; TAF7; NR2F2; UBA52; ZFP36; ZNF24; VEZF1; KAT6A; TAF15; FZD4; MTA1; MAGED1; PUM1; BCLAF1; THRAP3; ALYREF; RBM14; TADA3; CAMKK2; GCN1; PHF8; WWC1; RYBP; AUTS2; GNL3; YTHDF2; CHD7; ZMIZ1; CHD8; NIBAN2; PAGR1; TBL1XR1; ING5
positive regulation of nucleobase-containing compound metabolic process	BP	0.4088	74/181	4.3255	AGT; AR; ATF4; CDKN1C; CTBP2; DDX3X; DDX5; DHX9; FLT3LG; XRCC6; HDAC1; HNRNPD; HES1; HSF1; HSPA1A; HSPA8; HSP90AA1; IGF2; ILF2; ILF3; JUN; JUNB; KMT2A; COX2; MYO6; NCL; NFIA; NFE2L1; NFIC; NOS1; YBX1; PHF2; UPF1; TRA2B; SMARCA4; SP3; SP100; TAF7; TCP1; NR2F2; UBA52; ZFP36; ZNF24; VEZF1; KAT6A; TAF15; USP9X; FZD4; MTA1; MAGED1; PUM1; BCLAF1; THRAP3; ALYREF; RBM14; TADA3; CCT2; CAMKK2; GCN1; PHF8; WWC1; RYBP; AUTS2; GNL3; YTHDF2; UIMC1; CHD7; ZMIZ1; CHD8; NIBAN2; PAGR1; TBL1XR1; HDAC10; ING5
positive regulation of gene expression	BP	0.4061	80/197	4.4491	ADAR; AGT; ANK3; AR; ATF4; CDKN1C; CTBP2; DDX3X; DDX5; DHX9; FLT3LG; XRCC6; HDAC1; HNRNPD; HES1; HSF1; HSPA1A; HSPA8; IGF2; ILF2; ILF3; JUN; JUNB; LDLR; KMT2A; MYO1C; MYO6; NCL; NFIA; NFE2L1; NFIC; NOS1; YBX1; PHF2; TRA2B; SMARCA4; SP3; SP100; TAF7; NR2F2; UBA52; ZFP36; ZNF24; VEZF1; KAT6A; TAF15; FZD4; EIF3D; TAF1C; MAGED1; H2AFY; NCOR2; BCLAF1; THRAP3; ALYREF; RBM14; TADA3; SYNCRIP; CAMKK2; KHDRBS1; GCN1; PKP3; PHF8; WWC1; RYBP; SF3B1; AUTS2; GNL3; COA3; RPS27L; YTHDF2; DNAJA4; CHD7; VPS35; ZMIZ1; CHD8; NIBAN2; PAGR1; TBL1XR1; ING5

2.8.6   new_dx vs normal

Recall that we identified 686 interesting/significant peptides for this contrast. Based on these peptides, the gene-set-analysis yields the following waterfall plot.

Interpretation for the waterfall plot remains the same as above. We also tabulate the enriched/overrepresented GO terms. The last column of the table shows the genes associated with proteins that have at least one significant peptide in the contrast or pairwise comparison.

26

Term	Ontology	set.mean	set.size	z.score	in.genes
nucleoplasm part	CC	0.4599	63/137	4.2887	ACTB; ADD1; AR; DDX1; DHX9; EPAS1; EZH2; H1F0; HDAC1; HSPA1A; NBR1; KMT2A; AFDN; MYO6; PCBP1; PNN; POLR2E; BRD2; SRSF1; SNRNP70; SNRPB2; SON; SP3; SP100; TPP2; U2AF1; KAT6A; EED; MTA1; TRIP12; RBM39; NCOR2; PUM1; BCLAF1; MAML1; THRAP3; HIPK3; SRRM1; RBM14; TADA3; ATXN2L; CASC3; FNBP4; SF3B1; SRRM2; BRD1; PNISR; VIRMA; TDP2; PCF11; NOP58; UIMC1; YEATS2; SLC2A4RG; ENY2; ZMIZ1; THOC2; NUFIP2; CHD8; MEAF6; TBL1XR1; HDAC10; GTF3C6
DNA binding	MF	0.4595	85/185	5.0673	ACTB; ADAR; PARP1; APLP2; AR; ATF4; BCL6; ZFP36L2; CEBPD; CUX1; DDX1; DHX9; EPAS1; EZH2; XRCC6; GOLGB1; MSH6; GTF2I; H1F0; HIST1H1C; HDAC1; HNRNPD; HSPD1; RBPJ; ILF3; JUNB; JUND; MCM3; KMT2A; NCL; NFIA; NFE2L1; NFIB; NFIC; NME1; NME2; NPAS2; PCBP1; PNN; POLR2E; UPF1; RPL6; RPL7; RPS3; RPS15; SMARCA1; SMARCA4; SMARCC2; SON; SOX4; SP3; SP100; SSRP1; ZFP36; KAT6A; TAF15; DDX3Y; EED; MTA1; BCLAF1; THRAP3; DNAJB6; AKAP9; RBM5; SRRM1; ZMPSTE24; HOXB13; RAI1; SMG1; NUPR1; REPIN1; SIDT2; TDP2; SRRT; CHD7; ZNF395; SLC2A4RG; BBX; SCYL1; CHD8; ZSCAN18; TBL1XR1; ZNF587; GTF3C6; CREB3L4

3 Section II: Antibody Responses over Time after Treatments

3.1 Preamble

Now, we want to investigate how treatments induce changes in antibody repertoires in individuals over time. To address this question, we used serum samples available from the 40 patients with nmCSPC who were treated with one of two therapies. 20 patients received standard androgen deprivation therapy (ADT; GnRh analogue given every 3 months), and 20 patients received a DNA vaccine encoding prostatic-acid phosphatase (PAP; pTVG-HP given every 14 days for 6 administrations). Samples were collected (3 replicates) from each of these patients at baseline, 3 months, and 6 months following initiation of treatment.

Again, we take $\log_2$ transformation on the fluorescence levels prior to subsequent steps in our analysis.

3.2 Normalization of Fluorescence Data

In order to verify normalization of the fluorescence level, we also plot the boxplots of median (across replicates) $\log_2$ fluorescence level of all peptides for each patient at each time point.

27

Boxplots of Peptide Fluorescence Levels for Patients at 3 time points
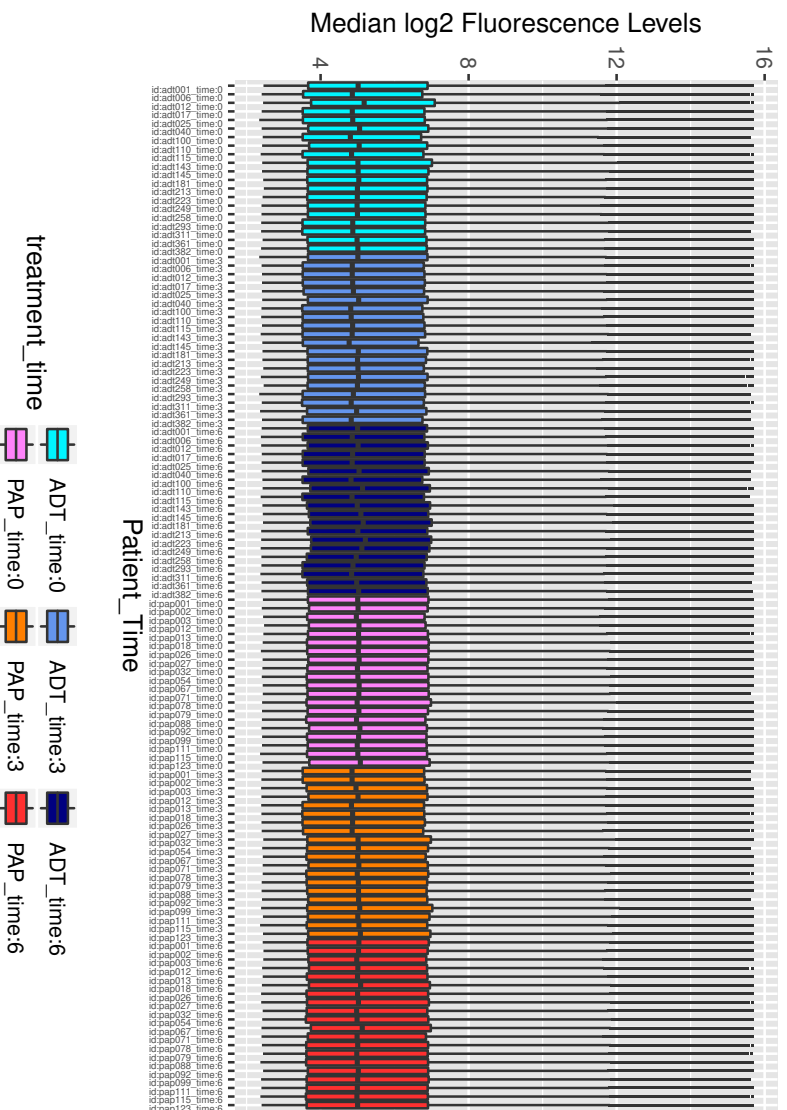
It appears that the fluorescence levels of the peptides are normalized.

3.3 Tests on Time Effect

To analyze how the two treatments (PAP or ADT) induces changes in antibody responses in individuals over time, we analyze the time effect of treatments in the patients for this study separately for the PAP group and for the ADT group. Specifically, for each peptide and each of the two treatment groups (consisting of 20 patients), we fit the following linear mixed model

$$y_{i\tau} = \beta_0 + \beta_1\tau + b_{0i} + b_{1i}\tau + \epsilon_i,$$

where

- $y_{i\tau}$ be the median fluorescence level on $\log_2$ scale for the ith patient at time τ
- $i = 1, \cdots, 20$ and $\tau = 0, 3$ or 6 months
- $\beta_0 =$ the baseline antibody response level for all patients in the treatment group
- b_{0i} is the random intercept of the jth patient
- b_{1j} is the random slope of the jth patient
- $\begin{pmatrix} b_{0i} \\ b_{1i} \\ \epsilon_i \end{pmatrix} \sim N_3 \left(\begin{bmatrix} 0 \\ 0 \\ 0 \end{bmatrix}, \Sigma = \begin{bmatrix} \sigma_0^2 & \rho\sigma_0\sigma_1 & 0 \\ \rho\sigma_0\sigma_1 & \sigma_1^2 & 0 \\ 0 & 0 & \sigma_\epsilon^2 \end{bmatrix} \right)$

For each peptide and for each treatment group, we test the following:

$H_0: \beta_1 = 0$, ie. Treatment does not induce changes in antibody response over time.

$H_1: \beta_1 \neq 0$, ie. Treatment induces changes in antibody response over time.

28

Rationale of the model: Since each patient has multiple measurements, the random effects of the mixed model allow us to capture the within-subject interdepencies. Every patient's antibody response is unique and possibly changes across time due to individual circumstances, so we want our model to include random intercept (representing patient-specific randomness) and random slope (of time). Since measurements were taken across only 3 time points, we refrain from considering more complicated terms involving time effect (eg. higher-order polynomial function of time).

Model-fitting and Test Statistics: Hypothesis testing in linear mixed-models is still an active area of research. Due to the large number of peptides, any non-parametric tests like permutation tests (shuffling treatment identifiers among patients by respecting time blocks) are prohibitively expensive in terms of computation. There are three usual parametric approximate tests for fixed effects in linear mixed models [Luke, 2017]:

- Kenward-Roger (KR) approximate F-test, with model estimates fitted using the Restricted Maximum Likelihood (REML) approach,
- Satterthwaite approximate F-test, with model estimates also fitted with REML, and
- likelihood ratio test (LRT), with model estimates fitted using the usual Maximum Likelihood (ML) approach.

Roughly, unlike the ML approach, the REML method gives unbiased estimate of $\widehat{\Sigma}$. This is imperative, since $\widehat{\Sigma}$ feeds into the F-test calculations. Both Kenward_Roger and Satterthwaite approximations aim to adjust the degrees-of-freedom in the F-test to account for the additional estimation of covariance terms in the random effects of mixed models, as compared to a vanilla F-test in basic linear models [Luke, 2017]. Likelihood ratio test is only meaningful when parameter estimates are fitted with ML, otherwise the likelihood ratio test statistic may even end up as a negative value.

The consensus is that likelihood ratio test (LRT) could be slightly more liberal than the other two methods [Luke, 2017]. KR and Satterthwaite approximations usually give comparable results, and the Satterthwaite method is also the default linear-mixed-model setting in SAS and in the R package *lmerTest* [Kuznetsova et al., 2017]. We deploy only the KR and Satterthwaite approximate F-tests and compare their p-values. We zoom-in the plots to consider p-values ≤ 0.2.

29
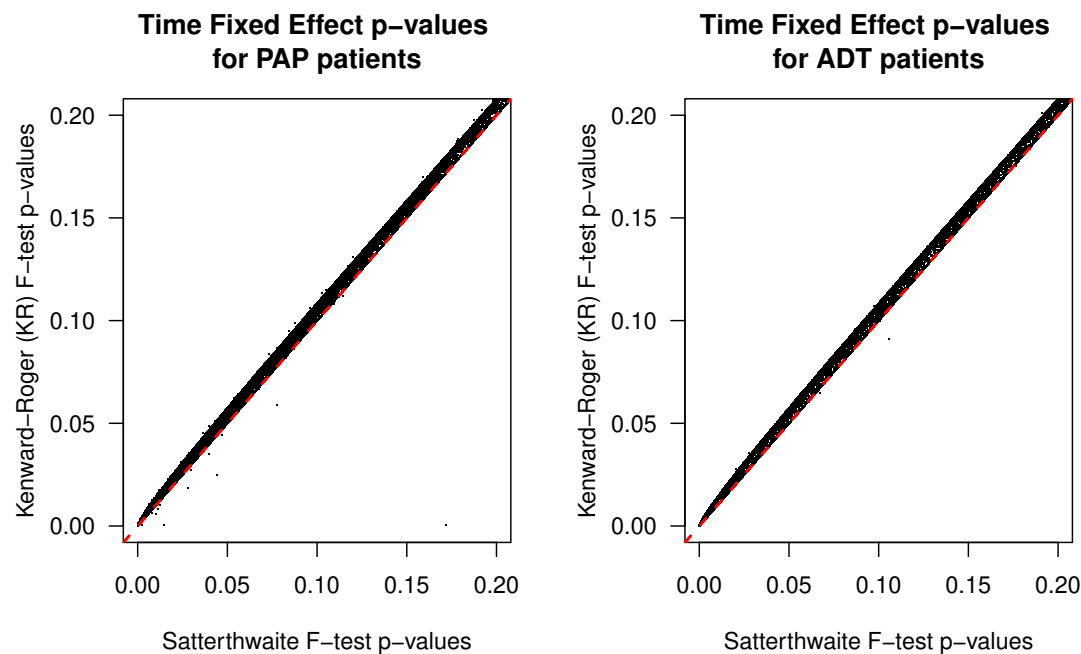
It appears that the KR-approximation is slightly more conservative than the Satterthwaite approximation in most cases. We also plot the density histograms of both sets of F-test p-values for both treatment groups at the same scale.

Density Histograms of F–test p–values
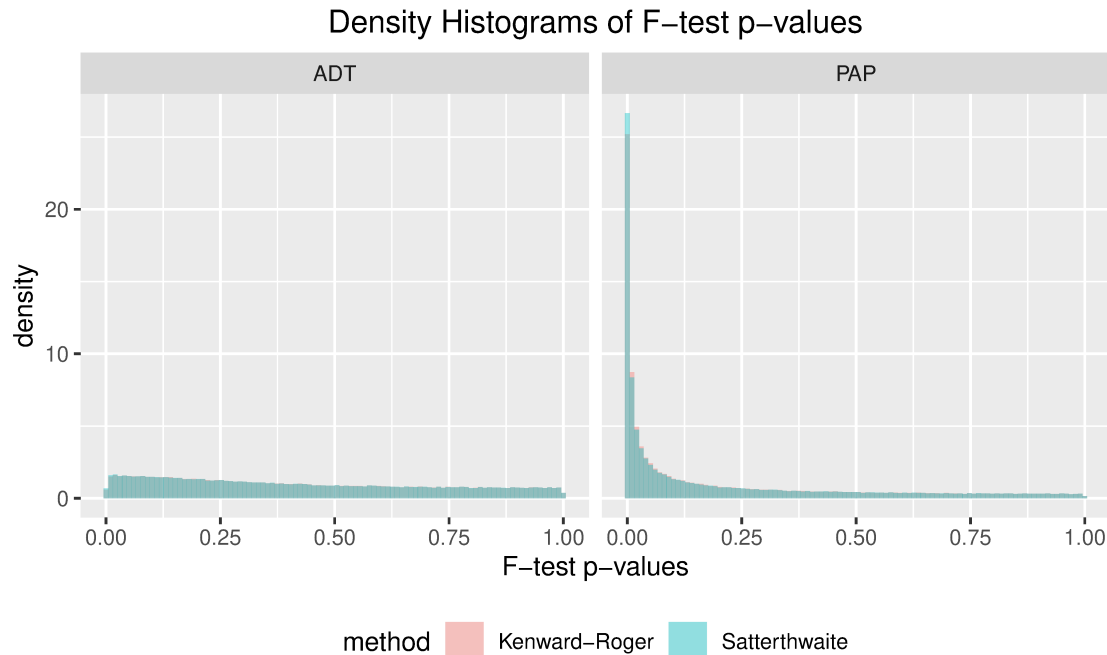
Again, the KR F-test p-values are slightly more conservative than the Satterthwaite approximation for the PAP patients. Where the ADT group is concerned, the p-value histograms are relatively flat for both approximation methods. After applying the BH method, no peptides from the ADT group are found to be significant even at 20% FDR for either of the two approximation methods. For the PAP group, we tabulate the peptide counts at various BH FDR thresholds.

BH_FDR_thresholds	Peptide_counts_KR	Peptide_counts_Satterthwaite
0.01	35039	39071
0.02	45356	48858
0.03	52742	55816
0.04	58713	61466
0.05	63747	66252

For instance, out of the 63747 peptides at 5% FDR based on KR p-values, 35034 of them are among the 63745 peptides at 5% FDR based on the Satterthwaite p-values. Where the PAP group is concerned, we will only consider peptides that meet **5% BH FDR cut-off for both KR and Satterthwaite methods**. In addition, we are only interested in peptides that demonstrate **at least two-fold increase in fluorescence after every 3-months, ie.** $\beta_1 \geq 0.3333$. There are 5680 peptides which meet these two requirements. The list of these peptides is also exported to the sheet "*PAP_Longitudinal*" in the Excel file "*09_Significant_Peptides.xlsx*".

3.4 Visualization

We first obtain the volcano plots of $-\log_{10}$ (KR) F-test p-values versus $\hat{\beta}_1$ for the PAP and ADT groups at the same scale. The 5680 significant peptides that meet the 5% BH FDR and estimated time effect cut-offs

are colored red. The vertical blue dashed line represents the 0.3333 threshold of estimated coefficient of time fixed effect.

The volcano plots corroborate with the patterns we observe from the p-value density histograms. More patients in the PAP groups exhibit more significantly higher changes in antibody responses over time.


PAP's volcano plot **ADT's volcano plot**
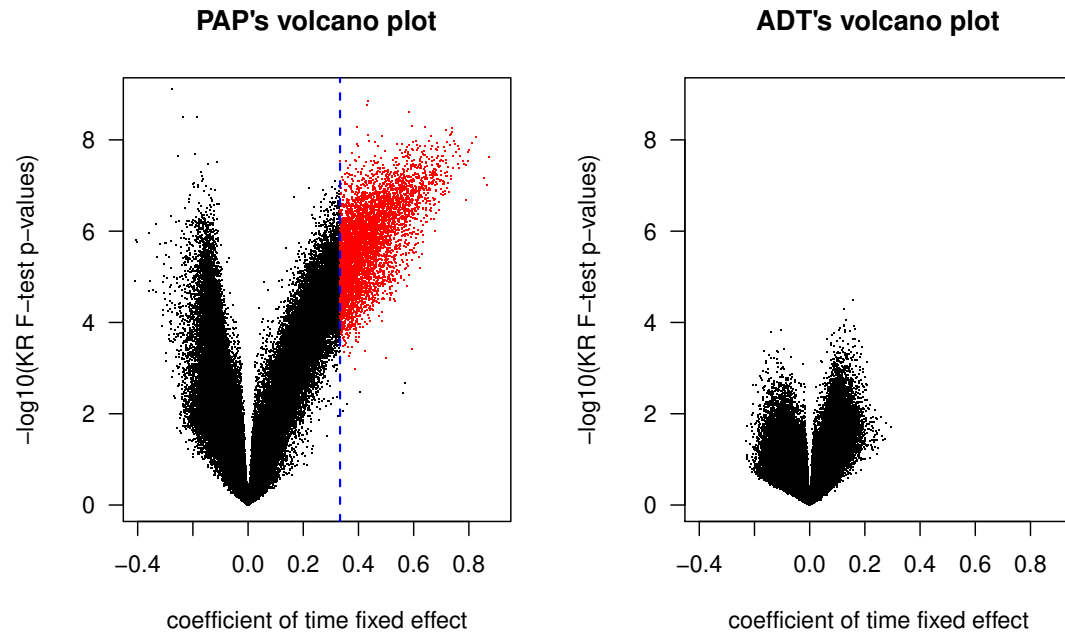
Next, we will illustrate the time fixed effect for the PAP patients among these 5680 significant peptides via a heatmap. First, we obtain the estimated residuals from null model, ie. for each of the 5680 peptides among the PAP patients, we fit the model

$$y_{i\tau} = \beta_0 + b_{0i} + b_{1i}\tau + \epsilon_i,$$

(which corresponds to setting $\beta_1 = 0$) and obtain the residuals for the PAP patients. All the other terms in the model are left unchanged so they retain the same explanation from above. Any pattern among these residuals will demonstate the time fixed effect not covered in the null model.

The fluorescence residuals are then winsorized at -1.7 and 1.7, which correspond to roughly bottom 5% and top 5% of the residuals. We then use these winsorized fluorescence residuals to plot the heatmap without any row-wise scaling. The color scheme of the heatmap is specified as navy for -1.7 which gradually transitions to firebrick for 1.7. Note that the order of the patients are the same across the 3 time points to show how these individuals' antibody response changes over time. Overall, the heatmap clearly illustrates that the individuals' antibody response levels increase over time.

The heatmap also illustrates the fact that each patient's antibody response across the 3 time points is still different. For example, fluorescence levels of (most of) the 5680 peptides for patients with ID *pap078*, *pap099*, *pap032* and *pap111* are pretty 'flat' across the first 3 months before rising profusely in the next 3 months. Patients with ID *pap018*, *pap002*, *pap013*, *pap001*, *pap026*, *pap027*, *pap115*, *pap088*, *pap079* and *pap067* exhibit a drop in antibody response level at time 3 months followed by a substantive increase at time 6 months. In a way, these peptides made the aforementioned dual-cutoff (at most 5% BH FDR and time fixed-effect coefficient ≥ 0.3333) because antibody response levels increase tremendously by time 6 months for all 20 patients.
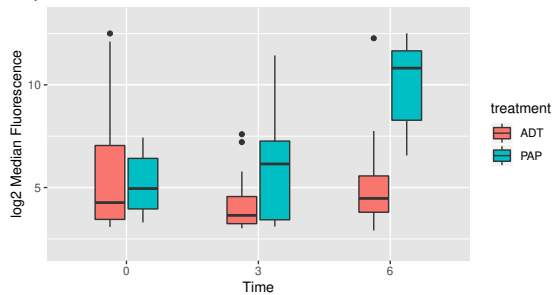
31
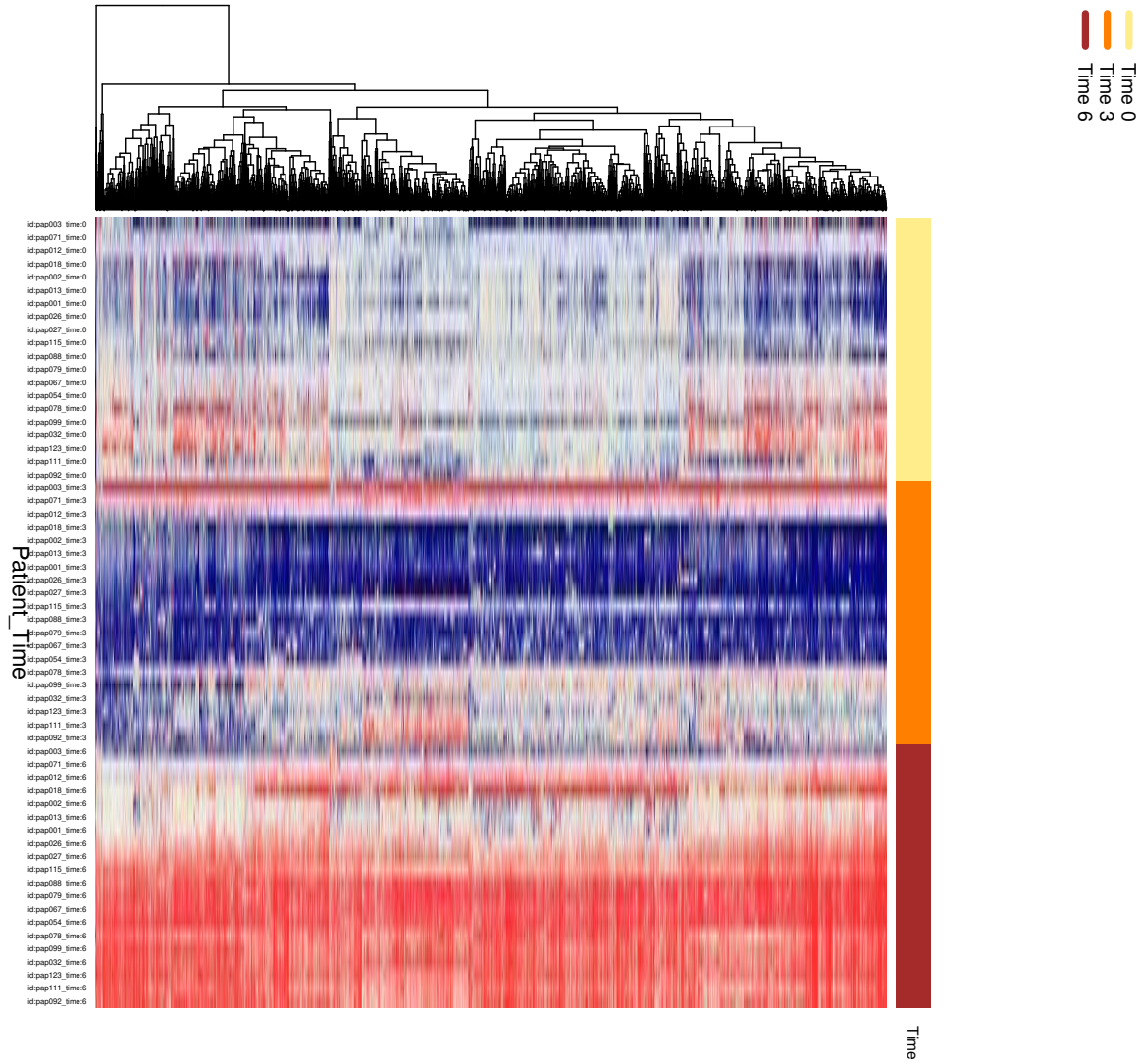
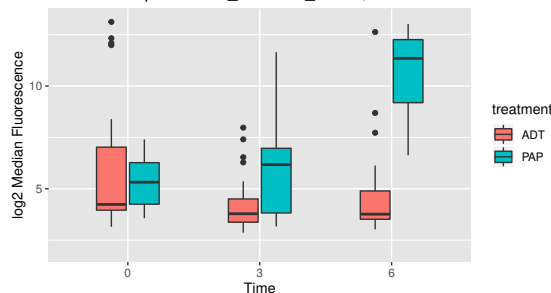We also provide boxplots of fluorescence of a few of these 5680 peptides.

32

Boxplots of Fluorescence Levels for Peptide: CAT151.3_T027960_G006287_2_15387_15731_345;101
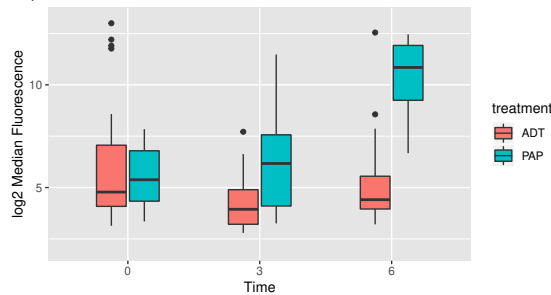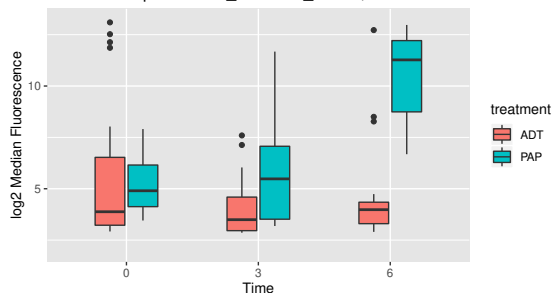
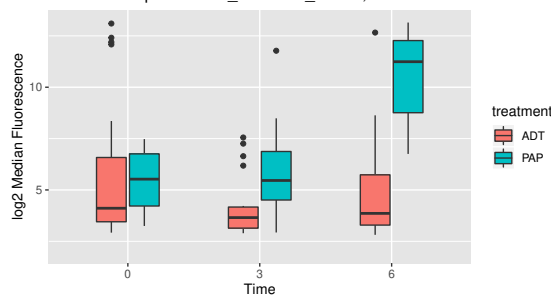Boxplots of Fluorescence Levels for Peptide: FBXL19_AS1_T130509_G030577_1_4499_4918_420;5

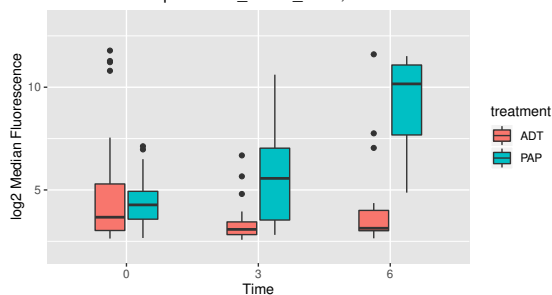Boxplots of Fluorescence Levels for Peptide: 1052_ARL6IP4_51329;285

Boxplots of Fluorescence Levels for Peptide: 1052_ARL6IP4_51329;289

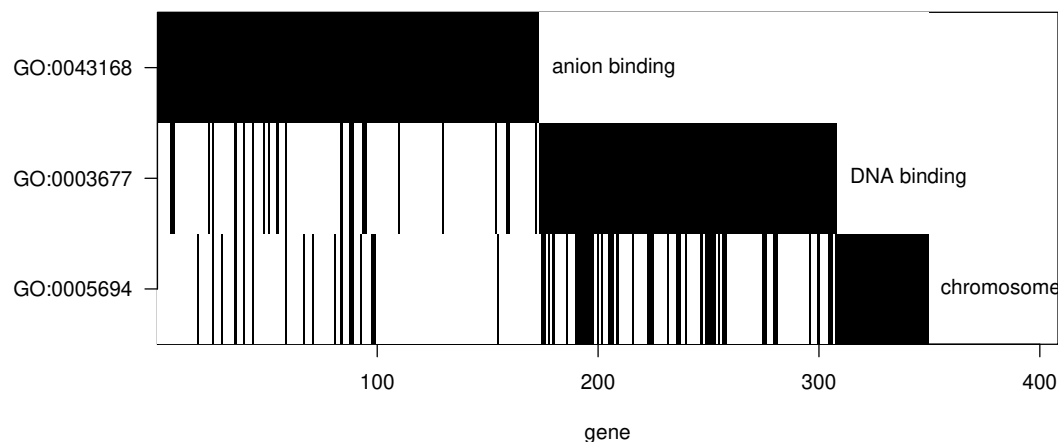Boxplots of Fluorescence Levels for Peptide: 1052_ARL6IP4_51329;293

Boxplots of Fluorescence Levels for Peptide: 946_NKTR_4820;425

3.5 Gene-Set-Analysis

We also perform gene-set analysis based on the 5680 interesting/significant peptides identified for the PAP group. Again, the explanations for gene-set-analysis remain the same. Again, we use the same parameters for the gene-set-analysis: We shall consider gene-sets containing at least 2 interesting/significant genes (`n.cell` = 2) with Bonferroni-corrected enrichment p-values not exceeding 5% (`nominal.alpha` = 0.05) . We also limit our analysis to those GO gene-sets which contain at least 5 genes (`n.low` = 5) and at most 300 genes (`n.upp` = 300).

The gene-set-analysis yields the following waterfall plot. Interpretation for the waterfall plot is similar as before.

33

Supplemental material

BMJ Publishing Group Limited (BMJ) disclaims all liability and responsibility arising from any reliance placed on this supplemental material which has been supplied by the author(s)

J Immunother Cancer

We also tabulate the enriched/overrepresented GO terms. The last column of the table shows the genes associated with proteins that have at least one significant peptide in the contrast or pairwise comparison.

Term	Ontology	set.mean	set.size	z.score	in.genes
chromatin	CC	0.9200	69/75	4.3797	AR; CEBPB; DHX9; EZH2; MSH6; H1F0; HIST1H1C; HIST1H2AD; H3F3A; H3F3B; HDAC1; HMGB2; HMGN1; HMGN2; HNRNPC; HNRNPK; HSF1; EIF3E; JUN; JUNB; JUND; MYC; PRM2; RAD21; RAN; UPF1; SMARCA1; SMARCA4; SMARCC2; TCF3; TCP1; KAT6A; HIST3H3; HIST1H2AK; HIST1H2AM; HIST2H2AC; HIST1H2BL; HIST1H2BF; HIST1H2BH; HIST1H4C; HIST1H4L; EED; HIST1H2AG; MTA1; MAGED1; H2AFY; NCOR2; IST1; MORF4L1; CBX1; CBX3; POGZ; PDS5A; TARDBP; SUZ12; NOP53; BICRA; HP1BP3; PHF10; H2AFJ; FAM111A; NUCKS1; HIST1H2AH; HIST1H2BK; HIST3H2A; H2AFV; HIST2H2AB; H3F3C; HIST2H2AA4
chromosome	CC	0.8739	104/119	4.4726	PARP1; AR; BCL6; CEBPB; CENPE; DHX9; DYNC1LI2; FBL; EZH2; XRCC6; MSH6; H1F0; HIST1H1C; HIST1H2AD; H3F3A; H3F3B; HDAC1; HMGB1; HMGB2; HMGN1; HMGN2; HNRNPC; HNRNPK; HSF1; EIF3E; JUN; JUNB; JUND; MCM3; MYC; SEPTIN2; NKX3-1; PAFAH1B1; PHF2; PPP1CC; PRM2; PURB; RAD21; RAN; RBBP6; UPF1; RPA1; CLIP1; SMARCA1; SMARCA4; SMARCC2; SP100; SSB; SSRP1; TCF3; TCP1; UBE2I; VCP; KAT6A; HIST3H3; HIST1H2AK; HIST1H2AM; HIST2H2AC; HIST1H2BL; HIST1H2BF; HIST1H2BH; HIST1H4C; HIST1H4L; EED; HIST1H2AG; MTA1; MAGED1; H2AFY; NCOR2; IST1; ARPC3; PCGF3; P3H4; PTGES3; MORF4L1; CBX1; CBX3; POGZ; PDS5A; TARDBP; SUZ12; SPIDR; ORC6; REPIN1; NOP53; BICRA; HP1BP3; GAR1; PHF10; H2AFJ; NSFL1C; THOC2; FAM111A; NUCKS1; MEAF6; HIST1H2AH; HIST1H2BK; HIST3H2A; H2AFV; TOP1MT; CENPX; HIST2H2AB; H3F3C; HIST2H2AA4
chromosomal part	CC	0.8727	96/110	4.2564	PARP1; AR; BCL6; CEBPB; CENPE; DHX9; DYNC1LI2; EZH2; XRCC6; MSH6; H1F0; HIST1H1C; HIST1H2AD; H3F3A; H3F3B; HDAC1; HMGB2; HMGN1; HMGN2; HNRNPC; HNRNPK; HSF1; EIF3E; JUN; JUNB; JUND; MCM3; MYC; SEPTIN2; NKX3-1; PAFAH1B1; PHF2; PPP1CC; PRM2; PURB; RAD21; RAN; UPF1; RPA1; CLIP1; SMARCA1; SMARCA4; SMARCC2; SP100; SSB; TCF3; TCP1; UBE2I; VCP; KAT6A; HIST3H3; HIST1H2AK; HIST1H2AM; HIST2H2AC; HIST1H2BL; HIST1H2BF; HIST1H2BH; HIST1H4C; HIST1H4L; EED; HIST1H2AG; MTA1; MAGED1; H2AFY; NCOR2; IST1; ARPC3; P3H4; PTGES3; MORF4L1; CBX1; CBX3; POGZ; PDS5A; TARDBP; SUZ12; ORC6; REPIN1; NOP53; BICRA; HP1BP3; GAR1; PHF10; H2AFJ; THOC2; FAM111A; NUCKS1; MEAF6; HIST1H2AH; HIST1H2BK; HIST3H2A; H2AFV; CENPX; HIST2H2AB; H3F3C; HIST2H2AA4

34

Supplemental material

BMJ Publishing Group Limited (BMJ) disclaims all liability and responsibility arising from any reliance placed on this supplemental material which has been supplied by the author(s)

J Immunother Cancer

(continued)

Term	Ontology	set.mean	set.size	z.score	in.genes
DNA binding	MF	0.8486	157/185	4.9247	ADAR; PARP1; APLP2; APP; AR; ATF4; BCL6; ZFP36L2; CEBPB; CEBPD; CUX1; DDX1; DHX9; EEF1D; EPAS1; ERH; EZH2; XRCC6; GOLGB1; MSH6; GTF2I; GTF3A; H1F0; HIST1H1C; H3F3A; H3F3B; HDAC1; HMGB1; HMGB2; HMGN1; HMGN2; HNRNPC; HNRNPD; HNRNPK; HES1; HSF1; HSPD1; RBPJ; ILF2; ILF3; JUN; JUNB; JUND; LBR; MCM3; KMT2A; MYC; NACA; NCL; NFIA; NFE2L1; NFIB; NFIC; NFIL3; NKX3-1; NPAS2; NPM1; YBX1; PA2G4; PNN; POLR2L; PRM2; PURB; UPF1; RPA1; RPL6; RPL7; RPS3; RPS15; RPS27; SET; SMARCA1; SMARCA4; SMARCC2; SON; SOX4; SP3; SP100; SSRP1; TAF7; TCEA1; TCF3; TDG; NR2F2; TSG101; ZFP36; ZNF24; ZKSCAN1; VEZF1; ZFAND5; KAT6A; TAF15; HIST1H2BL; HIST1H2BF; HIST1H2BH; HIST1H4C; HIST1H4L; DDX3Y; EDF1; EED; TAF1C; MTA1; H2AFY; IER2; BCLAF1; THRAP3; DNAJB6; AKAP9; RBM5; SRRM1; ZMPSTE24; BASP1; HOXB13; KHDRBS1; RAI1; ZNF275; SUB1; FOXJ3; TCF25; SMG1; RYBP; TARDBP; SUZ12; EHF; NUPR1; FOXP1; REPIN1; HP1BP3; SIDT2; LEF1; CXXC5; TDP2; SRRT; XRN1; ZFAND6; BANP; IFT57; STRBP; CHD7; ZNF395; SLC2A4RG; BBX; SCYL1; CHD8; ZNF350; NUCKS1; IRX3; TBL1XR1; RAX2; HIST3H2A; GTF3C6; TOP1MT; ZNF664; CREB3L4; ZMAT2; CENPX; H3F3C
anion binding	MF	0.8357	173/207	4.8214	ABAT; ACADVL; ACTN2; AK2; ALDH1A3; ANXA1; APLP2; APP; ARF1; ARF4; ASNS; ATP1A1; ATP1B1; ATP6V1A; BMPR1B; DDR1; CBS; CCT6A; CENPE; CHKA; CKB; CSNK1D; CSNK1E; DDX1; DDX5; DHX9; DHCR24; CYB5R3; DLD; DYNC1LI2; DPYSL3; EEF1A1; EIF5; FABP5; FOLH1; XRCC6; GNAS; GNAQ; MKNK2; MSH6; GUCY1A1; HADH; HK2; HMGB1; DNAJA1; HSPA1A; HSPA8; HSP90AA1; HSPD1; IARS; ILF2; ITPK1; KIF5C; KRAS; LBR; LRPAP1; MARS; MAT2A; MCM3; MDK; MAP3K5; MGST1; MYH9; MYH11; MYO1C; MYO6; SEPTIN2; NME3; NOS1; PEBP1; PAFAH1B1; PDPK1; PFKM; PITPNA; PRKAR2A; PKN2; MAP2K3; PSMA6; PSMC1; PTPRF; RAN; RAP1B; RARS; UPF1; RPL22; RPL29; SGK1; SMARCA1; SMARCA4; SQLE; SRPRA; TARS; TCP1; TDG; NR2F2; HSP90B1; CCT3; UBE2I; VCP; PIP4K2B; ULK1; STK24; OGT; DGKD; DDX3Y; SNX3; RAB3D; MICAL2; EIF4A3; MFN2; THRAP3; FARSB; ABCC5; ATP9A; HIPK3; ECI2; UBE2E3; CCT7; CCT4; CAMKK2; PMVK; RRAGA; SEPTIN9; HSPH1; RAB10; FASTK; RAB35; UBE2C; ADAMTS5; SNRNP200; SMG1; KIF13B; GTPBP4; WIPI2; GNL3; ATP2C1; EIF2AK1; ARFIP1; ACAD9; HIPK2; SNX12; CRYL1; SAR1B; HSD17B12; DDX47; IP6K2; RTCB; CHMP3; RASD1; RIPK4; LAPTM4B; DNAJA4; DHTKD1; UBE2Q1; CHD7; NSFL1C; WDR45B; MCCC1; ATP8B2; SCYL1; CHD8; GOLPH3; RRAGC; WNK1; DDX50; ATP13A3; MYO19; ALPK1; ACSS1; NEK9; BBS5; ANKK1; NRBP2

4   Conclusion

To investigate whether different prostate cancer stages lead to different antibody responses:

- We utilized both calls data and median fluorescence (across replicates) data.
- Calls data is very conservative – most calls are zero and nothing interesting pops up.
- For median fluorescence data, we deployed the Kruskal-Wallis tests and performed the Benjamini-Hochberg (BH) procedure to control for false discovery rate (FDR). With this approach, we identified 13729 peptides at 5% FDR.
- For these 13729 peptides, we zoomed-in on the following 6 contrasts or pairwise-comparisons. For each contrast, we deployed the Wilcoxon-Rank-Sum tests and performed the BH procedure on these 13729 Wilcoxon p-values. We are interested in peptides that meet the 5% BH-FDR cutoff based on these Wilcoxon p-values as well as having at least a two-fold difference between the medians of the two groups. The counts of peptides that fulfill the two conditions are tabulated below.

pairwise_comparison	peptide_counts
cancer vs normal	110
mCRPC vs others	4246
mCRPC vs nmCRPC	790
nmCRPC vs nmCSPC	3655
nmCSPC vs new_dx	637
new_dx vs normal	686

- We further performed gene-set-analyses based on the peptides identified as interesting/significant for each contrast.
- Visualization techniques via the heatmap and PCA (principal component analysis) reveal the effects of cancer stages on individuals' antibody responses.

To analyze how treatments (PAP vaccine or ADT) influence change in antibody responses over time,

- We deployed linear mixed effects model for each peptide, separately for the group of PAP-vaccinated patients and for the group of patients administered with ADT.
- We also applied the BH procedure on the F-test p-values of the time fixed effects for both groups of patients.
- No significant peptides are identified for the ADT group, even at 20% FDR.
- For the PAP group, we identified 5680 peptides at 5% BH FDR which also exhibit at least two-fold increase in median fluorescence levels every 3 months. Gene-set analysis is also performed based on the proteins associated with this list of peptides.
- The heatmap clearly illustrates that PAP-vaccinated patients had significantly higher antibody responses (measured by those peptides) over the course of 6 months.

The lists of significant peptides identified in both studies are exported to the Excel file "*09_Significant_Peptides.xlsx*". Boxplots of median fluorescence levels of some example peptides for different cancer stages are generated in .png images.

References

Douglas Bates, Martin Machler, Ben Bolker, and Steve Walker. Fitting linear mixed-effects models using lme4. *Journal of Statistical Software*, 67(1):1–48, 2015.

Yoav Benjamini and Yosef Hochberg. Controlling the false discovery rate: A practical and powerful approach to multiple testing. *Journal of the Royal Statistical Society. Series B (Methodological)*, 57(1):289–300, 1995.

Alexandra Kuznetsova, Per B. Brockhoff, and Rune H. B. Christensen. lmerTest package: Tests in linear mixed effects models. *Journal of Statistical Software*, 82(13):1–26, 2017.

Steven G. Luke. Evaluating significance in linear mixed-effects models in r. *Behavior Research Methods*, 49: 1494–1502, 2017.

J.H. McDonald. *Handbook of Biological Statistics*. Sparky House Publishing, Baltimore, Maryland, third edition, 2014.

Michael Newton, Subhrangshu Nandi, Ning Leng, and Aimee Teo Broman. *allez: Random-set calibration of gene-set statistics*, 2018. R package version 2.0.7.

John D. Storey and Robert Tibshirani. Statistical significance for genomewide studies. *Proceedings of the National Academy of Sciences of the United States of America*, 100(16):9440–9445, 2003.

Korbinian Strimmer. A unified approach to false discovery rate estimation. *BMC Bioinformatics*, 9(303), 2008.

Larry Winner. *Introduction to Biostatistics*. Department of Statistics, University of Florida, 2004. URL http://users.stat.ufl.edu/~winner/sta6934/st4170_int.pdf.

Supplemental Figure 1